

CHAPTER 1

General and theoretical aspects of the peroxide group

DIETER CREMER

*Lehrstuhl für Theoretische Chemie, Universität Köln, Köln,
West Germany*

I. INTRODUCTION	2
II. STRUCTURE	4
A. Topology of Atomic Assemblies XO_2 and X_2O_2	4
B. The Configuration Space of XO_2 and X_2O_2	5
III. ORBITAL DESCRIPTION	5
A. Qualitative Valence Bond Treatment	5
1. Molecular oxygen	6
2. Radical, biradical and ionic states of XO_2	7
3. X_2O_2 geometries with chain, Y or bridged structures	8
B. Qualitative Molecular Orbital Treatment	8
1. MO description of O_2	8
2. The hydrogenperoxyl radical	13
3. XO_2 : ozone	13
4. Hydrogen peroxide	13
5. X_2O_2 : F_2O_2	21
IV. PROPERTIES OF XO_2 AND X_2O_2 PROTOTYPES	21
A. Stationary Points on the Potential Hypersurface	21
B. The Conformational Subspace of H_2O_2	36
C. Total Energies, Heats of Formation and Bond Dissociation Enthalpies	40
D. Orbital Energies and Ionization Potentials	44
E. Geometry and Vibrational Analysis	47
F. Charge Density and One-electron Properties	53
G. Excited States	58
V. SUBSTITUENT EFFECTS	61
A. General Trends	61
1. Peroxy compounds XO_2	61

2. Peroxides XOOH and XOOX	63
B. Special Compounds	66
1. Peroxy acids and acyl peroxides	66
2. Polyoxides	68
3. Ozonides and other cyclic peroxides	69
VI. ABBREVIATIONS, SYMBOLS, CONSTANTS AND CONVERSION FACTORS	73
A. List of Abbreviations	73
B. List of Symbols	74
C. Constants and Conversion Factors	77
VII. ACKNOWLEDGEMENTS	77
VIII. REFERENCES	78

I. INTRODUCTION

Compounds containing the OO linkage are key species in oxidation reactions. Knowledge of their chemical properties is essential in the elucidation of atmospheric and stratospheric chemistry, the chemistry of combustion and flames, pollution, polymerization, biochemical synthesis and metabolism. This has been shown in previous monographs and review articles on hydrogen peroxide^{1,2} and organic peroxides³⁻⁷, oxidation reactions⁷⁻⁹, especially those involving singlet oxygen^{10,11} and ozone¹², combustion¹³, decomposition of peroxides^{7,14-16}, smog reactions^{17,18}, degradation of polymers¹⁹, oxidation in biochemical and biological systems^{11,20,21} and metal-dioxygen complexes^{22,23}.

In most cases where a peroxy compound is formed its precursor has been molecular oxygen. Since O₂ is the second most abundant molecule in the atmosphere, one might ask why only a vanishing small amount is converted to per- or poly-oxides. What force prevents O₂ from polymerizing in chains and rings held together by O—O single bonds?

The presentation given here is an attempt to answer this, and related questions, by providing an insight into the electronic features of molecules possessing OO bonds. In order to establish the scenario of per- and poly-oxide chemistry, it seems appropriate to first compare and contrast the OO group with other groups of chemical importance.

Table 1 contains some data relevant to the question of the stability of the O—O single bond. The average bond energies²⁴ listed in Table 1 indicate that oxygen prefers bonding to H, C, N or F rather than to another O atom. Actually, this tendency has been traced to the difference in electronegativities of singly bonded atoms X and O²⁵. The larger this difference, the more ionic the X—O bond (Table 1). Since bond strength is always enhanced by ionic character, X—O bond energies are generally larger than the 34 kcal mol⁻¹ of the O—O bond.

TABLE 1. Bond parameters of molecules containing a X—O single bond

Parameter	H—O	C—O	N—O	O—O	F—O	Ref.
Bond energy (kcal mol ⁻¹)	110	84	53	34	44	24
Electronegativity difference						
$\epsilon_{\text{O}} - \epsilon_{\text{X}}^{\text{a}}$	1.4	1	0.5	0	-0.5	25
Ionic character of bond (%)	18	15	7	0	6	24

^aAccording to the Pauling scale the electronegativity of oxygen is 3.5.

The average O—O single-bond energy, however, is also smallest when compared with values for X—X single bonds where X is a neighbouring atom of the same period (Table 2) or the same group (Table 3). For example, the C—C bond energy is 50 kcal mol⁻¹ larger than that of the O—O bond while the S—S bond energy is more than 20 kcal mol⁻¹ larger. Table 3 reveals that single-bond energies of Group VI elements do not decrease with atomic number as double-bond energies do. Both the S—S and Se—Se bond are stronger than O—O and Te—Te bonds, the latter being comparable in strength. In this respect, O is similar to N and F, both of which also form weaker homonuclear single bonds than their higher homologues. This anomaly of N, O and F also becomes apparent when looking at average X—X bond lengths. These are larger by 5–12% than bond lengths predicted from covalent radii, which have been derived from C—X bond lengths.

Both these anomalies of the O—O bond are indicative of the weakening effect of lone-pair–lone-pair repulsion. If destabilization resulting from lone-pair repulsion is lowered, a strengthening of the OO linkage occurs. This is best achieved in the O₂ molecule where two of the four lone pairs are no longer localized at one atom. By delocalization they gain bonding character (see Section III.A.1). This explains the high bond energy of O₂ (119.2 kcal mol⁻¹, Table 3).

Lone-pair–lone-pair repulsion also causes a weakening of SS or SeSe bonds. However, due to the larger covalent radii of these atoms (Table 3) and the corresponding increase of the bond lengths the effect is much smaller than for the OO linkage. This difference constitutes the source of the anomaly of Group VI single-bond energies discussed above.

The atomization energy of O₂ is 59.6 kcal mol⁻¹ of atoms to be compared with 34 kcal mol⁻¹ of atoms for an oxygen polymer. This means that polymerization of O₂ would be endothermic by 26 kcal mol⁻¹ of atoms, which corresponds to a change in the free enthalpy larger than 26 kcal mol⁻¹ as polymerization would be accompanied by a decrease of entropy. Therefore, oxygen polymers are not likely to occur in nature.

The fact that the O—O single bond can easily be broken is responsible for the unusual reactivity of peroxy compounds.

TABLE 2. Bond parameters of homonuclear single bonds X—X^a

Parameter	H—H	C—C	N—N	O—O	F—F
Bond energy (kcal mol ⁻¹)	104 ^b	84	38	34	38 ^b
Bond length (Å)	0.71	1.54	1.47	1.46	1.43
Covalent radius r_{c} of X (Å)	—	0.77	0.74	0.73	0.71
			(0.70) ^c	(0.66) ^c	(0.64) ^c

^aAll values from Ref. 24.

^bDissociation enthalpy of X—X.

^cEvaluated from X—C bond lengths.

TABLE 3. Average bond energies and covalent radii of Group VI elements^a

Parameter	OO	SS	SeSe	TeTe
Single-bond energy (kcal mol ⁻¹)	34	58	44	34
Double-bond energy (kcal mol ⁻¹)	119	102	63	53
Covalent radius r_{c} (Å)	0.73	1.04	1.16	1.35

^aAll values from Ref. 24.

II. STRUCTURE

Molecules with the stoichiometric formulas XO_2 or X_2O_2 will be considered in this chapter provided that they contain the subunit OO , i.e. that there exists some kind of bonding interaction between the O atoms. At the moment, it suffices to indicate these interactions by a string \sim tying the atoms together. Then, the following question has to be answered: What are the possible structures of molecules XO_2 and X_2O_2 ?

A. Topology of Atomic Assemblies XO_2 and X_2O_2

If the number of bonding interactions involving X and O is not limited, two topologically different structures can be expected for XO_2 and ten for X_2O_2 . These are shown in Figure 1.

To distinguish between them we may term them chain (1, 3, 4), Y or branched (5), cyclic or polycyclic (2, 6–12) forms. Since X,X interactions are of secondary interest, we can consider 4, 6 and 9 as special cases of 1 and 2 and, similarly, 7, 11 and 12 as being special cases of 5, 8 and 10. If we assume that both atoms X interact in a similar manner with the OO moiety, then 8 can be dropped as an unlikely candidate for a peroxide structure*. That leaves us with the chain structures 1, 3, the branched or Y structure 5, the cyclic structure 2 and the bicyclic or bridged one (10).

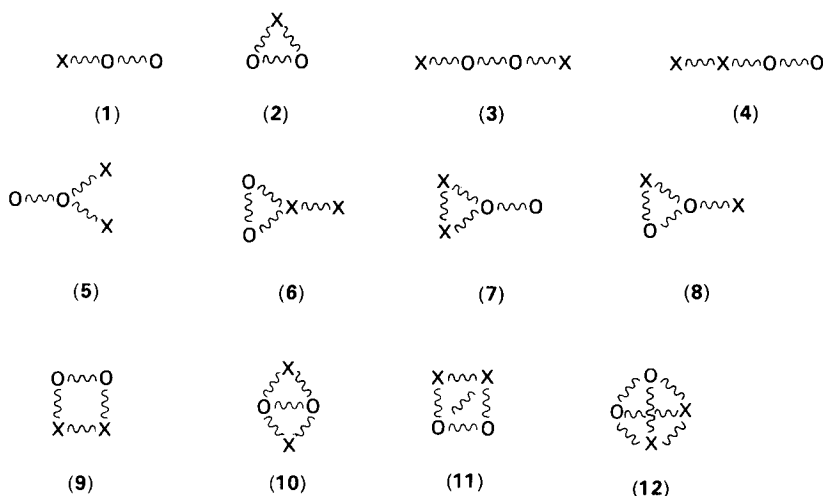


FIGURE 1. Topologically different structures of XO_2 and X_2O_2 compounds.

* Actually, this line of reasoning can only be followed if the stability of 8 is compared with those of the other peroxide structures. We anticipate the result of such a stability analysis in order to simplify the topological analysis. However, if two different substituents X and Y are attached to the OO moiety, structure 8 may very well correspond to a stable peroxide form (see, e.g. CH_2OOH^+) and, therefore, cannot be dropped.

B. The Configuration Space of XO_2 and X_2O_2

In order to get a better understanding of the topological arrangements 1, 2, 3, 5 and 10, we shall now discuss specific geometrical forms generated from these structures. The configuration space of XO_2 can be spanned by the three internal coordinates R , R' and α , where R and R' denote the OO and OX bond length, respectively, and α is the OOX bond angle. In Figure 2 the interconversion of 1 to 2 is depicted. It involves linear, bent and cyclic geometries of XO_2 , which are related by the angle α . In this respect interconversion can be viewed as corresponding to a movement approximately parallel to the α axis of the XO_2 space. This is indicated in Figure 2. Movements roughly parallel to the R or R' axis ultimately lead to dissociation of XO_2 .

As for X_2O_2 , the chain structure 3 is certainly the one most familiar to chemists. Geometries generated from 3 comprise linear-linear, linear-bent and bent-bent forms. The latter can be further distinguished by the dihedral angle τ . Characteristic geometries are obtained for $\tau = 0^\circ$ (*cis* form), $\tau = 180^\circ$ (*trans* form) or $0^\circ < \tau < 180^\circ$ (skewed forms). They are shown in Figure 3.

The Y structure (5) was historically one of the first discussed in connection with the elucidation of the hydrogen peroxide structure¹. It can be either planar or pyramidal as shown in Figure 3. A similar distinction can be made for the bicyclic or bridged geometries, which have hardly been considered in peroxide chemistry.

The main interconversional modes together with some dissociative paths of X_2O_2 molecules are sketched in Figure 3. There the total six-dimensional space of the four-atom system has been projected onto a four-dimensional subspace by keeping the two R' and two α coordinates equal. Again, movements in geometrical space have been constrained to occur roughly parallel to one of the four axes, defined by R , R' , α and τ .

III. ORBITAL DESCRIPTION

A. Qualitative Valence Bond Treatment

In order to understand the bonding situation in XO_2 and X_2O_2 it is helpful to 'synthesize' them in a step-by-step manner from atoms O and X via the 'intermediate' O_2 .

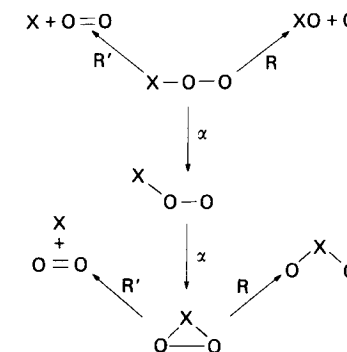


FIGURE 2. Possible interconversions occurring in the XO_2 configuration space approximately parallel to the space axes (R , R' , α). Note that lines between atoms symbolize bonding interactions rather than electron-pair bonds.

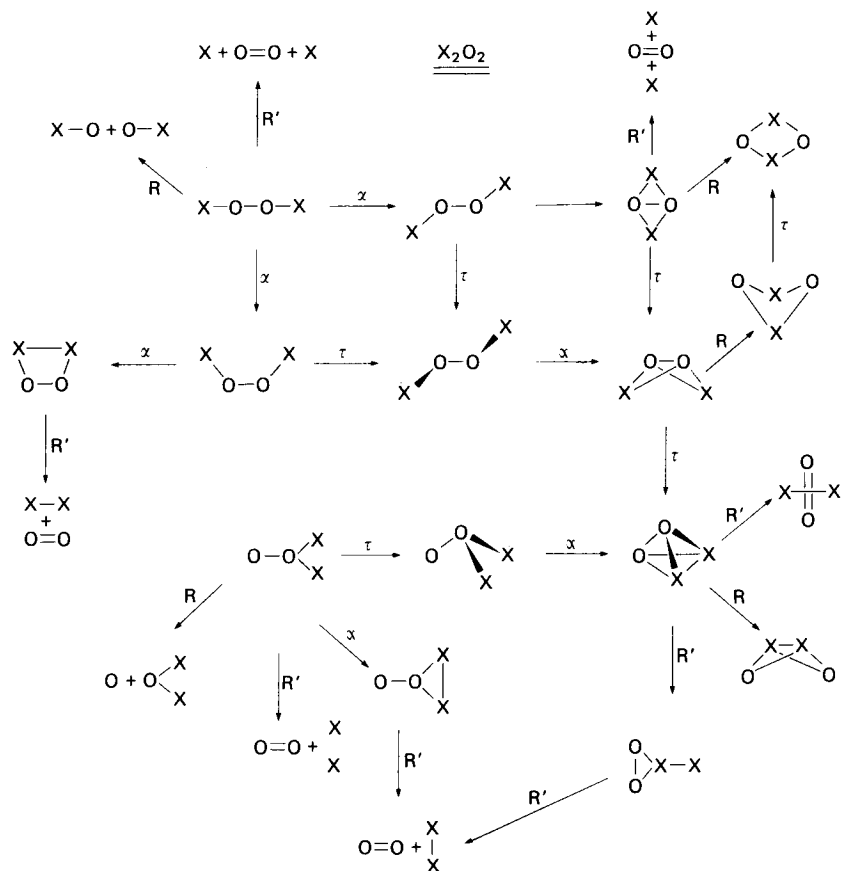
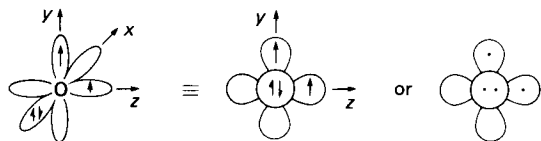


FIGURE 3. Possible interconversions occurring in the X_2O_2 configuration space. See caption of Figure 2.

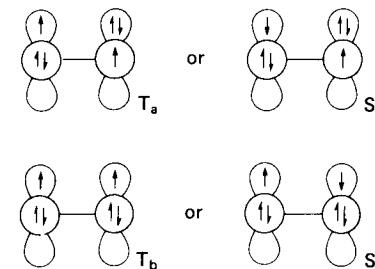
1. Molecular oxygen

Atomic oxygen possesses the electron configuration $(1s)^2(2s)^2(2p)^4$, which leads to a 3P ground state and 1D and 1S excited states. Ignoring the low-lying and doubly occupied $1s$ and $2s$ AOs, the $O(^3P)$ state can be visualized as:



There are 81 different ways of combining two $O(^3P)$ atoms leading to a total of 81 O_2 states. If a strong σ bond is formed by coupling of the $2p_z$ AOs, essentially two possibilities

a and b remain to combine the other $2p$ electrons. Each combination mode splits into a singlet (S) and a triplet (T) state of O_2 :



Combination mode a is clearly preferred, since it allows the electron pair on one O atom to delocalize onto the second O atom, thus reducing destabilizing Coulomb repulsions typical for combination mode b. The delocalization effect involving three $2p\pi$ electrons has been estimated to account for about 30 kcal mol^{-1} of the bond strength²⁶. Accordingly, π bonding should contribute 60 kcal mol^{-1} to the total bond strength of O_2 . The singly occupied orbitals are orthogonal in case a. Exchange interactions stabilize the triplet but destabilize the singlet state, just as would be predicted if Hund's rule of maximum multiplicity would be applied. Hence T_a represents the ground state (GS) of O_2 , while S_a , S_b and T_b describe excited states.

2. Radical, biradical and ionic states of XO_2

If an atom X, with a single electron in a $1s$, $2s$ or $2p\sigma$ AO, approaches O_2 , it can form a σ bond with O via one of the singly occupied $2p$ orbitals of the T_a state. A bent XO_2 radical results. This should be the GS if X is a monovalent atom or group, like H, Li, CH_3 , NH_2 , etc. The GS is characterized by the term symbol $1^2\pi(3\pi)$ where the plane containing the three atoms serves to classify the symmetry of the singly occupied orbital (σ or π) and the total number of π electrons is given in parentheses (see Figure 4).

Excited states of XO_2 are derived from the $1^2\pi(3\pi)$ state by $p\sigma \rightarrow p\pi$ promotion or a $p\pi \rightarrow p\pi$ charge transfer. Thus, a covalent (cov) $1^2\sigma(4\pi)$ state with the single electron occupying the $p\sigma$ orbital and an ionic $2^2\pi(3\pi)$ state of XO_2 , both with bent geometries, are obtained. They are shown in Figure 4.

A cyclic XO_2 state becomes possible when X has a second unpaired electron available for bonding. If $X = O$, F^+ , S etc., there is in addition an electron lone pair and the configuration at atom X may be either $(p\sigma)^1(p\pi)^2$ or $(p\sigma)^2(p\pi)^1$. As indicated in Figure 5, the latter is more favourable since it avoids the destabilizing pair-pair Coulomb repulsion between π electrons at adjacent atomic centres of XO_2 . Accordingly, the 4π states of XO_2 should be more stable than its 5π states.

If the $p\pi$ orbitals at atom X and the terminal oxygen did not overlap, the biradical XO_2 would be more stable in the T state $^3\pi\pi(4\pi)$ according to Hund's rule. But $p\pi$ orbitals separated by more than 2 \AA still have a finite overlap. This brings the S (4π) state below the T state²⁶.

Excited 5π and 6π states are generated from the 4π states by $p\sigma \rightarrow p\pi$ promotion(s). The $1^1\sigma\sigma(6\pi)$ state, characterized by bad Coulomb repulsions, can stabilize itself by decreasing α and forming a three membered ring. Ionic states of XO_2 are obtained by $p\pi \rightarrow p\pi$ or $p\sigma \rightarrow p\pi$ charge transfer to one of the terminal atoms (Figure 5). They correspond to resonance descriptions of XO_2 in terms of Lewis structures.

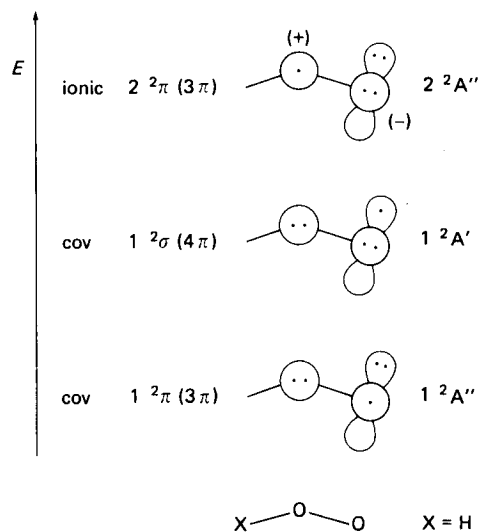


FIGURE 4. Schematic representation of low-lying states of XO_2 with monovalent X. Sigma bonds are denoted by solid lines, σ orbitals by lobes, π orbitals by circles and electrons by dots. Appropriate state symbols are given for HO_2 . The covalent (cov) or ionic nature of each state is indicated.

3. X_2O_2 geometries with chain, Y or bridged structures

In Figure 6, four different geometries of X_2O_2 are rationalized by adding another monovalent atom X to each of the three lowest states of XO_2 . Assuming that the energy content of XO_2 is carried over to X_2O_2 , the orthogonal bent-bent geometry should be more stable than both *trans* and *cis* forms, which in turn should be more stable than the pyramidal Y form.

Some of the other possible X_2O_2 geometries can only be derived from high-lying XO_2 states (Figure 6). Accordingly, their energies should be considerably higher than those of the bent-bent geometries. This can be verified by counting the number of electron-pair-electron-pair repulsions.

Bridged geometries of X_2O_2 cannot be rationalized in this way. However, one can predict that the planar bridged form is also destabilized because of pair-pair repulsions.

B. Qualitative Molecular Orbital Treatment

1. MO description of O_2

One of the early triumphs of MO theory was the explanation of the paramagnetism of molecular oxygen. In Figure 7, the MOs of O_2 are schematically shown²⁷. With respect to their shape and energy (Figure 7, left-hand side), they differ from those which one obtains by a simple pairwise combination of oxygen 2s and 2p AOs (Figure 7, right-hand side and middle). This is due to mixing of valence MOs with the same symmetry as indicated by the interaction lines of Figure 7.

1. General and theoretical aspects of the peroxide group

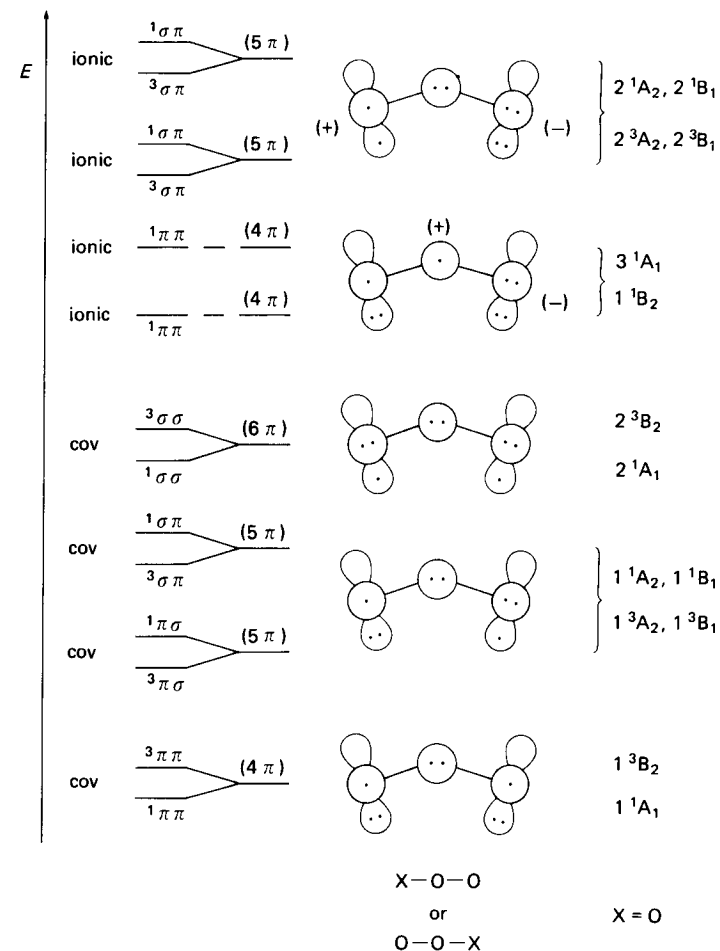


FIGURE 5. Schematic representation of low-lying states of XO_2 with divalent X. Note that the order of states depends on the nature of X. Appropriate state symbols are given for O_3 . See caption of Figure 4.

Assigning 18 electrons to the MOs of O_2 , the electron configuration

$$O_2: (1\sigma_g)^2(1\sigma_u)^2(2\sigma_g)^2(2\sigma_u)^2(3\sigma_g)^2(1\pi_u)^4(1\pi_g)^2 = [N_2](1\pi_g)^2$$

results. Ten electrons occupy bonding σ_g and π_u MOs, while six are in antibonding σ_u and π_g MOs. Hence, O_2 possesses two bonds, one formed by the $3\sigma_g$ and one by a $1\pi_u$ electron pair.

There are only two electrons occupying the $1\pi_g$ set, which can hold a total of four electrons. When spin is considered, there exist

$$\binom{4}{2} = \frac{4 \times 3}{2} = 6$$

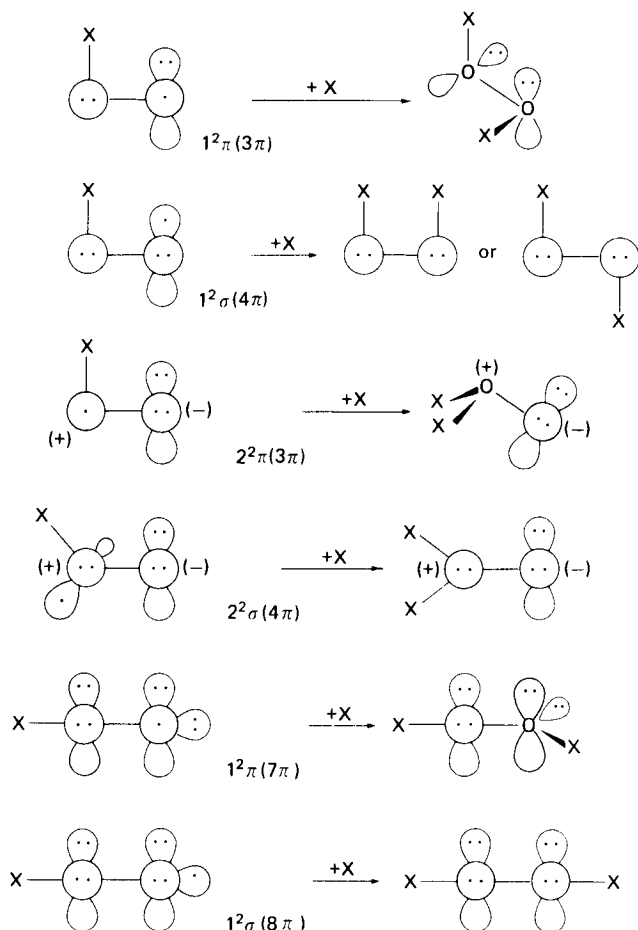


FIGURE 6. Formal 'syntheses' of X_2O_2 geometries. From top to bottom the energy of the XO_2 'precursor' increases. Compare with Figure 4.

possible assignments of the two electrons to the four $1\pi_g$ spin orbitals. They are given in Table 4. By writing for each assignment the corresponding Slater determinant, six state functions are obtained, which are depicted in Table 5 in terms of both real and complex spin orbitals²⁸.

The real state functions gain physical significance if O_2 is approached by a reacting molecule. For the free molecule, however, the distinction between the x and y directions is completely arbitrary. Then, the state functions have to be expressed in terms of complex spin orbitals $\pi_g^{m_l}$. The cylindrical symmetry of the latter complies with the requirements of the cylindrical point group $D_{\infty h}$ of the O_2 molecule.

The six state functions describe the three electronic states $^3\Sigma_g^-$, $^1\Delta_g$ and $^1\Sigma_g^+$ of O_2 (Tables 4 and 5). According to Hund's rule of maximum multiplicity and the orbital diagrams shown in Table 5 for the real state functions of O_2 , these states should

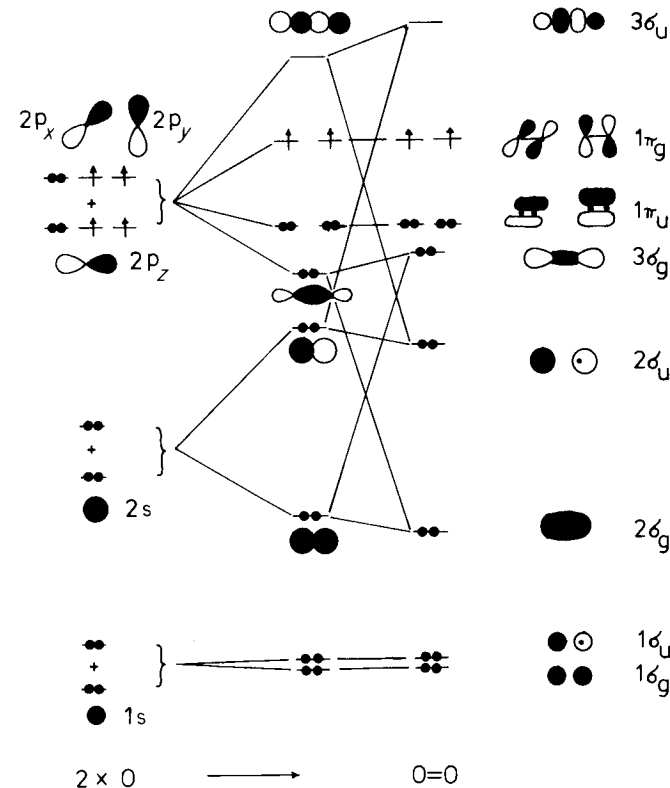


FIGURE 7. Qualitative MO correlation diagram for O_2 . The shape of the MOs before (middle) and after (left-hand side) mixing is indicated. Solid lines between different MO levels denote orbital mixing.

TABLE 4. Assignments of the π_g electrons of $O_2^{a,b}$

Assignment	$\pi_g^1\alpha$	$\pi_g^1\beta$	$\pi_g^{-1}\alpha$	$\pi_g^{-1}\beta$	M_L	M_S	Term
1	1	1	0	0	2	0	$^1\Delta_g$
2	1	0	1	0	0	1	$^3\Sigma_g^-$
3 ^c	1	0	0	1	0	0	$^3\Sigma_g^-$, $^1\Sigma_g^+$
4 ^c	0	1	1	0	0	0	$^3\Sigma_g^-$, $^1\Sigma_g^+$
5	0	1	0	1	0	-1	$^3\Sigma_g^-$
6	0	0	1	1	-2	0	$^1\Delta_g$

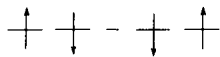
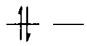
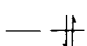

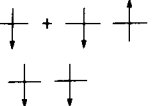
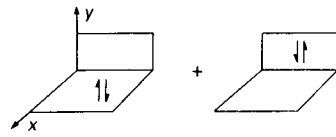
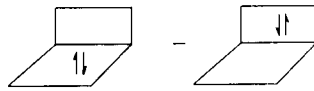
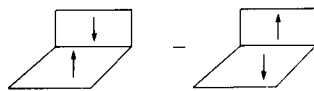
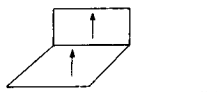
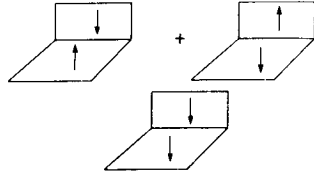
^a M_L and M_S are the eigenvalues of the total orbital and spin angular momentum operator \hat{L}_z and \hat{S}_z .

^b Assignments are given for complex spin orbitals $\pi_g^1 = \frac{1}{\sqrt{2}}(\pi_g^x + i\pi_g^y)$ and $\pi_g^{-1} = \frac{1}{\sqrt{2}}(\pi_g^x - i\pi_g^y)$ where

the superscript ± 1 corresponds to the eigenvalue m_l of the operator \hat{L}_z . The complex spin orbitals $\pi_g^{m_l}$ are more easily obtained when starting from complex atomic orbitals $2p_{m_l} = f(r, \theta) \cdot e^{im_l\phi}$ expressed in terms of spherical polar coordinates r, θ, ϕ . For a more detailed description, see, for example, Ref. 28.

^c Assignments are degenerate. To obtain the correct state functions, in-phase and out-of-phase combinations of the corresponding Slater determinants have to be taken.

TABLE 5. Complex and real state functions of O₂^a

State	Complex state functions	Description
¹ Σ _g ⁺	$\frac{1}{\sqrt{2}} [\pi_g^+(1)\pi_g^-(2) + \pi_g^-(1)\pi_g^+(2)]$ $\times \frac{1}{\sqrt{2}} [\alpha(1)\beta(2) - \beta(1)\alpha(2)]$	
¹ Δ _g	$\left. \begin{aligned} &[\pi_g^+(1)\pi_g^+(2)] \\ &[\pi_g^-(1)\pi_g^-(2)] \end{aligned} \right\} \times \frac{1}{\sqrt{2}} [\alpha(1)\beta(2) - \beta(1)\alpha(2)]$	
		
³ Σ _g ⁻	$\frac{1}{\sqrt{2}} [\pi_g^+(1)\pi_g^-(2) - \pi_g^-(1)\pi_g^+(2)]$ $\times \begin{cases} \alpha(1)\alpha(2) \\ \frac{1}{\sqrt{2}} [\alpha(1)\beta(2) + \beta(1)\alpha(2)] \\ \beta(1)\beta(2) \end{cases}$	
		
State	Real state functions	Description
¹ Σ _g ⁺	$\frac{1}{\sqrt{2}} [\pi_g^x(1)\pi_g^x(2) + \pi_g^y(1)\pi_g^y(2)]$ $\times \frac{1}{\sqrt{2}} [\alpha(1)\beta(2) - \beta(1)\alpha(2)]$	
¹ Δ _g	$\left. \begin{aligned} &\frac{1}{\sqrt{2}} [\pi_g^x(1)\pi_g^x(2) - \pi_g^y(1)\pi_g^y(2)] \\ &\frac{1}{\sqrt{2}} [\pi_g^y(1)\pi_g^y(2) + \pi_g^x(1)\pi_g^x(2)] \end{aligned} \right\} \times \frac{1}{\sqrt{2}} [\alpha(1)\beta(2) - \beta(1)\alpha(2)]$	
		
³ Σ _g ⁻	$\frac{1}{\sqrt{2}} [\pi_g^x(1)\pi_g^y(2) - \pi_g^y(1)\pi_g^x(2)]$ $\times \begin{cases} \alpha(1)\alpha(2) \\ \frac{1}{\sqrt{2}} [\alpha(1)\beta(2) + \beta(1)\alpha(2)] \\ \beta(1)\beta(2) \end{cases}$	
		

^aComplex state functions have been obtained by expanding the Slater determinants derived from Table 4. Their form is schematically represented by orbital diagrams. The two linear combinations correspond to degenerate electron assignments (Table 4, footnote c). The real state functions have been obtained using the relation between complex and real MOs (Table 4, footnote b). In case of the two ¹Δ_g functions linear combinations of the resulting functions have to be taken in order to cancel imaginary terms.

correspond to the GS and the first and second excited state of O₂, i.e.

$$E(^3\Sigma_g^-) < E(^1\Delta_g) < E(^1\Sigma_g^+),$$

which is experimentally confirmed (Section IV.A).

2. The hydrogenperoxyl radical

The MOs of the HO₂ radical are closely related to those of molecular oxygen, as can be judged from a comparison of Figures 7 and 8. Figure 8 contains contour-line representations of the actual MOs of HO₂, calculated with HF theory for the linear (13), bent (14) and bridged (15) geometries. For each MO the appropriate symmetry notation is given. They should be used to understand Figure 9 where a qualitative MO correlation diagram for O₂ and HO₂, the latter with varying bond angle α, is given.

Figure 9 can be analysed in terms of increasing or decreasing bonding overlap²⁹. Since the 2π-7a' MO is stabilized for 90° < α < 180°, bent geometries of HO₂ should be the most stable ones, irrespective of the occupation of the 2π-2a'' MO. This means that the HO₂ cation, radical and anion should all prefer geometry 14 rather than 15 or 13.

3. XO₂: ozone

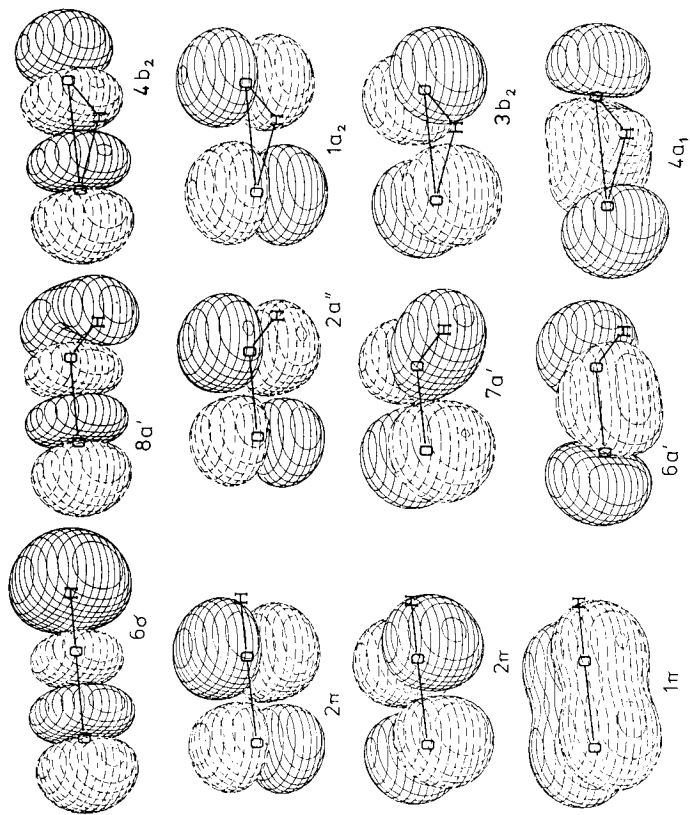
If X disposes of suitable 2pπ AOs three degenerate pairs of π MOs determine the electronic features of the linear XO₂ form. They possess OO bonding, nonbonding and antibonding character (Figure 10). In case of bending of the molecule, degeneracy is removed and the MO levels split (Figure 11). Both the in-plane (σ) and out-of-plane (π) nonbonding MOs are destabilized, while the two other σ,π pairs, bonding and antibonding, become more stable. This is due to developing 1,3 bonding or antibonding interactions in the bent form as can be seen from inspection of the corresponding MOs of ozone depicted in Figure 10.

Depending on the occupancy of these MOs XO₂ prefers the bent rather than the linear structure. This is demonstrated in Table 6 where predictions with regard to the most probable GS geometry of XO₂ systems with 14–20 valence electrons are given. These are based on Figures 10 and 11 and suggest that XO₂ peroxides with 14–16 valence electrons are linear, while those with 17–20 valence electrons adopt bent geometries with 100 < α < 130°^{30–32}.

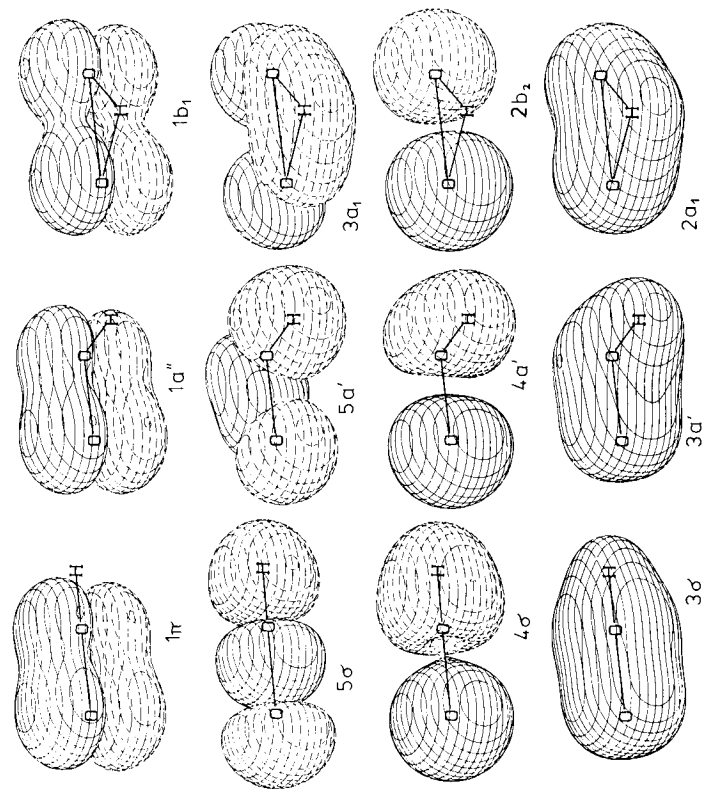
As indicated in Figure 11 conversion of bent to cyclic ozone is symmetry forbidden and, therefore, should be characterized by a relatively high energy barrier. The orbital diagram of Figure 11 suggests that the cyclic state of O₃ should be more stable than the bent one. A quantitative analysis of O₃, however, reveals that configuration interaction (CI), especially between the GS electron configuration and the ... (1a₂)⁰(4b₂)²(6a₁)²(2b₁)² configuration leads to stabilization of the bent form below the cyclic structure. So far only one XO₂ system has been observed experimentally in a cyclic form, namely dioxirane (X = CH₂)³³.

4. Hydrogen peroxide

Linear H₂O₂ (16) possesses degenerate π_u and π_g MOs, similar to those of O₂, but fully occupied. The ¹Σ_g⁺ state is the GS of 16. In the Y (17) and the bridged form (18), the in-plane components of the π MOs gain OH bonding character (Figure 12), thus leading to a lowering of the corresponding orbital energies (Figure 13) and an overall stabilization of these forms. According to the qualitative MO diagram of Figure 13, one can expect 17 to



(13)



(14)

(15)

FIGURE 8. Three-dimensional plots of valence MOs of **13**, **14** and **15**. An amplitude of ± 0.05 a.u. is used for the contour level. The group theoretical symmetry notation is given below each MO.

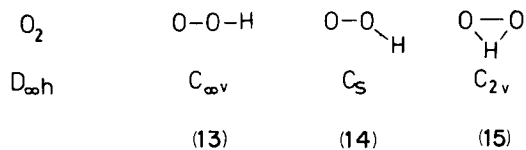
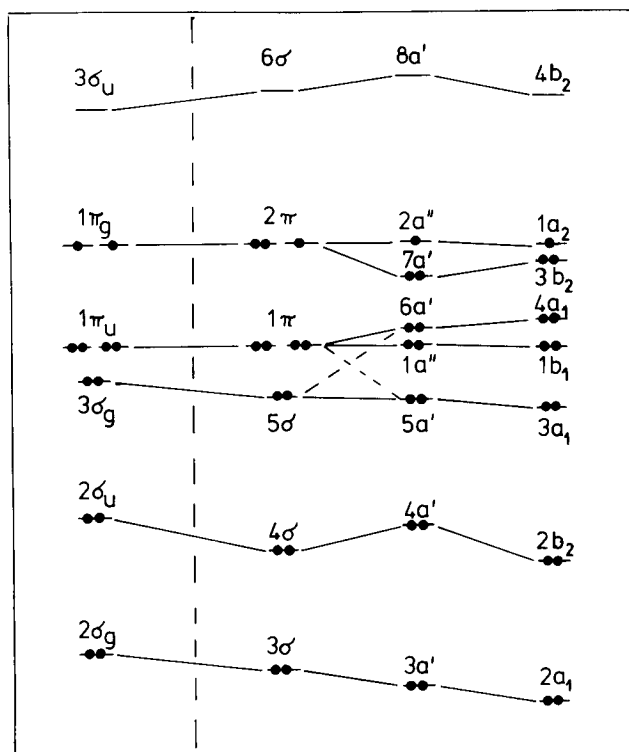


FIGURE 9. Qualitative MO correlation diagram for O_2 and linear (13), bent (14) and bridged (15) HO_2 based on UHF calculations and experimental ionization potentials. A crossing of the $5a'$ and $6a'$ MO, indicated by dashed lines, is symmetry forbidden (noncrossing rule). Compare with Figure 8.

be more stable than 18. In both cases the nonplanar forms, i.e. the pyramidal Y form (19) and the puckered bridged form (20), are characterized by additional OH bonding as one (20) or both (19)²⁹ π MOs can mix with the $1s(H)$ orbitals. Hence, Figures 12 and 13 suggest the following ordering of total energies:

$$E(16) > E(18) > E(20) > E(17) > E(19).$$

Undoubtedly the argument of increased stabilization due to developing OH bonding in the highest occupied MOs applies even more strongly to the bent-bent forms with $\tau = 0^\circ$ (21), 120° (22) or 180° (23). This is documented by the shape of the $3b_1-4b-1b_g$ and $1a_2-5a-4a_g$ MOs depicted in Figure 14. (A quantitative MO correlation diagram for the

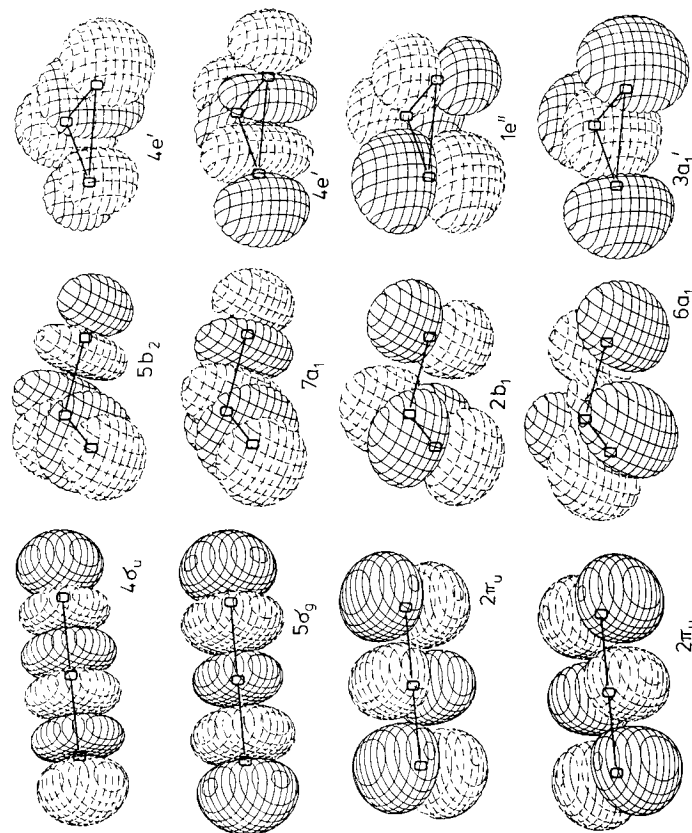


FIGURE 10. Continued overleaf.

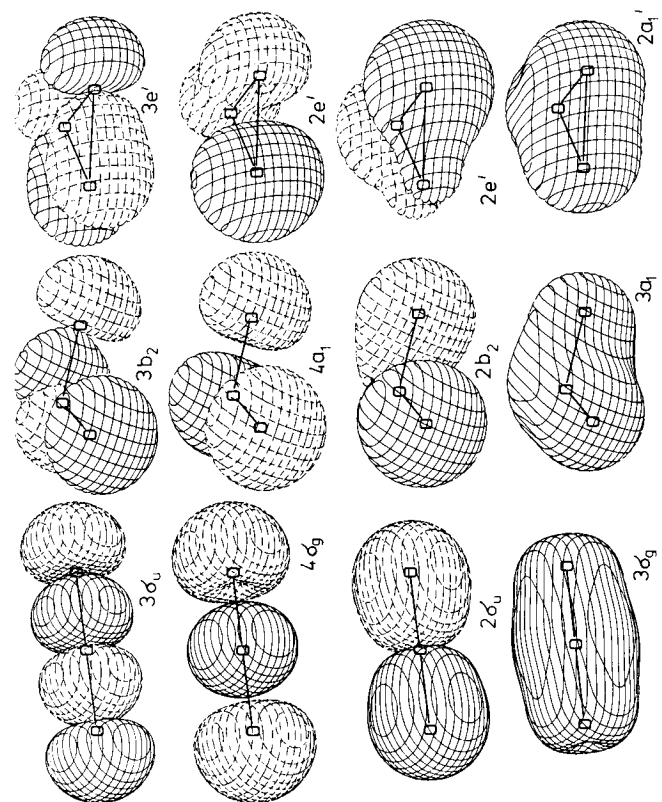
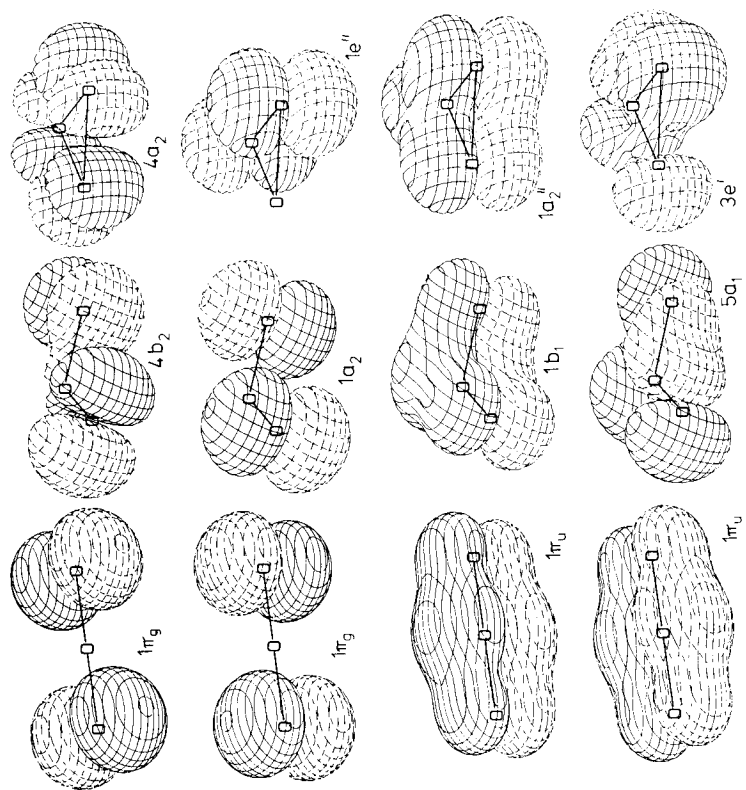


FIGURE 10. Three-dimensional plots of valence MOs of linear, bent and cyclic O_3 . See caption of Figure 8.

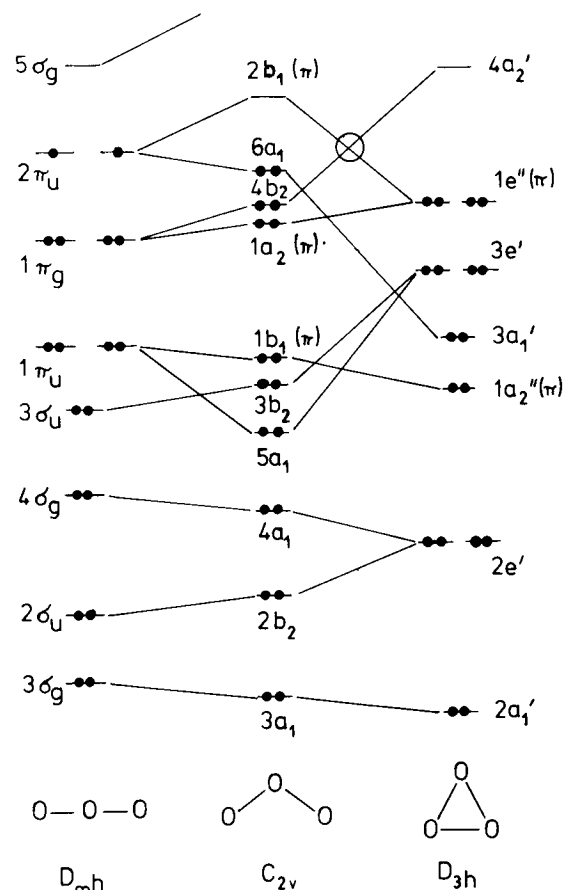


FIGURE 11. Qualitative MO correlation diagram for linear, bent and cyclic O_3 based on UHF and RHF calculations and experimental ionization potentials. The symmetry-forbidden crossing of the $2b_1$ - $1e''$ and $4b_2$ - $4a_2'$ MOs is indicated. Note that the $2b_1$ MO—if occupied—possesses a considerably lower energy. Compare with Figure 10.

bent-bent geometries is shown in Section IV.B, Figure 19).

According to an argument given by Gimarc³⁴, the higher stability of skewed H_2O_2 can be explained in the following way: The change of the orbital energy of the $4b$ and $5a$ MO for τ increasing from 0° to 180° is approximately parallel to the change in the $1s(H)$ - $2p(O)$ orbital overlap, which in turn depends on $\cos \tau$. For simplicity the $2p_x$ and $2p_y$ AOs are kept fixed and interconversion from **21** to **23** is considered to comprise clockwise and counterclockwise rotation of the OH groups by $\tau' = 90^\circ$. At $\tau' = 45^\circ$ ($\tau = 90^\circ$) the $4b$ and $5a$ MO cross, both possessing then some OH bonding character (Figure 14). Overlap in the orthogonal form is larger than for **21** and **23** by a factor of $2 \cos 45^\circ = 1.7$. Hence skewed H_2O_2 with τ close to 90° should be the most stable bent-bent form. Actually, the lowest energy is found for **22**, since τ depends on a delicate balance among various electronic factors (see Section IV.B).

TABLE 6. Ground-state geometry of XO_2 peroxides

Valence electrons	Molecule	Electron configuration ^a	State ^a	Geometry	α (deg.) ^b
14	BeOO	$\dots(1\pi_u)^4(1\pi_g)^2$	${}^3\Sigma_g^-$	Linear	180°
15	BOO	$\dots(1\pi_u)^4(1\pi_g)^3$	$2\Pi_g$	Linear	
16	BOO ⁻	$\dots(1\pi_u)^4(1\pi_g)^4$	${}^1\Sigma_g^+$	Linear	
	HBOO			Linear	180°
	NOO ⁺			Linear	
17	NOO	$\dots(1a_2)^2(4b_2)^2(6a_1)^1$	2A_1	Bent	122
	OOO ⁺			Bent	132
18	H ₂ COO	$\dots(1a_2)^2(4b_2)^2(6a_1)^2$	1A_1	Bent	120°
	HNOO			Bent	119
	NOO ⁻			Bent	118
	OOO			Bent	118
	FOO ⁺			Bent	113
19	OOO ⁻	$\dots(1a_2)^2(4b_2)^2(6a_1)^2$	2B_1	Bent	116
	FOO	$(2b_1)^1$		Bent	109
20	FOO ⁻	$\dots(1a_2)^2(4b_2)^2(6a_1)^2(2b_1)^2$	1A_1	Bent	

^aElectron configuration and appropriate state symbol are given for the isoelectronic ozone ion (O_3^{4+} , $\dots O_3^{2-}$). Compare with Figures 10 and 11.

^bSources of α values are given in Section V.A.1.

^cCyclic form is more stable; see Table 36, Section V.A.1.

5. X_2O_2 : F_2O_2

X_2O_2 compounds with 26 valence electrons are best known in peroxide chemistry. They prefer bent-bent geometries³⁵ as is revealed by Figures 15 and 16, which depict the valence MOs and the corresponding orbital correlation diagram of F_2O_2 . Overlap arguments similar to those used in the H_2O_2 case suggest the existence of a stable skewed form.

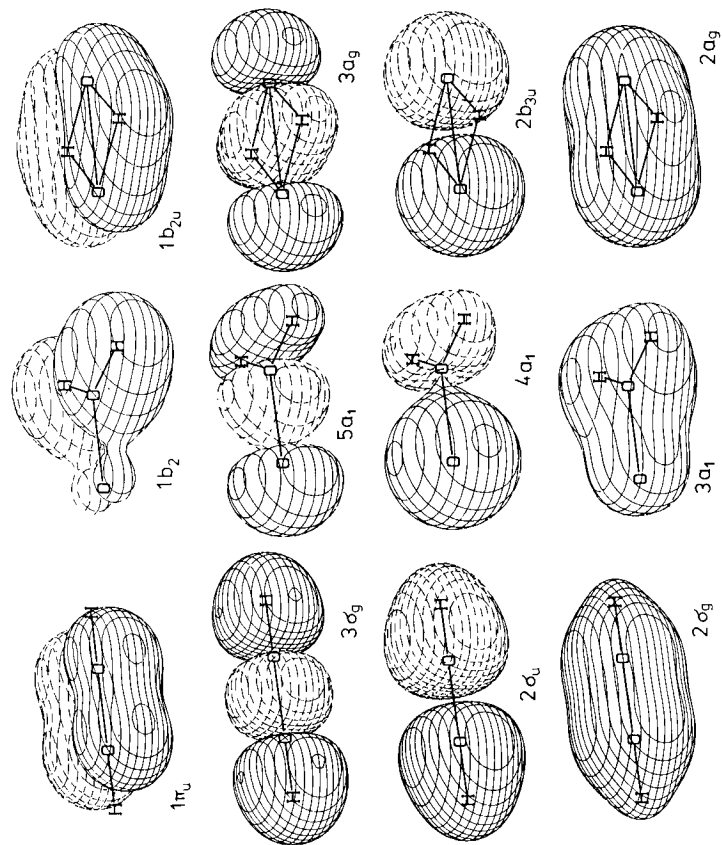
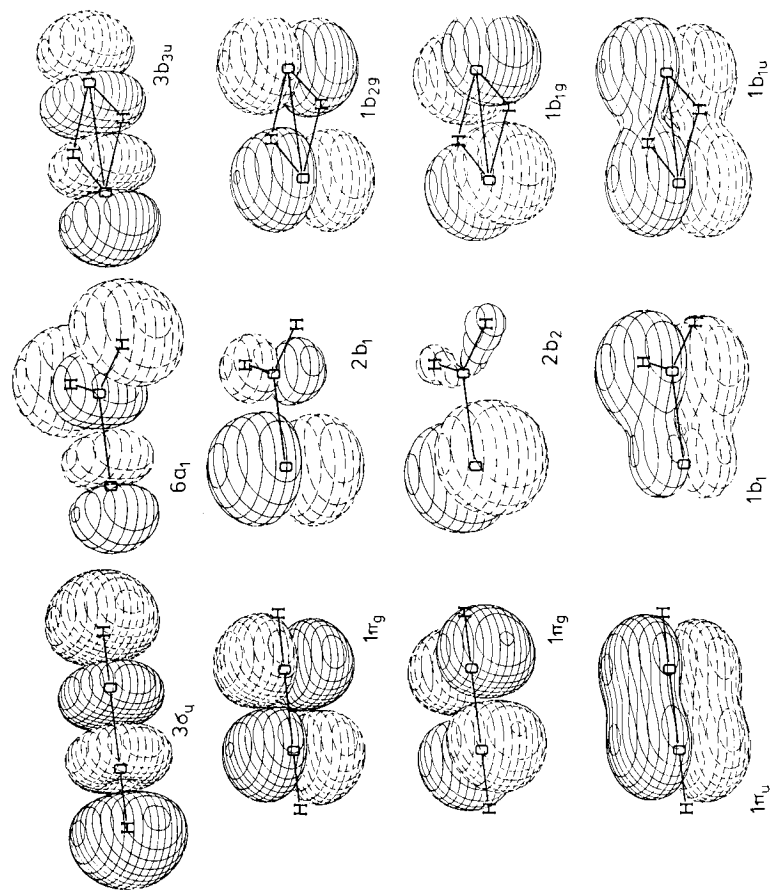
Knowledge of X_2O_2 compounds with 16–24 valence electrons is scarce. Some of these peroxides can be formed as diradical intermediates by a homolytic X–X cleavage reaction of cyclic peroxides $\bar{X}-O-O-\bar{X}$. As can be inferred from studies on dioxetanes¹⁵, decomposition to X=O fragments (X = Be, BH, CH₂, NH, O) should be rapid in all cases.

According to theory, stable X_2O_2 systems with 18 (X = BeH) or 22 (X = BH₂) valence electrons should exist³². Their orbital diagrams differ considerably from that of F_2O_2 . Predictions with regard to their geometry are difficult to make without a complete MO analysis (see Section V.A.2).

IV. PROPERTIES OF XO_2 AND X_2O_2 PROTOTYPES

A. Stationary Points on the Potential Hypersurface

Few molecules have been studied as extensively, both theoretically and experimentally, as the O_2 molecule. The vast literature on O_2 through early 1971 has been reviewed by Krupenie³⁶. Since then several very accurate calculations of GS and excited states of O_2 and its ions have been carried out^{37–44}. They confirm the qualitative ordering of the three



(16)

(17)

(18)

FIGURE 12. Three-dimensional plots of valence MOs of 16, 17 and 18. See caption of Figure 8.

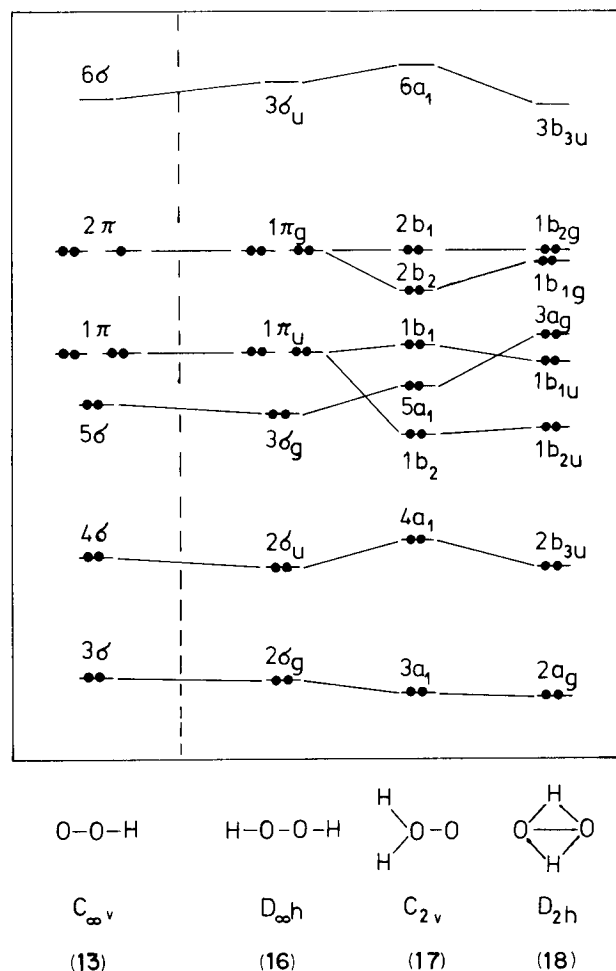


FIGURE 13. Qualitative MO correlation diagram for linear HO_2 , linear (16), Y (17) and bridged (18) H_2O_2 based on UHF and RHF calculations. Compare with Figures 8 and 12.

lowest states with the $^3\Sigma_g^-$ GS being more stable by 22.5 and 37.5 kcal mol $^{-1}$ than the $^1\Delta_g$ and $^1\Sigma_g^+$ states³⁶.

Also available are detailed theoretical data on special features of the O_3 hypersurface⁴⁵⁻⁶¹, some of which are summarized in Table 7. They show that calculations which go beyond the HF level of theory predict the bent 4π state to be more stable by 5-40 kcal mol $^{-1}$ than the cyclic state of O_3 with 6π electrons. More recent calculations seem to suggest a value of about 23-28 kcal mol $^{-1}$ ^{51,60}. Bent ozone is separated from its cyclic form by a barrier of about 30-40 kcal mol $^{-1}$ ^{52,57,62}.

Wright has suggested that cyclic O_3 with C_{2v} symmetry may be an intermediate on the decomposition path leading to $\text{O}_2(^3\Sigma_g^-)$ and $\text{O}(^3\text{P})$ ⁴⁶. His assumption is based on the

discovery of an ozone precursor in radiolysis experiments. An experimental estimate of the activation energy of O_3 decomposition (24 kcal mol $^{-1}$), reported by Benson and Axworthy⁶³, excludes this possibility by describing O_3 decomposition as an endothermic process with no activation barrier. A recent theoretical evaluation of the decomposition surface of the bent form is in line with this estimate⁶⁰. (For a different view see Reference 56.)

Widening of the angle α is accompanied by an increase of the energy. Linear O_3 is less stable than the bent form by 77⁴⁹ to 89 kcal mol $^{-1}$ ⁵⁹. It adopts a triplet GS, $^3\Sigma_g^-$ (see Figure 11), which correlates with the first $^3\text{B}_1$ state of bent ozone (Figure 5). The $^1\text{A}_1$ GS of ozone, however, correlates with a degenerate $^1\Delta_g$ state of the linear configuration lying about 13 kcal mol $^{-1}$ above the $^3\Sigma_g^-$ state⁴⁹.

In the past, the GS of ozone has been mostly described by a zwitterionic structure in order to explain the observed reactivity of O_3 . Recent calculations carried out with different methods unanimously find a relative high biradical character for this and related XO_2 species in the gas phase^{26,64-68} (Table 8). Harding and Goddard have shown that biradical character is consistent with the electrophilic nature observed for ozone and that there is no need to postulate zwitterionic structures⁶⁹. The latter can become important in solution-phase reactions of XO_2 systems, especially when X bears a π -donating substituent $\text{R}(\text{X} = \text{NR}, \text{CR}_2)$ ^{58,69}.

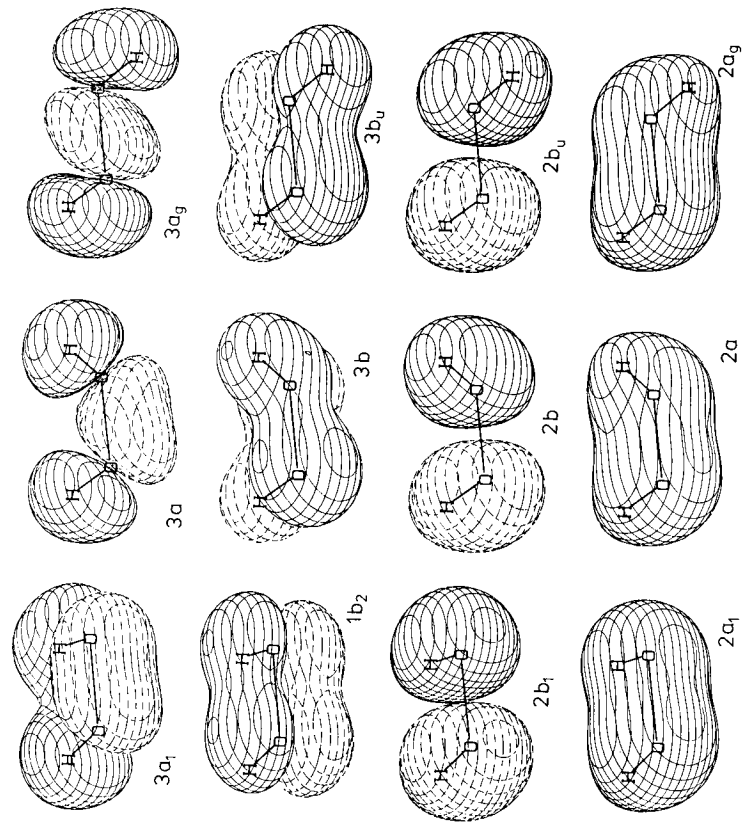
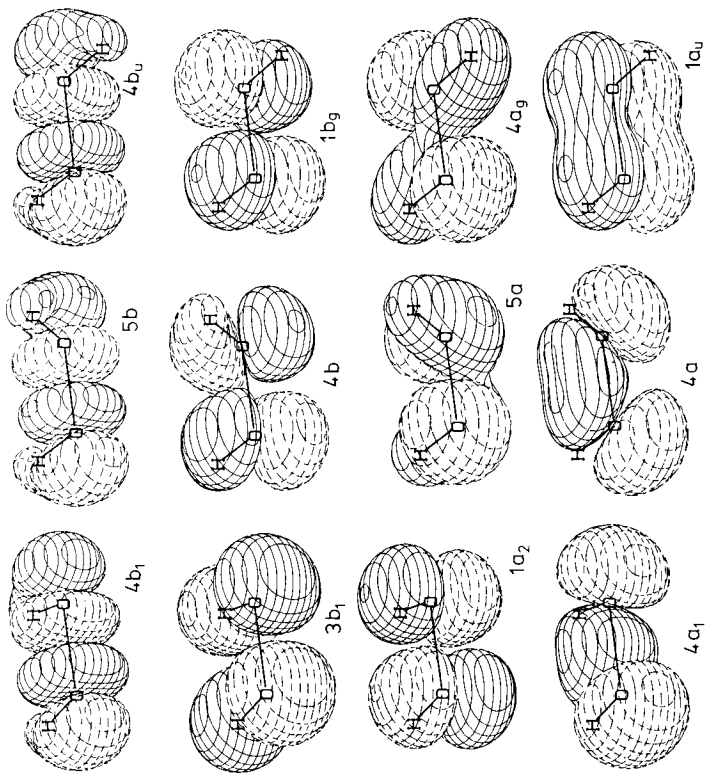
Several theoretical investigations on the HO_2 radical in its most stable GS configuration have been published recently⁷¹⁻⁸¹. They describe HO_2 as possessing C_s symmetry with an equilibrium angle α close to 104° which is in accordance with qualitative MO arguments (Section III.B.2, Figure 9) and experiment⁸². Specific results are compared in Table 9.

In recent studies by Melius and Blint⁷⁸ and Langhoff and Jaffe⁷⁹ large portions of the HO_2 potential energy surface have been computed employing CI methods and augmented basis sets. Contour plots of various sections of the theoretical surface⁷⁸ are presented in Figure 17. They indicate that either widening or closing of the angle α causes an increase of the total energy with the linear form being more destabilized than the bridged one. The lowest linear HO_2 state, $^2\Pi$, correlates with the $^1\text{A}''$ GS and the $^1\text{A}'$ excited state. The barrier to linearity is computed to be 60-70 kcal mol $^{-1}$ ^{79,83}. It is interesting to note that CI calculations describe the linear state to be ionic because of a transfer of the H electron to the π_g MO of O_2 ⁷⁹.

Unfortunately, only a C_s geometry ($R' = 0.968$ and 1.198 \AA at $\alpha = 60^\circ$) of bridged HO_2 has been computed⁷⁹. It lies about 40 kcal mol $^{-1}$ above the GS of bent HO_2 . Geometry optimization should lead to a value of about 35 kcal mol $^{-1}$. An early estimate of the energy of the bridged form⁸⁴ suggesting a minimum is unreliable because it is based on *ab initio* calculations of HO_2^+ and HO_2^- rather than a direct calculation of HO_2 .

The theoretical analysis of the HO_2 surface suggests a small barrier (≤ 2 kcal mol $^{-1}$) at $\alpha = 120^\circ$, $R' = 1.99$ and $R = 1.23 \text{ \AA}$ (Figure 17) for the reaction $\text{H} + \text{O}_2 \rightarrow \text{HO}_2$ due to partial breaking of the π bond of O_2 . HO_2 is more stable by 44 kcal mol $^{-1}$ than the reactants, which has to be compared with an experimental value of 46 kcal mol $^{-1}$ ⁸⁵. Breaking of the O-O bond of HO_2 requires 56 kcal mol $^{-1}$ (63 kcal mol $^{-1}$, obs.⁸⁶). The corresponding reaction channel proceeds uphill directly towards the products HO and O, i.e. there is no activation barrier for the reverse process leading to HO_2 .

Although H_2O_2 has been the subject of numerous quantum-chemical calculations, only the conformational subspace of its bent-bent form (see Section IV.B) has been explored so far. Therefore, we have carried out *ab initio* calculations on forms 16-20 at various levels of theory⁸⁷. Some of our results are listed in Table 10. They confirm the order of stabilities given in Section III.B.4. Thus, inversion at one of the O atoms of 23 is an unlikely process ($\Delta E = 71$ kcal mol $^{-1}$, Table 10). Equally unstable are the bridged forms 18 and 20. The Y form, however, may occur under certain conditions. Depending on the level of theory



(21)

(22)

(23)

FIGURE 14. Three-dimensional plots of valence MOs of 21, 22 and 23. See caption of Figure 8.

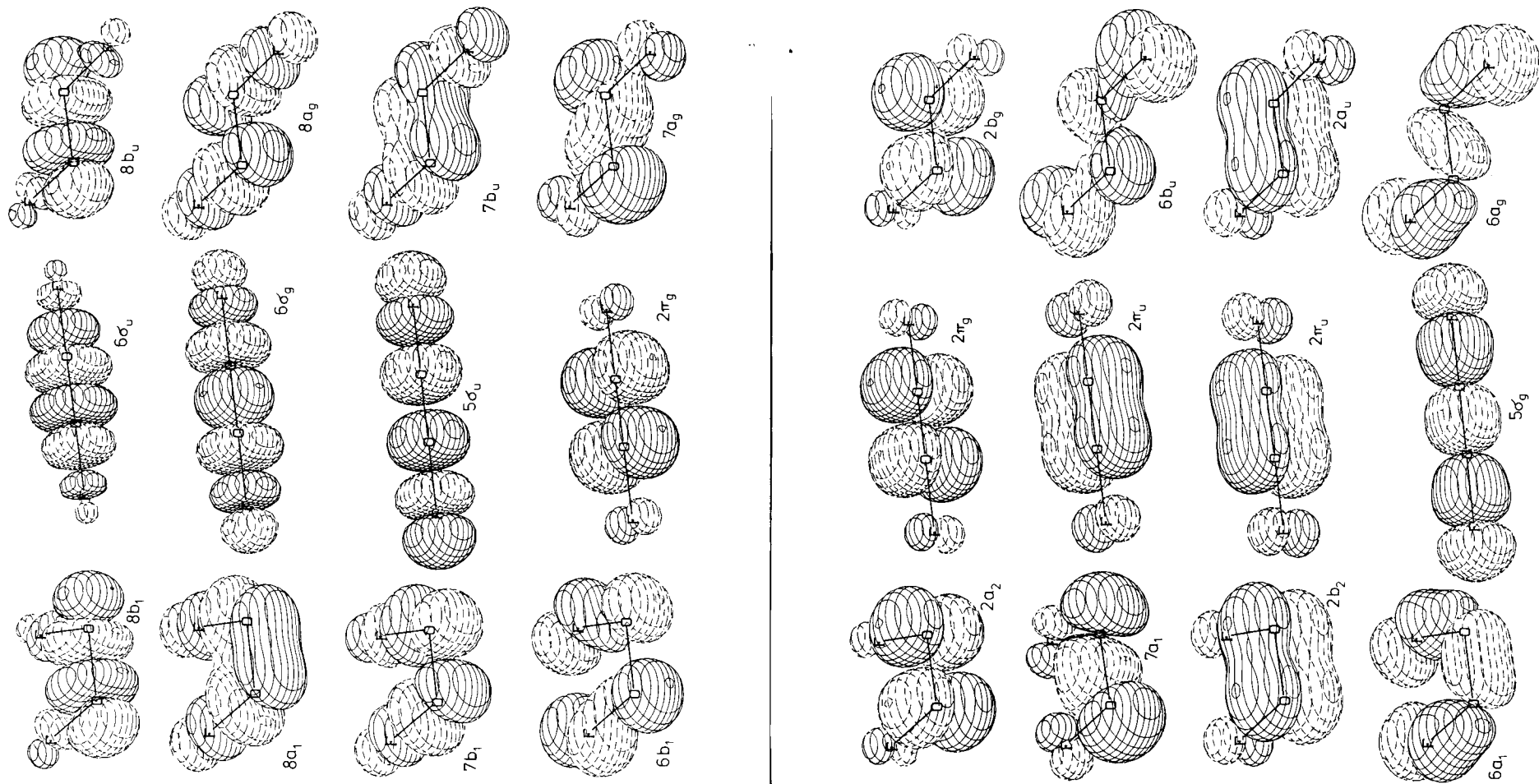


FIGURE 15. Continued overview.

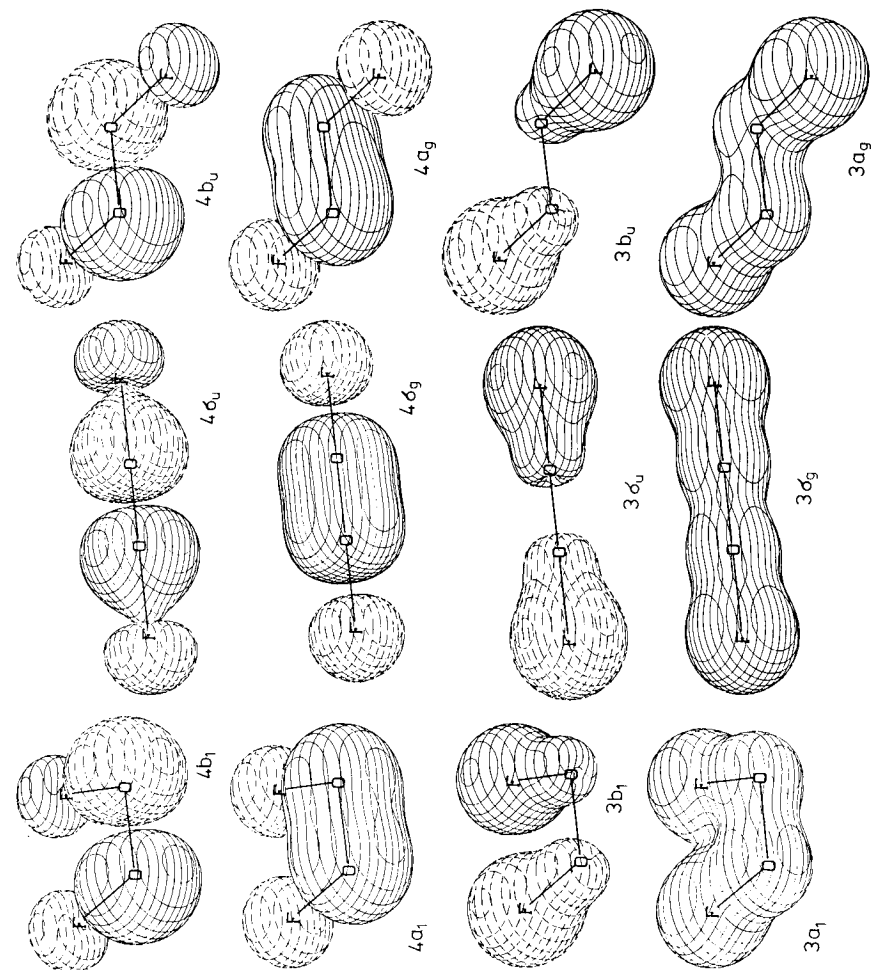
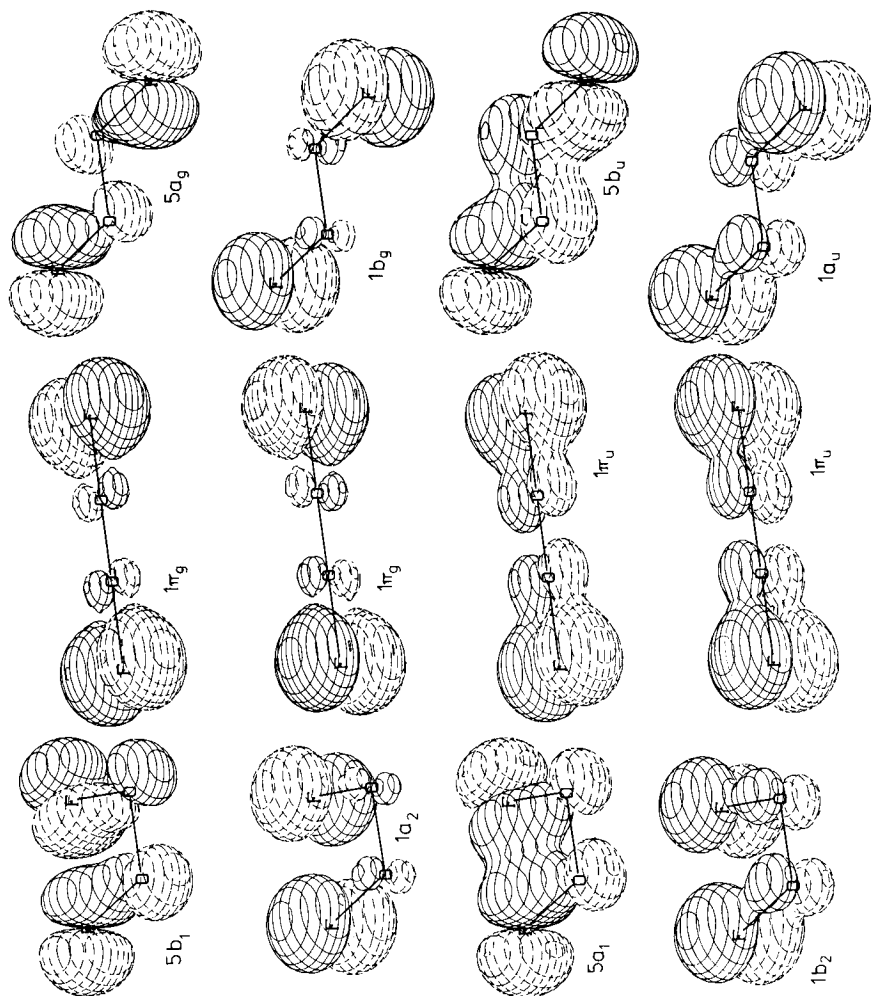


FIGURE 15. Three-dimensional plots of valence MOs of *cis*, linear and *trans* F_2O_2 . See caption of Figure 8.

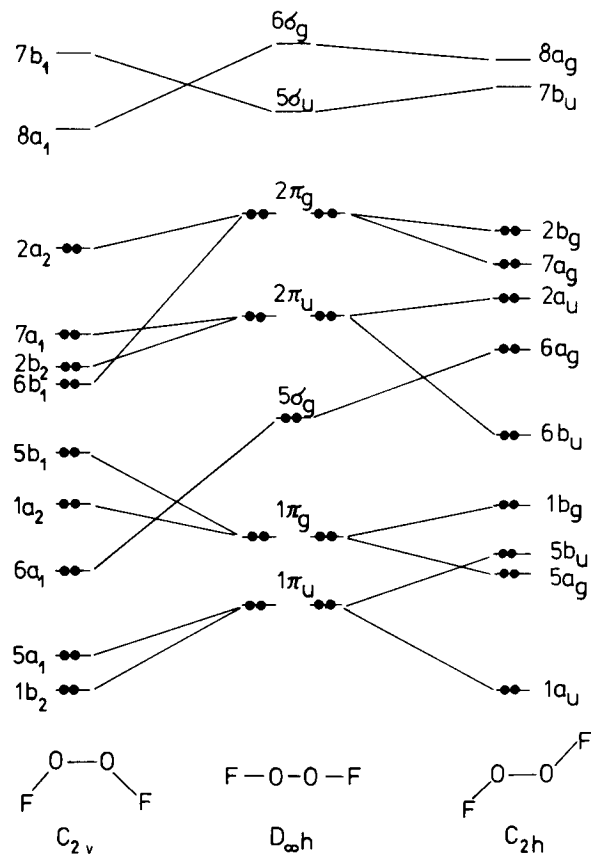


FIGURE 16. Qualitative MO correlations for *cis*, linear and *trans* F_2O_2 based on RHF calculations. Compare with Figure 15.

TABLE 7. Energies and geometries of bent (C_{2v}) and cyclic ozone^a

Method	Absolute energy (bent)	Relative energy (cyclic)	Geometry				Ref.
			Bent		Cyclic		
			R	α	R	α	
HF/DZb	-224.2386	-7.0	1.244	118	1.397	(60)	52
INO CI/DZb	-224.4226	16.1	1.322	115	1.482	62	52
CEPA/DZb	-224.7710	4.6 ^b	1.264	117.3	1.435	(60)	56
GVB-CI/DZd	-224.78578 ^c	28.1	1.299	116	1.449	(60)	50
HF-CI/DZd	-224.80065	21.0	(1.278)	(116.8)	(1.44)	(60)	55
RSMP/DZd	-225.05309	38.6	1.289	116.8	1.450	(60)	58
Exp. ^d	-225.557	23-28	1.272	117.8	1.45	(60)	70

^aAbsolute energies in hartree, relative energies in kcal mol^{-1} , distances in Å, angles in deg.; values in parentheses are assumed.

^bIn a more recent study, Burton proposes a value of 12 kcal mol^{-1} ⁵⁶.

^cCalculated at experimental geometries.

^dExperimental r_e geometry of ozone (C_{2v}). Absolute energy from Table 14, Section IV.C. Estimates of relative energy from Refs. 60 and 51.

TABLE 8. Biradical character χ of some XO_2 compounds (%)

Molecule	RHF/CI (Ref. 64)	GVB ^b (Ref. 26)	UHF/CI ^b (Ref. 66)	VB ^c (Ref. 67)	MC SCF-CI (Ref. 68)
$\cdot OOO\cdot$	30 ^a	48	55	59	23 ^a
$\cdot NHOO\cdot$				55	
$\cdot CH_2OO\cdot$			42	43	
$\cdot OO\cdot$	100	100	100	100	100

^aCalculated from coefficients of $\bar{\Psi} = 1/\sqrt{2}[C_1\Phi(\dots(1a_2)^2(2b_1)^0) + C_2\Phi(\dots(1a_2)^0(2b_1)^2)]$;

$\chi = 100C_2^2/(1/\sqrt{2})^2 = 200C_2^2$.

^bCalculated from overlap S in the highest occupied orbital set: $\chi = [1 - 2S/(1 + S^2)] \times 100$; $S = 0.28$ (GVB) and 0.24 (UHF/CI) for O_3 .

^cCalculated by expanding $\bar{\Psi}_{HF}$ in terms of VB functions.

TABLE 9. Energies and geometries for the $^2A''$ state of the HO_2 radical^a

Method	Absolute energy	Geometry			Ref.
		R	R'	α	
UHF/MBS	-148.1967	1.357	1.004	104.1	74
UHF/DZ	-150.1579	1.384	0.968	106.8	71
UHF/DZ	-150.2360	1.315	0.948	105.7	79
CI/DZ	-150.2448	1.458	0.973	104.6	75
MC SCF-CI/DZdp ^b	-150.2998	1.365	0.995	104.2	78
GVB-CI/DZdp	-150.4271	1.369	0.991	103.3	81
Exp.		1.335	0.977	104.1	82

^aEnergies in hartree, distances in Å, angles in deg.

^bMCSCF energy given.

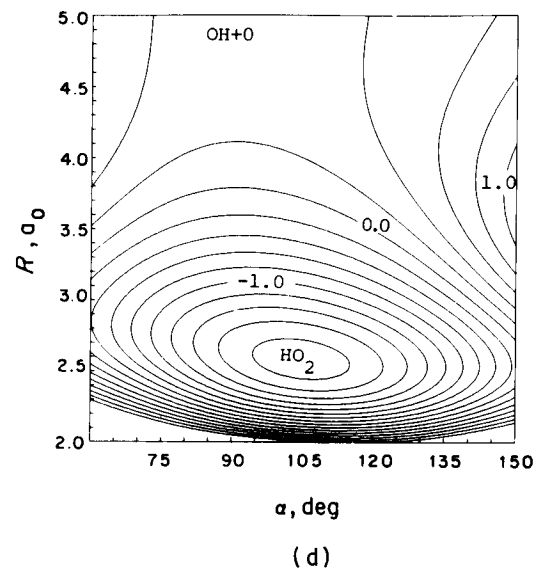
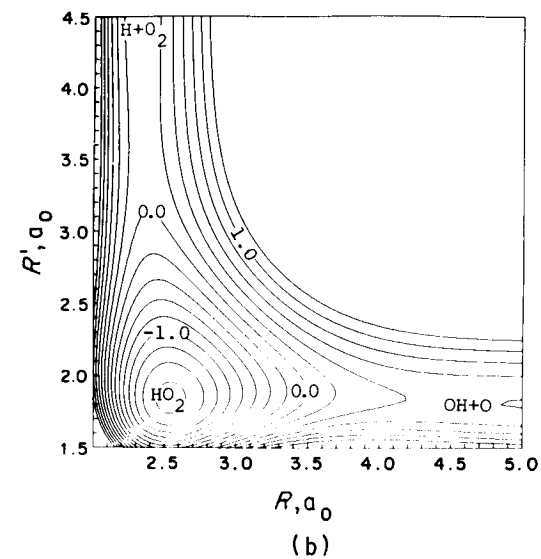
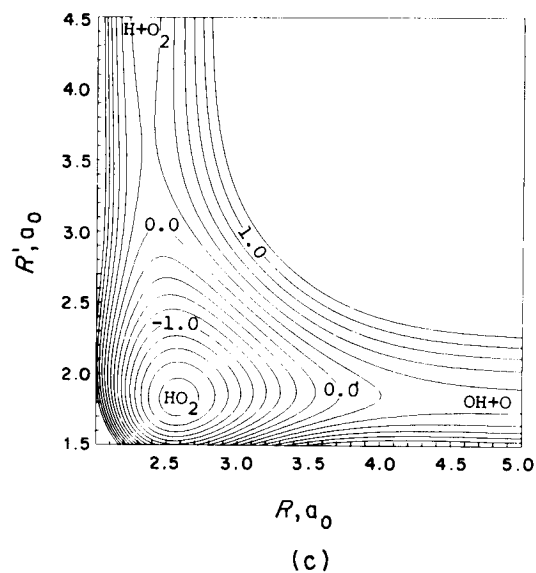
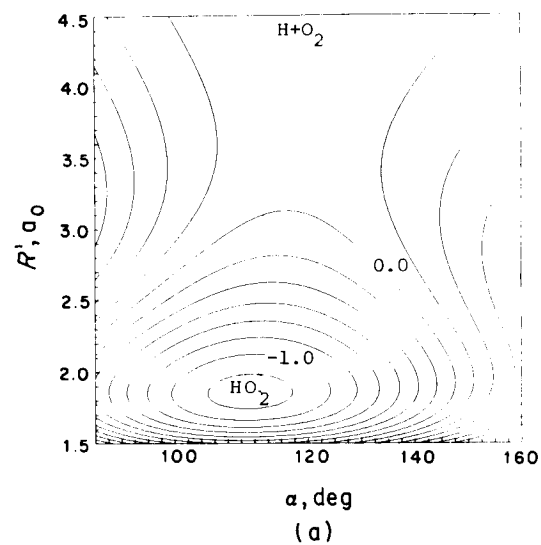


FIGURE 17. Equal potential energy contour plots of the HO_2 potential surface: (a) α versus R' ($R = 1.233 \text{ \AA}$), (b) R versus R' ($\alpha = 120^\circ$), (c) R versus R' ($\alpha = 104^\circ$) and (d) α versus R ($R' = 0.979 \text{ \AA}$). The contour spacings are 0.2 eV . The zero-energy contour is taken with respect to the $\text{H} + \text{O}_2$

reactants. Contour levels greater than 1.2 eV are not included. $a_0 = 0.52918 \text{ \AA}$. Reproduced by permission of North-Holland Publishing Company from C. F. Melius and R. J. Blint, *Chem. Phys. Letters*, **64**, 183 (1979).

TABLE 10. Theoretical energies and geometries of various H₂O₂ structures^a

Structure	Form	R	R'	α	Energy
Chain	Bent-bent (23)	1.476	0.967	97.2	-151.15613
	Linear (16)	1.333	0.941	180.0	155.4
	Linear-bent	1.406	0.945	180.0	70.7
Y	Planar (17)	1.487	0.959	119.8	63.2
	Pyramidal (19)	1.521	0.969	100.7	52.8
					108.7
Bridged	Planar (18)	1.720	1.167	42.5	71.4
	Puckered (20) ^b	1.662	1.179	45.2	68.3

^aRSMP/SVdp calculations, Ref. 87. Absolute energy of 23 in hartree, relative energies in kcal mol⁻¹, bond lengths in Å, angles in deg.

^bThe puckering angle δ is 57°. It corresponds to $\tau = 123^\circ$ ($\delta = 180 - \tau$). The puckering amplitude q is 0.40 Å.

employed, the relative energy of 17 ranges from 26–63 kcal mol⁻¹⁸⁷. Form 17 can gain about 10 kcal mol⁻¹ by pyramidalization. Since the dipole moment of the pyramidal geometry 19 is rather high (4.3 D, RHF/SVdp), solvation in polar solvents will lead to further stabilization of the Y form.

B. The Conformational Subspace of H₂O₂

One of the benchmark tests in quantum chemistry is the computation of the rotational potential of H₂O₂. The pros and cons of newly developed methods and techniques have been scrutinized by comparing computed and observed barrier data^{88–107}. In addition, attempts to explain the origin of the H₂O₂ barriers have revealed merits and limitations of interpretative models^{108–113}. Aspects relevant to this work have been discussed in several reviews on the quantum-chemical treatment of internal rotation in molecules^{114–117}.

Despite the fact that H₂O₂ is the simplest molecule to show internal rotation, it was not until the early seventies that a reasonable account of the rotational barriers could be provided by *ab initio* calculations of the RHF type.

In Figure 18 15 selected H₂O₂ barriers and the corresponding RHF molecular energies are plotted, where the latter may be considered as roughly reflecting the size of the basis set employed. It is obvious that only with elaborate basis sets are reliable barrier values obtained.

In contrast to the situation for ethane where RHF/MBS calculations performed for a rigid rotor model are satisfactory, *ab initio* calculations of H₂O₂ must fulfill at least two criteria: (1) The basis set employed has to be augmented by polarization functions. (2) All geometrical parameters have to be optimized for all values of τ to be considered.

Cremer has demonstrated that rescaling of the basis set functions during rotation leads to a further improvement of the barrier values¹⁰⁷. Inclusion of correlation effects into the theoretical approach does not lead to more accurate results¹⁰⁷. This is in line with purely theoretical considerations by Freed who has shown that correlation effects should contribute little to rotation or inversion barriers¹¹⁸.

In Table 11 experimental^{119–122} and *ab initio* barriers^{101,107} are compared. There exists no ambiguity with regard to the stability of the skew form at $\tau = 120^\circ$ and its *trans* barrier. A value of 1.1 kcal mol⁻¹ has been widely accepted. With regard to the *cis* barrier, reported barrier data, both experimental and theoretical, are less conclusive (Table 11). Ewig and

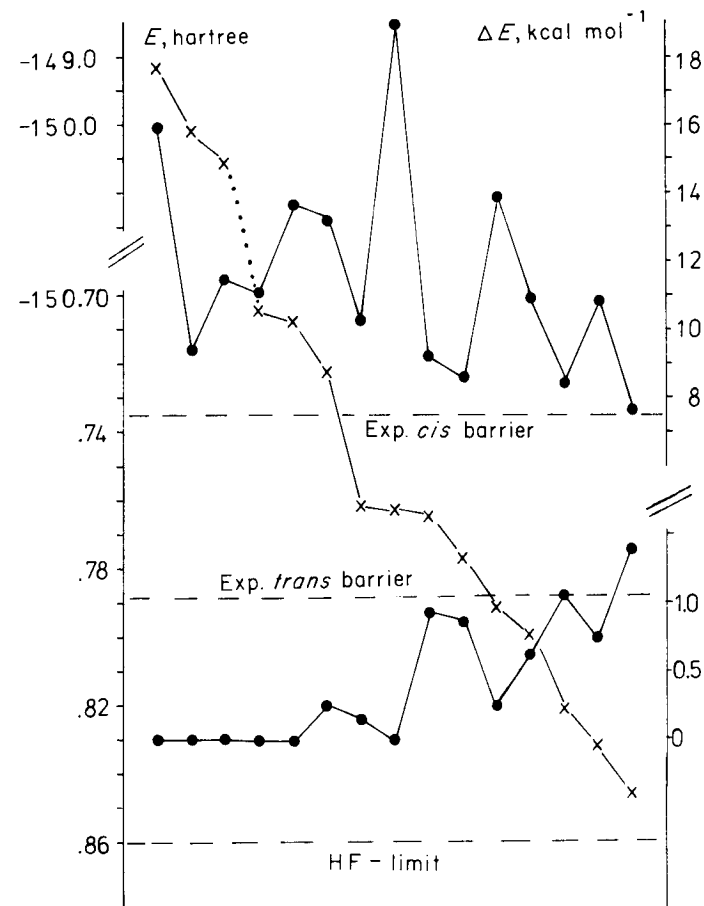


FIGURE 18. Total molecular energies E (crosses: \times) and barrier values ΔE (dots: \bullet) of H₂O₂ according to 15 selected RHF calculations taken from References 101 and 107.

Harris¹²² have demonstrated that small changes in the torsional frequencies of H₂O₂ increase the *cis* barrier height from 7.6 to 14.4 kcal mol⁻¹, while the *trans* barrier and the shape of the torsional potential between 140° and 220° remain unchanged. A value of 7.4 kcal mol⁻¹, predicted on the basis of large basis set calculations¹⁰⁷, seems to be the best estimate of the *cis* barrier available at present.

The preference of the skewed conformation has also been observed in gas-phase investigations of substituted peroxides^{123–127}. Depending on the size and the electronic features of the group X replacing H, the dihedral angle τ may vary from 90 to 170°. Smaller angles τ are observed for persulphides^{128–130}.

Various hypotheses have been put forward concerning the origin of the rotational barriers of ethane-like molecules. A critical review, published by Payne and Allen¹¹⁷, compares no less than 14 distinctly different models for explaining conformational behaviour.

TABLE 11. Comparison of experimental and *ab initio* barriers of H₂O₂

Authors	Year	Reference	ΔE (<i>trans</i>) (kcal mol ⁻¹)	ΔE (<i>cis</i>) (kcal mol ⁻¹)	τ (deg.)
Redington, Olson and Cross ^a	1962	119	0.85	3.71	109.5
Hunt and coworkers ^a	1965	120	1.10	7.03	111.5
Oelfke and Gordy ^b	1969	121	1.1	7.0	120
Ewig and Harris ^a	1969	122	1.10	7.57	112.8
Dunning and Winter ^c	1975	101	1.10	8.35	113.7
Cremer ^c	1978	107	0.94	7.69	119.3 ^d

^aFrom infrared spectrum.^bFrom millimetre-wave spectrum.^cFrom RHF calculations.^dFrom RSMP calculations.

Despite the appealing character of some of the proposed models, their quantitative verification turns out to be especially difficult in the case of H₂O₂. Rather inconclusive have been attempts to trace the origin of the *cis* and *trans* barriers back to orbital orthogonality or exchange contributions imposed by the Pauli Principle^{112,131}, interference effects between the weak vicinal 'tails' of OH or lone-pair (n) LMOs^{111,132}, bond-antibond interactions¹³³, the dominance of attractive or repulsive energy terms^{109,116,134,135} or the prevailing role of special MOs.

In Figure 19, RHF/SVd orbital energies ϵ_i for the five highest occupied MOs of H₂O₂ are plotted as functions of τ . They reveal that reliable predictions with regard to the relative stabilities of **21**, **22** and **23** cannot be made with the aid of ϵ_i values. This holds for the two HOMOs discussed in Section III.B.4 as well as for the total orbital energy $2 \sum_i^{\text{occ}} \epsilon_i$ as was first shown by Fink and Allen⁸⁹.

An elegant way to avoid these difficulties has been pursued by Radom, Hehre and Pople¹⁰⁰. These authors have expanded the *ab initio* rotational potential of H₂O₂ in form of a truncated Fourier series (equation 1) and have used the constants V_i^c to analyse the *cis* and *trans* barriers. Figure 20 illustrates this procedure. In Table 12, the corresponding V_i^c constants of H₂O₂ are compared with those of some other peroxides.

$$V(\tau) = V_1(\tau) + V_2(\tau) + V_3(\tau) \\ = \frac{1}{2}V_1^c(1 - \cos \tau) + \frac{1}{2}V_2^c(1 - \cos 2\tau) + \frac{1}{2}V_3^c(1 - \cos 3\tau) \quad (1)$$

The $V_1(\tau)$ term can be considered as indicating repulsive ($V_1^c < 0$, H₂O₂, Table 12) or attractive ($V_1^c > 0$, HOOF, Figure 21) interactions between OH or OX bond dipole moments. The V_2^c term has been connected with the degree of lone-pair (n) delocalization. According to Pople and coworkers¹⁰⁰, there seems to be a general tendency of n orbitals to become coplanar with adjacent polar bonds, thus guaranteeing an overall stabilization of N or O containing rotors in the corresponding conformation¹⁰⁰. Hence, a negative V_2^c is indicative of maximum n delocalization at $\tau = 90^\circ$. Actually, this description is related to the explanation of the anomeric effect given by Altona and coworkers¹³⁷. Both ways of interpreting $V_2(\tau)$ are illustrated in Figure 21.

Figure 20 as well as Table 12 reveal that the rotational minimum at $\tau = 120^\circ$ results from a delicate balance of $V_1(\tau)$ and $V_2(\tau)$, which clearly dominate the conformational behaviour of H₂O₂ and other peroxides. The V_3^c term is relatively small and negative suggesting a slight preference for staggering of bonds.

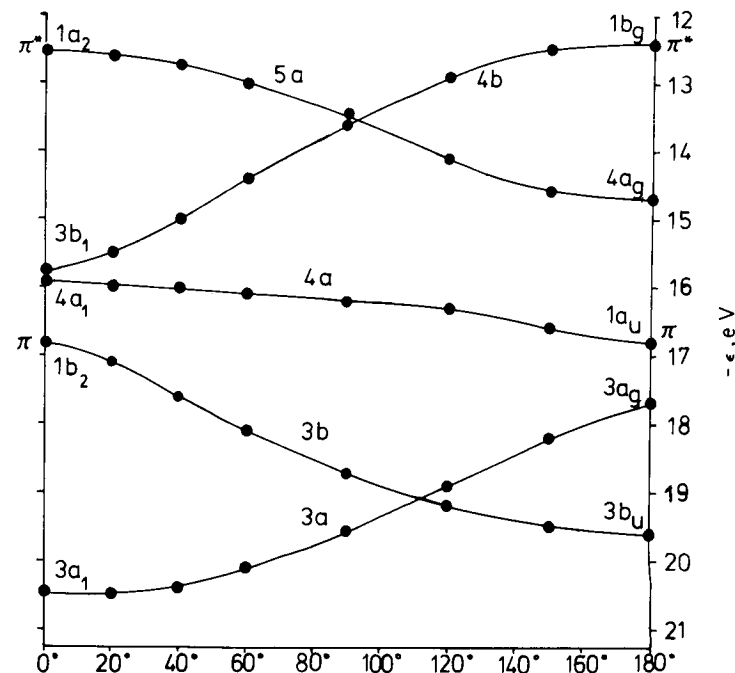
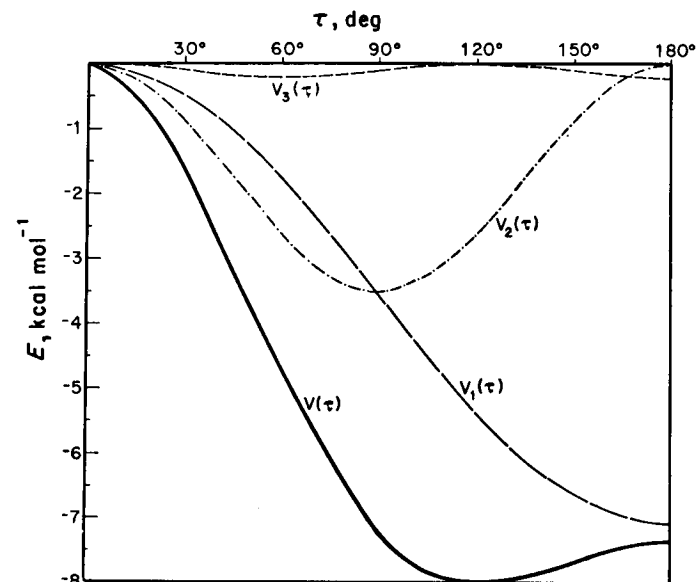
FIGURE 19. Functional dependence of RHF/SVd orbital energies on τ calculated for H₂O₂ (D. Cremer, unpublished results).FIGURE 20. Fourier decomposition of potential function $V(\tau)$ for H₂O₂. Adapted from L. Radom, W. J. Hehre and J. A. Pople, *J. Amer. Chem. Soc.*, **94**, 2371 (1972), by permission of the American Chemical Society.

TABLE 12. Potential constants (kcal mol⁻¹) for internal rotation in peroxides^a

Molecule	V ₁ ^c	V ₂ ^c	V ₃ ^c	Method	Ref.
HO—OH	-7.1	-3.5	-0.2	RHF/SV	100
	-8.0	-3.7	-0.3	RHF/SVdp	114
CH ₃ O—OH	-7.5	-2.9	-0.4	RHF/SV	100
FO—OH	4.2	-5.2	-0.1	RHF/SV	100
CF ₃ O—OH	-5.6	-3.9	-0.4	RHF/SV	136
CF ₃ O—OF	-4.1	-6.1	-0.7	RHF/SV	136

^aEnergy of the *cis* form ($\tau = 0^\circ$) is taken as the reference point.

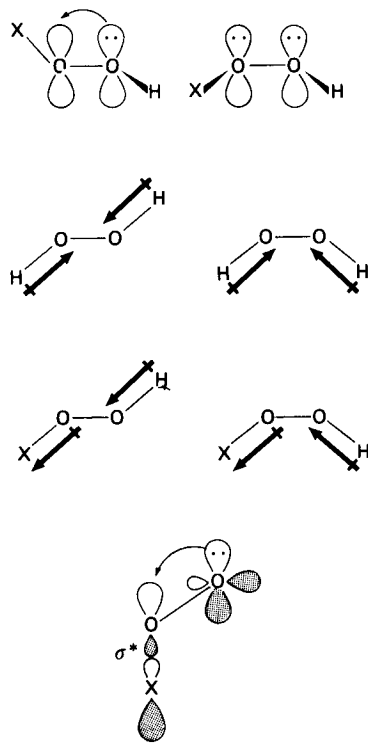


FIGURE 21. Schematic illustration of lone-pair delocalization, interaction between bond dipole moments, and the anomeric effect.

C. Total Energies, Heats of Formation and Bond Dissociation Enthalpies

Thermochemical data on XO₂ and X₂O₂ compounds are sparse¹³⁸⁻¹⁴¹. That is why Benson and Shaw in their review on the thermochemistry of organic per- and polyoxides¹⁴² have dwelt on empirical methods to estimate heats of formation $\Delta H_f^\circ(298)$ and bond dissociation enthalpies $DH^\circ(298)$. Subsequent work of Benson and

coworkers¹⁴³⁻¹⁴⁸, based on group additivity principles, has led to an improvement and extension of ΔH_f° estimates for polyoxides and polyoxide radicals. Some of these values are listed in Table 13^{143,148}.

A theoretical determination of ΔH_f° is only possible with recourse to an appropriate reference state and its experimental ΔH_f° value (equation 2). By calculating molecular (MOL) and reference state (REF) energies and using known $\Delta H_f^\circ(0)^{\text{REF}}$ data, $\Delta H_f^\circ(0)^{\text{MOL}}$ can be determined from equation (2). The crucial point is the evaluation of the 'experimental' energy $E(\text{EXP})$ ¹⁴⁹. As is illustrated in Figure 22, this requires the knowledge of (a) HF limit energies $E(\text{HF})$, (b) their correlation corrections $E(\text{CORR})$ to obtain Schrödinger energies $E(\text{S})$, (c) relativistic corrections $E(\text{REL})$ to obtain true theoretical energies $E(\text{THEO})$ and (d) vibrational corrections $E(\text{VIB})$, which primarily comprise zero-point vibrational energies ZPE .

$$E(\text{EXP})^{\text{MOL}} - \sum^k E(\text{EXP})^{\text{REF}} = \Delta H_f^\circ(0)^{\text{MOL}} - \sum^k \Delta H_f^\circ(0)^{\text{REF}} \quad (2)$$

For polyatomic molecules none of these energies can be accurately determined by theory. However, it is possible to obtain estimates of the molecular energies $E(\text{HF})$, $E(\text{S})$, $E(\text{THEO})$ and $E(\text{EXP})$ if *ab initio* and experimental data are combined¹⁴⁹. In Table 14 $E(\text{EXP})$ values as well as some other characteristic molecular energies, obtained in this way, are given for O₂, H₂O₂, O₃, H₂O₃, MeO₂H and MeO₂Me¹⁴⁹. The theoretical estimates lead to ΔH_f° values, generally not more accurate than ± 5 kcal mol⁻¹. This is also true when differences $\Delta E(\text{EXP})$ are approximated by computed SCF energies $E(\text{X})$ (X: SV or DZ basis)^{150,151,153} or estimates of $E(\text{HF})$ ¹⁵² using closed-shell molecules (H₂, H₂O, H₂O₂, XH_n, XOH, etc.) or ions (O₂²⁺) as reference states¹⁵⁰⁻¹⁵³.

Due to the relatively large uncertainties of theoretical ΔH_f° values, the data of Table 13 are used to discuss dissociation enthalpies DH° of peroxy compounds. A cleavage of the O—O bond of H₂O₂ requires¹⁴²:

$$DH^\circ(\text{HO—OH}) = 2\Delta H_f^\circ(\text{HO}\cdot) - \Delta H_f^\circ(\text{H}_2\text{O}_2) = 51 \text{ kcal mol}^{-1}$$

TABLE 13. Estimated $\Delta H_f^\circ(298)$ values (kcal mol⁻¹) for polyoxides and polyoxide radicals^{143,148 b}

	X ¹ , X ²				
	H, H	Me, Me	<i>t</i> -Bu, <i>t</i> -Bu	Me, H	<i>t</i> -Bu, H
<i>Polyoxides</i>					
X ¹ O ₂ X ²	-32.5 ^a	-30.0 ^a	-83.4 ^a	-31.3	-58.0 ^a
X ¹ O ₃ X ²	-15.7	-13.2	-66.6	-14.5	-41.2
X ¹ O ₄ X ²	1.1	3.6	-49.8	2.3	-24.4
X ¹ O ₅ X ²	17.9	20.4	-33.0	19.1	-7.6
<i>Polyoxide Radicals</i>					
X ¹ O·	9.4 ^a	3.9	-22.8		
X ¹ O ₂ ·	3.0	6.2	-22.5		
X ¹ O ₃ ·	17.8	23.0	-7.7		
X ¹ O ₄ ·	32.6	39.8	7.1		
X ¹ O ₅ ·	47.4	56.0	21.9		

^aExperimental values.

^bAdapted with permission from P. S. Nangia and S. W. Benson, *J. Phys. Chem.*, **83**, 1138 (1979).

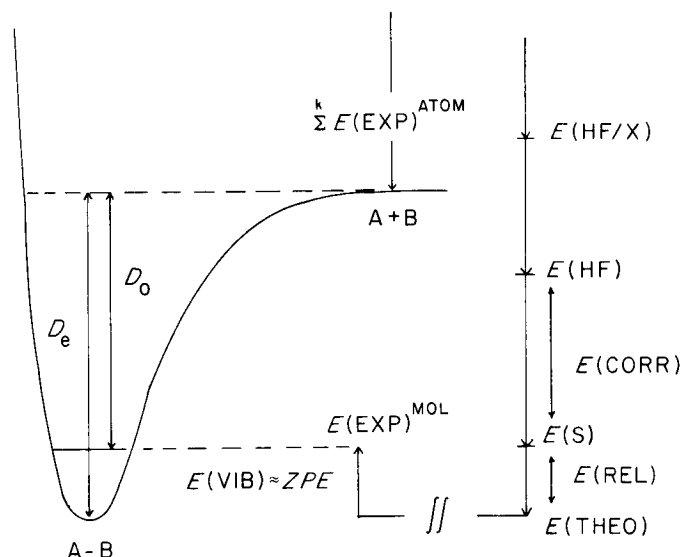


FIGURE 22. Theoretical determination of dissociation energies D_e and D_0 for a molecule AB. (See text for an explanation of the various energies.) Note that different energy scales are used on the right- and left-hand sides of the drawing.

TABLE 14. Theoretical energies (hartree) and heats of formation (kcal mol^{-1}) of some compounds containing the OO moiety^a

Energy	O ₂	H ₂ O ₂	MeOOH	MeOOME	O ₃	H ₂ O ₃
$E(\text{HF})$	-149.670	-150.860	-189.901	-228.956	-224.391	-225.678
$E(\text{CORR})$	-0.647	-0.693	-0.946	-1.199	-1.032	-1.024
$E(\text{REL})$	-0.100	-0.100	-0.128	-0.150	-0.150	-0.150
$E(\text{THEO})$	-150.417	-151.653	-190.961	-230.283	-222.573	-226.852
ZPE	0.004	0.025	0.054	0.083	0.008	0.030
$E(\text{EXP})$	-150.408	-151.621	-190.898	-230.188	-225.557	-226.814
$\Delta H_f^0(0)$	0	-31.1	-23.1	-23.2	34.8	-24.2
$\Delta H_f^0(298)$	0	-32.6	-26.5	-28.5	34.1	-26.5

^aTaken from Ref. 149. For O₂, H₂O₂ and O₃ experimental ΔH_f^0 values have been used to obtain correlation energy increments upon which the estimation of $E(\text{CORR})$ energies of higher peroxides is based. ZPE values have to be enlarged by corrections for the nuclear motion relative to the centre of mass when calculating $E(\text{VIB})$; $ZPE = \frac{1}{2} h N_A \sum_i^{3k-6} \nu_i$, where k is the number of atoms and the ν_i are the experimental frequencies. Reference states are the atoms H, O and C.

and that of the O—H bond¹⁴³:

$$\begin{aligned} DH^0(\text{HO}_2-\text{H}) &= \Delta H_f^0(\text{HO}_2\cdot) + \Delta H_f^0(\text{H}\cdot) - \Delta H_f^0(\text{H}_2\text{O}_2) \\ &= 88 \text{ kcal mol}^{-1}. \end{aligned}$$

Thus, $DH^0(\text{O—O})$ nicely fits into the series of $DH^0(\text{X—X})$ values of isoelectronic X₂H_{2n} molecules as can be seen from Table 15 (compare also with Table 2, Section I).

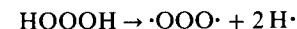
TABLE 15. Dissociation enthalpies DH^0 (kcal mol^{-1}) of isoelectronic X₂H_{2n} molecules

Molecule	$DH^0(\text{X—X})$	$DH^0(\text{X—H})$	Reference
C ₂ H ₆	88	99	141
N ₂ H ₄	69	104 ^a	141
O ₂ H ₂	51	88	142
F ₂	38	—	141

^aEstimated value.

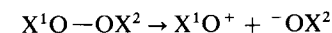
It is interesting to compare O—O, C—O and O—H dissociation enthalpies for organic polyoxides. According to the data listed in Table 16, the O—O bond is considerably weakened if H is replaced by Me or an additional O atom is inserted into the O—O linkage. Delocalization of the 3π electrons of a peroxy radical (see Section III.A.2) strengthens the O—O bond by about 15 kcal mol^{-1} . The same effect makes the O—H bond of H₂O₂ more susceptible to bond rupture than that of an alcohol. This holds also for C—O bonds (Table 16).

The π delocalization energy of O₃ can be estimated by the formal reaction¹⁴⁵



where the unpaired electrons of the $\cdot\text{OOO}\cdot$ fragment are thought not to interact and the enthalpy change is taken as twice the $DH^0(\text{O—H})$ value of H₂O₂. Thus, a ΔH_f^0 value for the hypothetical $\cdot\text{OOO}\cdot$ species with 100% biradical character (i.e. when the overlap (S) equals zero, see Table 8, Section IV.A) can be evaluated and compared with the experimental heat of formation of ozone. Depending on the value of $\Delta H_f^0(\text{H}_2\text{O}_3)$, the 4π delocalization energy has been predicted to be 17–19 kcal mol^{-1} ^{69,145}. Since the actual dissociation enthalpy of O₃ is 25 kcal mol^{-1} (Table 16), only 6–8 kcal mol^{-1} can be assigned to the O—O σ bond.

A heterolytic cleavage of the O—O bond



requires a considerably higher amount of energy if X¹ and X² cannot stabilize the emerging ions. The reaction energy ΔE can be estimated utilizing the dissociation enthalpy for homolytic cleavage (equation 3)¹⁴⁴. From experimental ionization potentials I and

TABLE 16. Dissociation enthalpies DH^0 (kcal mol^{-1}) of molecules containing O—O, C—O and O—H bonds^{141,143,148,154}

Molecule	$DH^0(\text{O—H})$	Molecule	$DH^0(\text{O—O})$	Molecule	$DH^0(\text{C—O})$
H—O·	102	O=O	119	CH ₃ —OH	91
H—OH	119	HO—O·	66	CH ₃ —O ₂ ·	28
H—OCH ₃	104	CH ₃ O—O·	59	CH ₃ —O ₂ H	70
H—O ₂ ·	49	HO—OH	51	HCO—OH	107
H—O ₂ H	88	CH ₃ O—OH	45	HCO—O ₂ H	86
H—O ₂ CH ₃	90	CH ₃ O—OCH ₃	38		
H—O ₃ ·	68	O=O ⁺ —O ⁻	25		
		HO ₂ —OH	30		
		CH ₃ O ₂ —OCH ₃	23		

electron affinities $EA^{146,147}$, the energy of heterolytic O—O cleavage in the gas phase is predicted to be 5–8 times larger than homolytic cleavage (Table 17).

$$\Delta E \approx DH^0(X^1O-OX^2) + I(X^1O\cdot) + EA(X^2O\cdot) \quad (3)$$

However, heterolytic cleavage needs less energy if (a) an ion pair is formed at a distance r_{ip} separating the effective charge centres, and (b) formation of the ion pair occurs in solution. Then the energy of heterolytic cleavage is given by equation (4). Benson and coworkers^{143,147} have estimated r_{ip} to be $2.65 \pm 0.05 \text{ \AA}$. This leads to a Coulomb attraction energy of $124 \pm 2 \text{ kcal mol}^{-1}$. Accordingly, a dialkyl trioxide can undergo heterolytic cleavage, provided the solvation energy ΔE_{solv} of the ion pair compensates for a difference of about 20 kcal mol^{-1} . The energy ΔE_{solv} can be approximated by Kirkwood's formula¹⁵⁵ (equation 5), where ϵ is the dielectric constant of the solvent, μ the dipole moment ($\mu = 2.65 \times 4.8 = 12.72 \text{ D}$) and a the radius of a spherical cavity formed by solvent molecules surrounding the ion pair. With $a = 3.5 \text{ \AA}$ ¹⁴⁷ the solvation energy of a typical hydrocarbon solvent ($\epsilon = 2$) is predicted to be 11 kcal mol^{-1} . This energy will increase to 20 kcal mol^{-1} if a solvent with $\epsilon = 5.2$ is used.

$$\Delta E_{ip}(\text{solvent}) = \Delta E - e^2/r_{ip} - \Delta E_{solv} \quad (4)$$

$$\Delta E_{solv} \approx 14.39 \cdot \frac{\epsilon - 1}{2\epsilon + 1} \cdot \frac{\mu^2}{a^3} \quad (5)$$

D. Orbital Energies and Ionization Potentials

According to Koopmans' theorem¹⁵⁶ the values $-\epsilon_i$ of UHF orbital energies provide reasonable approximations to vertical ionization potentials (IPs), I_{vert} . As can be seen from Table 18, magnitudes of the energies ϵ_i obtained with UHF theory for O_2 ¹⁵⁷ are of the same order as the experimental IPs measured with ESCA^{158–160}. An exception occurs in the case of the $3\sigma_g$ and $1\pi_u$ MOs where the experimentally observed order is reversed. This failure of UHF theory results from the neglect of (a) Coulomb correlation of electrons and (b) MO relaxation effects upon ionization.

The correct MO sequence of O_2 has been obtained by the ΔE_{SCF} approach, i.e. by separately calculating the GS of O_2 and the ground and excited 'hole states' of O_2^+ listed in Table 18¹⁶¹. In this way relaxation effects are accounted for. Electron propagator calculations, which consider in addition correlation effects, provide the best agreement between experiment and theory (Table 18)¹⁵⁷.

A similar discrepancy between Koopmans' values and experimental IPs has been observed in the case of ozone. The experimental PE spectrum^{162–164} reveals considerable

TABLE 17. Energy for heterolytic O—O cleavage estimated according to equation (3)^a

Products	$I(\text{eV})$	$EA(\text{eV})$	$\Delta E(\text{kcal mol}^{-1})$
$HO^+ + ^-OH$	13.2	1.83	313
$CH_3O^+ + ^-OH$	8.3	1.83	194
$CH_3O^+ + ^-OCH_3$	8.3	1.57	193
$HO^+ + ^-O_2H$	13.2	1.85	292
$HO_2^+ + ^-OH$	11.5	1.83	253
$CH_3O_2^+ + ^-OCH_3$	6.75	1.57	142

^a I and E values from Refs. 146 and 147.

TABLE 18. Theoretical and experimental ionization potentials I_{vert} (eV) of O_2

Spin orbital	Ion state	UHF ^{a,d}	$\Delta E_{SCF}^{b,e}$	Electron propagator ^{a,e}	Expt. ^c
$1\pi_g\alpha$	$^2\Pi_g$	15.3	13.1	11.8	12.1
$1\pi_u\beta$	$^4\Pi_u$	15.8	14.3	17.0	16.1
$1\pi_u\alpha$	$^2\Pi_u$	22.8	15.6	17.4	17.0
$3\sigma_g\beta$	$^4\Sigma_g^-$	19.3	17.3	18.0	18.2
$3\sigma_g\alpha$	$^2\Sigma_g^-$	20.8	21.0	19.5	20.3
$2\sigma_u\beta$	$^4\Sigma_u^-$	27.5	26.0	24.1	24.6
$2\sigma_u\alpha$	$^2\Sigma_u^-$	33.0	33.5	26.7	27.9
$2\sigma_g\beta$	$^4\Sigma_g^-$	43.3	41.0	39.0	39.6
$2\sigma_g\alpha$	$^2\Sigma_g^-$	46.6	45.9	40.2	41.6
$1\sigma_u\beta$	$^4\Sigma_u^-$	563.4		542.7	
$1\sigma_u\alpha$	$^4\Sigma_u^-$	563.5	554.4	542.8	543.1
$1\sigma_g\alpha$	$^2\Sigma_g^-$	564.9		544.5	
$1\sigma_g\alpha$	$^2\Sigma_g^-$	565.0	556.6	544.5	544.2

^aRef. 157.

^bRef. 161.

^cRef. 158 (above 28 eV) and Ref. 159 (below 28 eV).

^dKoopmans' values.

^eFrom calculation of the ion states.

vibrational structure for the first ionization. This is not consistent with depopulation from the nonbonding $1a_2$ MO as suggested by HF calculations (see Table 19). Investigations, which go beyond the HF level of theory, agree on the assignment of the first IP as resulting from $6a_1$ ionization^{49,53,62,165–167}. In addition, they provide sufficient evidence for the MO sequence $6a_1, 4b_2, 1a_2, 1b_1$. This has been taken into consideration when summarizing the relevant data in Table 19 (see also Figure 11).

Available data on the IPs of the HO_2 radical are sparse. Foner and Hudson⁸⁵ deduced a preliminary value for the first IP , which has been confirmed theoretically by Shih and coworkers (Table 20)⁷⁷. It corresponds to ionization of a $7a'$ electron resulting in a triplet state, namely the $^3A''$ GS of the HO_2^+ ion⁷⁴. Shih and coworkers have tentatively assigned the second IP to $2a''$ ionization. Again, Koopmans' values lead to a different order of IPs ⁷⁷.

TABLE 19. Theoretical and experimental ionization potentials I_{vert} (eV) of O_3

MO	Ion state	RHF ^a (Ref. 59)	MBPT ^b (Ref. 166)	CI ^b (Ref. 53)	GVB ^b (Ref. 49)	Expt. (Refs. 162–164)
$6a_1$	2A_1	15.2	12.9	12.5	12.9	12.75
$4b_2$	2B_2	15.5	13.3	12.6	13.0	13.02
$1a_2$	2A_2	13.3	13.2	13.0	13.6	13.57
$1b_1$	2B_1	21.1				} 20.1
$3b_2$	2B_2	21.7				
$5a_1$	2A_1	22.6				
$4a_1$	2A_1	30.0				

^aKoopmans' values.

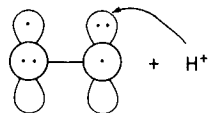
^bFrom calculations of the ion states.

TABLE 20. Ionization potentials I_{vert} (eV) of the HO₂ radical

MO	Ion state	SCF ^a (Ref. 77)	MRD-CI ^a (Ref. 77)	Exp. (Refs. 85, 168)
7a'	³ A'' ^b	10.9	11.6	11.5
2a''	¹ A'	12.9	12.3	12.2
7a'	¹ A''	12.2	12.6	

^aFrom calculations of the ion states.

^bNote that a 'synthesis' of HO₂⁺ from O₂ and H⁺ also leads to a triplet GS:



PE spectra of H₂O₂ are obscured due to decomposition of the sample to H₂O and O₂ in the electron source¹⁶⁹⁻¹⁷¹. Because of the contaminants, the uncertainty of the experimental IP s is rather large (0.2–1 eV)¹⁷¹. The Koopmans' values obtained with augmented basis sets¹⁰⁷ are 8–10% larger than the observed IP s (Table 21), which is in accordance with Robin's 8% rule¹⁷².

The first band of the PE spectrum of H₂O₂ reveals some vibrational fine structure ($\nu'' = 1050 \text{ cm}^{-1}$). Brown¹⁷⁰ has argued that ionization from an O—O antibonding MO should lead to a strengthening of the bond and, hence, to an increase of the O—O stretching frequency ν_3 of H₂O₂ ($\nu_3 = 863 \text{ cm}^{-1}$, see Section IV.E). Comparison with Figure 14 shows that both the 4b and 5a MO possess O—O antibonding character. With the auxiliary information about τ being larger than 90° and, hence, 5a below 4b (Figure 19), an assignment of the first and second IP to the 4b and 5a MO is straightforward.

The third IP resulting from ionization of the O—O bonding 4a electron (Figure 14) also exhibits a vibrational progression ($\nu'' = 1100 \text{ cm}^{-1}$). Arguments have been given, which connect this progression with an excitation of the symmetric OOH bending vibration ν_2 (1393 cm^{-1})¹⁷¹. If correct, the same reasoning, of course, could apply to the first PE band.

TABLE 21. Theoretical and experimental ionization potentials I_{vert} (eV) of H₂O₂

MO	$-\epsilon_i^a$ RHF/SVd	$-\epsilon_i^b$ RHF/SVd	Exp. I_{vert}	
			Ref. 169	Ref. 171
4b	12.9	11.9	11.7	11.7
5a	14.1	13.0	12.7	13.0
4a	16.3	15.0	15.3	15.4
3a	18.9	17.4	17.4	17.5
3b	19.2	17.7	17.4	18.5
2b	32.9	30.3		
2a	39.8	36.6		
1b				
1a	561.5	516.6		

^aKoopmans' values obtained with an augmented SV basis. See Section IV.B, Figure 19.

^bCorrected according to Robin's 8% rule, Ref. 172.

Assignment of 3a and 3b ionization on the basis of theoretical Koopmans' values depends very much on the use of the correct τ value ($\tau = 120^\circ$) of skewed H₂O₂. Figure 19 reveals that the 3a and 3b MOs cross at $\tau \approx 116^\circ$. Hence, any calculation with $\tau < 116^\circ$ ¹⁷³ leads to a wrong assignment.

For a series of organic peroxides PE spectra have been recorded^{170,171,174-177}. The spacing of the first two IP s has been used to determine the conformation of a peroxide. According to Figure 19 the splitting $\Delta\epsilon_1 = \epsilon(5a) - \epsilon(4b) = -\Delta I_1$ varies with τ , which can be described analytically by a truncated Fourier expansion (Figure 23) (equation 6). Rademacher and Elling¹⁷⁶ have calibrated equation (6) experimentally by utilizing known τ values of organic peroxides in conjunction with PE measurements. The function $\Delta I_1(\tau)$ thus obtained is depicted in Figure 23. It has been used to estimate the dihedral angle τ of cyclic peroxides (Table 22), for which $\tau < 90^\circ$ and, hence, the sign of ΔI_1 is known¹⁷⁶. Since the magnitude of both I_{vert} and ΔI_1 is influenced by the substituents attached to the peroxy group (compare with Figure 23), τ values determined with equation (6) on the basis of PE investigations are rather inaccurate. This becomes obvious when applying the analytic form of $\Delta I_1(\tau)$ given in Reference 176 to alicyclic organic peroxides ($\Delta I_1 = 0.45 \text{ eV}$ for ROOH; R = pentyl, hexyl or heptyl¹⁷¹).

$$\Delta I_1(\tau) = A \cos \tau + B \cos 2\tau + C \quad (6)$$

E. Geometry and Vibrational Analysis

Pertinent to a discussion of the O—O bond strength measured by the depth of the potential function (see, for example, Figure 22) is the analysis of the O—O bond length (location of the potential minimum) and its stretching frequency and force constant (width

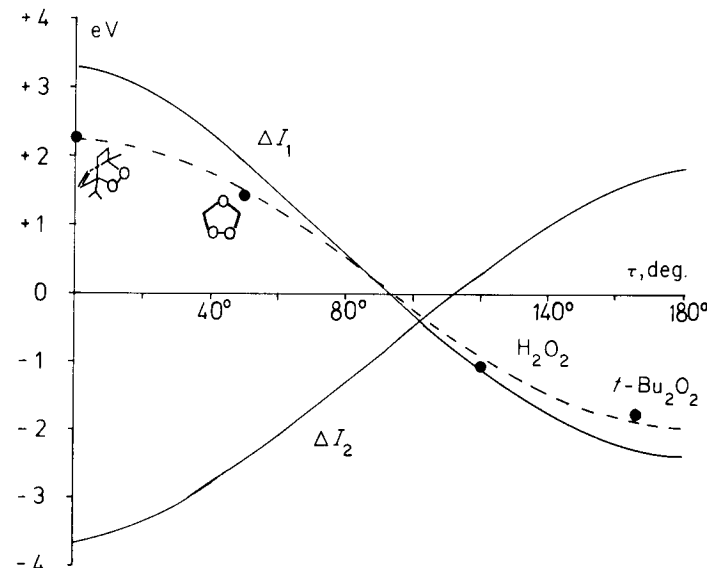
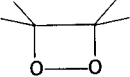
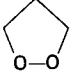
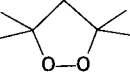
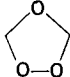
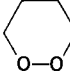
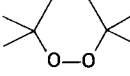
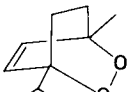
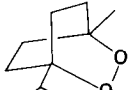


FIGURE 23. Functional dependence of the spacings $\Delta I_1 = I(4b) - I(5a)$ and $\Delta I_2 = I(3b) - I(3a)$ on the dihedral angle τ of H₂O₂ as obtained with RHF/SVd calculations [$\Delta I_1(\tau): A = 2.7, B = 0.2, C = 0.3 \text{ eV}$]. Experimental measurements of ΔI_1 are denoted by dots. They lead to $\Delta I_1(\tau) = 2.08 \cos \tau + 0.15$ (dashed line)¹⁷⁶.

TABLE 22. Determination of the dihedral angle τ from measured ionization potentials I_{vert} ¹⁷⁶

Molecule ^a	$I(b)$ (eV)	$I(a)$ (eV)	ΔI (eV)	τ (deg.)	Ref.
HO—OH*	11.51	12.56	-1.05	120	170
MeO—OMe	9.71	11.61	-1.90	170	177
<i>t</i> -BuO—OBu- <i>t</i> *	8.83	10.57	-1.74	166	176
	10.94	8.98	1.96	30	170
	11.13	9.86	1.27	57	175
	10.40	9.25	1.15	61	170, 174
	12.4	10.96	1.44	50	175
	10.35	10.17	0.18	89	176
	9.76	9.35	0.31	86	170, 174
	10.71	8.42	2.29	10	170
	10.36	8.50	1.86	35	170

^aStarred molecules have been used for determining the functional dependence $\Delta I(\tau)$.

of the potential function). In Table 23 some relevant data for O_2 and its ions^{36,151,178-182} are summarized. The dependence of these properties on the electron configuration is evident. Depopulation of the antibonding π_g MOs of O_2 increases the bond order (Section III.B.1, Figure 7) and bond strength. The strengthening of the OO bond is reflected by lower R_e and higher ν_e and D_e values. Conversely, if the partially vacant π_g MOs of O_2 are filled, thus lowering the bond order to 1.5 (superoxide ion) and 1 (peroxide ion), the OO distance increases, while stretching frequency and dissociation energy decrease.

The r_e and ν parameter of ozone^{70,183-189} suggest that its OO bonds resemble more O_2 than O_2^{2-} despite its low dissociation energy¹⁸⁸ (Table 24). Even its anion, O_3^- ,

TABLE 23. Electronic configuration and properties of O_2 and its ions

Molecule	Configuration	State	Bond order P^a	R_e (Å)	ν_e (cm ⁻¹)	D_e (eV)	T_e (eV)	Ref.
O_2^{2+}	... $(1\pi_g)^0(3\sigma_u)^0$	$^1\Sigma_g^+$	3	1.034 ^b				151
O_2^+	... $(1\pi_g)^1(3\sigma_u)^0$	$^2\Pi_g$	2.5	1.123	1876.4	6.55		36
O_2	... $(1\pi_g)^2(3\sigma_u)^0$	$^3\Sigma_g^-$	2	1.207	1580.2	5.21	0	36
		$^1\Delta_g$	2	1.216	1509.3	4.23	0.98	36
		$^1\Sigma_g^+$	2	1.227	1432.7	3.58	1.63	36
		$^2\Pi_g$	1.5	1.341	1089	4.09 ^c		178, 179
O_2^{2-}	... $(1\pi_g)^4(3\sigma_u)^0$	$^1\Sigma_g^+$	1	1.50 ^d	848 ^e			180, 182
$(O_2^{2-})_2$... $(1\pi_g)^4(3\sigma_u)^2$	$^1\Sigma_g^+$	0	Large		0		

^a $P = P_b - P_a$; P_b , P_a : number of electron pairs occupying bonding or antibonding MOs.

^bRHF/DZ value; see also Ref. 181 for RHF/SV calculations.

^c D_0 value.

^dDistance observed for alkali peroxides, Ref. 180.

^eAverage of the A_g vibrational frequencies computed for Li_2O_2 , Ref. 182.

TABLE 24. Electron configuration and molecular properties of ozone and some of its ions

Molecule	Configuration	State	Bond order P^a	R_e (Å)	α_e (deg.)	ν (cm ⁻¹)	D_0 (eV)	Ref.
O_3^+	... $(6a_1)^1(2b_1)^0$	2A_1	1.72	1.26 ^b	131.7		1.85	185, 189
O_3	... $(6a_1)^2(2b_1)^0$	1A_1	1.66	1.272	117.8	1103	1.05 ^c	70, 184
O_3^-	... $(6a_1)^2(2b_1)^1$	2B_1	1.22	1.38 (2)	116 (2)	982	1.39 ^d	186, 188
				1.35 ^b	114.1		2.41 ^e	189

^aEvaluated with the aid of Pauling's bond-order relationship²⁵: $R_e = (a - b) \ln P$, where $a = 1.452 \text{ Å}$ [$R_e(H_2O_2)$ for $P = 1$] and $b = -0.353 \text{ Å}$ from $R_e = 1.207 \text{ Å}$ for $P(O_2) = 2$.

^bTheoretical value of Ref. 189, corrected with the aid of exp. and theoret. ozone parameters.

^cHiller and Vestal¹⁸⁸ suggest a value of $\leq 0.75 \text{ eV}$ on the basis of photodissociation measurements on O_3^- .

^d $D_0(O_2 - O^-)$.

^e $D_0(O - O_2^-)$.

possesses an OO distance and stretching frequency¹⁸⁶ closer to the superoxide than the peroxide ion. Noteworthy is the reduction of the angle α in the series O_3^+ , O_3 , O_3^- , which is parallel to the stepwise occupation of 1,3 bonding MOs (Figure 10).

A first direct measurement of R for H_2O_2 was obtained by Giguère and Shomaker as early as 1943¹⁹⁰. Subsequent work on the r_0 structure of H_2O_2 by Redington, Olson and Cross¹¹⁹ led to a complete set of geometrical data. However, the experimental determination of a r_0 structure of H_2O_2 has to cope with the dilemma of extracting four internal parameters out of three rotational B_0 constants, since no accurate spectroscopic data on D_2O_2 are available. This problem has been solved by assuming an O—H length. Recently, convincing evidence has been gathered from neutron diffraction results of H_2O_2 ^{191,192}, D_2O_2 ¹⁹³ and D_2O ¹⁹⁴, from the microwave study of HOF¹⁹⁵ and an elaborate *ab initio* study¹⁰⁷, which suggest $R_e(OH) \approx R_0(OH) \approx 0.965 \text{ Å}$. With this parameter the r_0 structure of H_2O_2 published by Redington and coworkers¹¹⁹ has been revised^{107,196,197}. In addition, r_e parameters have been derived utilizing published

vibrational-rotational constants¹⁹⁶. In Table 25, the r_0 and r_e geometries are compared. Both theory and experiment support a R_e value of 1.452 Å for H_2O_2 . The corresponding difference $R_0 - R_e$ obtained by Cremer and Christen¹⁹⁷ is rather large, which has been criticized by Giguère and Srinivasan¹⁹⁸.

Out of the wealth of computed *ab initio* geometries of H_2O_2 a rather confusing picture emerges as is illustrated in Figure 24. Some theoretical R_e distances cluster around 1.39–1.40 Å, while the others are scattered between 1.40 and 1.56 Å, i.e. most *ab initio* distances are clearly outside the range of error of spectroscopic H_2O_2 geometries. This indicates that the calculation of the O—O bond length of H_2O_2 is very sensitive to basis set and correlation errors of the HF approach. HF calculations with extended basis sets

TABLE 25. Geometrical parameters of H_2O_2 as determined by experiment and theory

Parameter	r_0^a IR (Ref. 197)	r_e^b IR, MW (Ref. 196)	r_e RHF/SV (Ref. 107)	r_e RSMP/DZdp (Ref. 107)
R (Å)	0.965 ^c	0.965 ^c	0.965	0.967
R (Å)	1.464	1.452	1.460	1.451
α (deg.)	99.4	100.0	102.3	99.3
τ (deg.)	120.2	119.1	120.0 ^c	119.3

^aReinterpretation of infrared data of Ref. 119.

^bDeduced from infrared and microwave data of Refs. 119 and 121.

^cAssumed value.

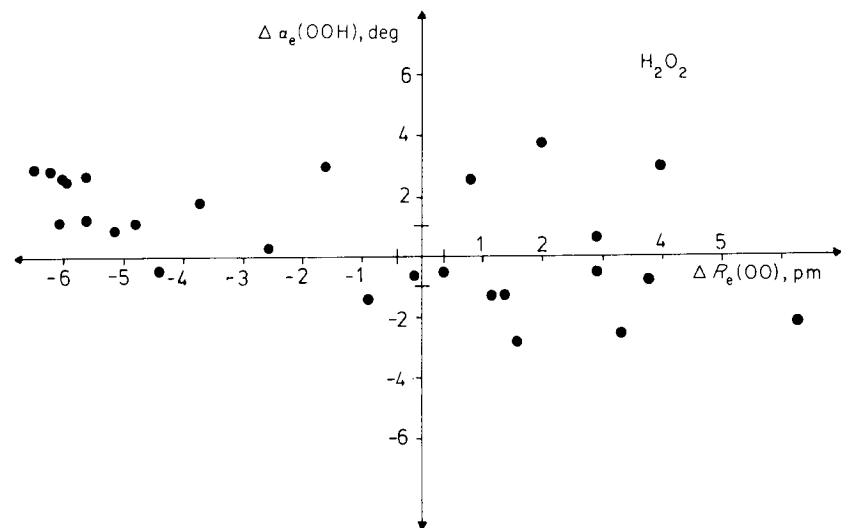


FIGURE 24. Deviation of *ab initio* geometries for skewed H_2O_2 . Origin at $R_e = 1.452$ Å and $\alpha_e = 100^\circ$ ¹⁹⁶. ΔR_e measured in picometre. Uncertainty of experimental r_e geometry is indicated.

severely underestimate R_e . This is the result of an artificial accumulation of electron charge close to the O nuclei, which increases the stabilizing Coulomb interactions between electrons and nuclei. The latter are shielded by the surrounding electron charge. Coulomb repulsion between the O nuclei is considerably reduced, which explains the short O—O bond lengths. As soon as electron correlation is considered, accumulation of charge in one area is no longer possible. Removal of electron charge from the inner to the outer valence sphere of the O nuclei causes a lengthening of the theoretical O—O bond towards the true R_e value¹⁰⁷.

Because of a distinctively different description of the inner and outer valence spheres of O and the polarity of the OH bond with MBS, SV, DZ or augmented DZ basis sets^{107,199}, theoretical R_e values of H_2O_2 depend strongly on the size of the basis set. This dependence is qualitatively described in Figure 25. It is responsible for the scattering of *ab initio* values of R_e reflected by Figure 24. In addition, it indicates that calculations carried out with relatively small basis sets can lead to reasonable R_e and R_0 values due to a fortuitous cancellation of basis set and correlation errors¹⁰⁷.

Crystallographic data on the O—O bond length in H_2O_2 ^{191,192}, D_2O_2 ¹⁹³ and perhydrates^{200–206} vary between 1.44 and 1.47 Å. It has been noted²⁰⁰ that R of H_2O_2 molecules in solids is generally smaller than for peroxides due to the presence of water. Correcting for this effect and the thermal motion in the crystal, Pedersen has predicted the average R value of H_2O_2 to be 1.456 Å²⁰⁰, which is in line with $R_e = 1.452$ Å.

The six normal modes of vibrational motion of H_2O_2 are sketched in Figure 26. Harmonized frequencies have been published by Khachkuruzov and Przhhevskii²⁰⁷, who examined the available spectroscopic data of H_2O_2 and D_2O_2 . Recent Raman measurements of H_2O_2 vapour²⁰⁸ provide evidence for an O—O stretching frequency, significantly different from liquid- or solid-phase values (Table 26). However, these

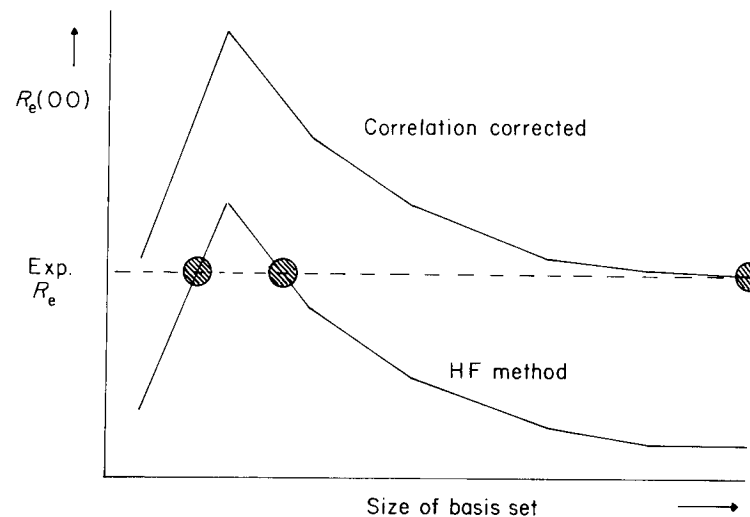
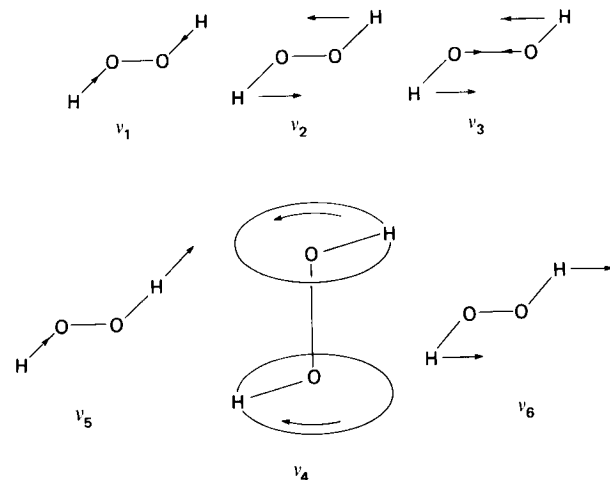


FIGURE 25. Qualitative illustration of the dependence of the theoretical O—O bond length R_e on the size of the basis set and the method. Two 'Pauling points' found for HF/small-basis-set calculations are indicated.

FIGURE 26. Normal modes of vibrational motion for H_2O_2 .TABLE 26. Vibrational frequencies (cm^{-1}) of HO_2 and H_2O_2

Frequency	Character	HO_2			H_2O_2 Exp. ^d
		Exp. ^a	UHF ^b	GVB-CI ^c	
ν_1	OH stretch	3414	3488	3655	3607
ν_2	OOH bend	1389	1357	1416	1393
ν_3	OO stretch	1101	1083	1181	863
ν_4	HOOH torsion				317
ν_5^e	OH stretch				3608
ν_6^e	OOH bend				1266

^aFrom matrix isolation studies, Ref. 209. Recently, $\nu_3 = 1097 \text{ cm}^{-1}$ has been found in the gas phase²¹⁰.

^bScaled UHF/DZdp calculations, Ref. 80.

^cGVB-CI/DZdp values from Ref. 81.

^dRef. 208. In the infrared spectra of liquid and solid H_2O_2 a value of 880 cm^{-1} has been observed for ν_3 .

^eAsymmetric modes of H_2O_2 (Figure 26).

differences are still within the margin of error of theoretical ν values as is revealed by a comparison of *ab initio*^{80,81} and experimental HO_2 frequencies^{209,210} (Table 26).

Theoretical attempts at evaluating absolute infrared intensities of HO_2 (via calculation of derivatives of the dipole moment with respect to the normal modes of vibration)⁸⁰ and H_2O_2 (via determination of a suitable hydrogen atomic tensor)²¹¹ have recently been published. Because of the extreme difficulties of measuring these quantities, the theoretical data, although only accurate to within 50%, help to investigate the existence of H_2O_2 and HO_2 in planetary atmospheres.

A general harmonic *ab initio* force field of H_2O_2 has been calculated by Botschwina, Meyer and Semkow at the HF level of theory¹⁰². Theoretical values of diagonal quadratic force constants are considerably overestimated, e.g. stretching force constants by 10–45%.

Correcting for correlation effects proves as important as in the case of r_e values. Alternatively, diagonal force constants can be adjusted empirically with the aid of observed frequencies. Force constants obtained in this way for H_2O_2 ¹⁰² are compared in Table 27 with experimentally based values published by Khachkuruzov and Przhevalskii²¹².

Trends in theoretical quadratic and cubic force constants of FOH , H_2O_2 , NH_2OH and CH_3OH are extensively discussed by Meyer and coworkers¹⁰². Absolute values of f_{rr} , f_{RR} , f_{rrr} and f_{RRR} increase monotonically from FOH to CH_3OH . The diagonal cubic stretching force constants are negative ($f_{rrr} = -60.8$, $f_{RRR} = -36.7 \text{ aJ } \text{Å}^{-3}$) and dominate the anharmonicity of the potential energy function.

The OO stretching force constants, either experimentally or theoretically determined, clearly indicate the weakening of the OO bond along the series O_2^+ , O_2 , O_2^- , O_2^{2-} or O_3 , O_3^- or O_2 , HO_2 , H_2O_2 . Evidence for these trends is summarized in Table 28, which complements Tables 23 and 24.

F. Charge Density and One-electron Properties

The electron density distribution ρ of H_2O_2 has been computed by *ab initio* methods and analysed with the aid of a Mulliken population analysis^{92,93,96,101,107,215}. Gross atomic charges q and overlap populations p obtained in this way reflect changes of the electron density distribution during rotation around the O—O bond as can be seen from Table 29. They can be used to substantiate the qualitative models discussed in Section IV.B. On the other hand, q and p values have to be interpreted with care since the Mulliken population analysis suffers from serious drawbacks^{216,217}. For certain basis sets $p(\text{OO})$

TABLE 27. Quadratic force constants of H_2O_2 at its equilibrium geometry

Force constant ^a	Exp. (Ref. 212) ^b	<i>Ab initio</i> /empirical (Ref. 102) ^c
f_{rr}	8.311	8.009
f_{RR}	4.493	4.322
f_{aa}	0.696	0.894
$f_{rr'}$	-0.045	-0.020
f_{rR}	0.069	-0.083
f_{ra}	-0.370	-0.040
$f_{ra'}$	-0.002	-0.001
f_{Ra}	0.385	0.605
$f_{aa'}$	0.074	0.079

^aFor reasons of simplicity the symbols designated in the text as $R(\text{OH})$ and $R(\text{OO})$ are abbreviated here to r and R . All values in $\text{aJ } \text{Å}^{-n}$ where n is the number of stretching coordinates involved in the partial differential quotient of the potential energy. $1 \text{ aJ (atto joule)} = 10^{-18} \text{ J} = 1 \text{ mdyne } \text{Å} = 0.2294 \text{ hartree} = 6.24 \text{ eV}$. See I. M. Mills in *Theoretical Chemistry*, Vol. I, The Chemical Society, London, 1974.

^bBased on $\nu_2 = 1390 \text{ cm}^{-1}$ and $\nu_3 = 880 \text{ cm}^{-1}$.

^cLeast squares adjustment to ν values of Table 26; OH vibrations harmonized (ν_1 : +176; ν_5 : +188 cm^{-1}) with anharmonicity constants of H_2O and D_2O : K. Kuchitsu and Y. Morino, *Bull. Chem. Soc. Japan*, **38**, 814 (1965).

TABLE 28. Experimental and theoretical OO stretching force constants of molecules containing the O₂ unit

Molecule	State	f_{RR} (aJ Å ⁻²)		Ref.
		Exp.	Theory	
O ₂ ⁺	² Π _g	16.5		213
O ₂	³ Σ _g ⁻	11.8 ^a	15.2	213, 73
	¹ Δ _g	10.7 ^a	15.1	213, 73
O ₂ ⁻	² Π _g	5.6		214
O ₂ ²⁻	¹ Σ _g ⁺		4.0	182 ^b
O ₃	¹ A ₁	6.2	10.6	184, 73
O ₃ ⁻	² B ₁	3.8 ^c		186
HO ₂	² A''	5.9	7.4	209, 73
H ₂ O ₃	¹ A		6.7	73
H ₂ O ₂	¹ A	4.5	6.3	212, 73

^a $f_e = 5.8883 \times 10^{-7} \mu_a \nu_e$ [aJ Å⁻²]; μ_a = reduced mass.

^bCalculated for Li₂O₂.

^cAssumed.

TABLE 29. Mulliken population analysis of RHF/SVdp calculations on H₂O₂^{a,b}

Parameter	cis	skew	trans
$q(\text{O})$	8.348	8.365	8.371
$q(\text{H})$	0.652	0.635	0.629
$p(\text{OO})$	0.123	0.138	0.128
$p(\text{OH})$	0.599	0.616	0.620
$p(\text{HH})$	-0.019	0.003	0.007

^aAll values in atomic units.

^bFrom Ref. 107.

may even become negative⁹³, which is in clear conflict with the chemical picture of the O—O bond.

Another way of analysing the electron density distribution at the O—O bond is to evaluate the deformation density function (equation 7) as suggested by Daudel and coworkers²¹⁸. In equation (7) $\rho(\mathbf{r})$ is the electron density at a point \mathbf{r} and $\sum \rho^A(\mathbf{r})$ that which would result if the atoms forming the molecule could be added together without perturbing each other. In the case of the O atom the function ρ is not spherical and it is not self-evident how to form ρ^A . One eludes this problem by averaging the electron density of O(³P) over all orientations in space, thus reintroducing spherical symmetry.

$$\Delta\rho(\mathbf{r}) = \rho(\mathbf{r}) - \sum_{\text{ATOM}} \rho^A(\mathbf{r}) \quad (7)$$

Applying this method to O₂, the O lone-pair electrons can be pictured. But at the same time a negative $\Delta\rho(\mathbf{r})$ is found in the internuclear region²¹⁸. This has been interpreted as a result of strong Coulomb repulsion between bonding electrons of O₂, which forces electron density to a region outside the space surrounding the bond axis.

A similar result has been obtained for H₂O₂ by Coppens and Stevens²¹⁹ using the RHF wave function published by Dunning and Winter¹⁰¹. The computed deformation density $\Delta\rho$ is negative in the O—O bond region. This has been verified by X-ray and neutron diffraction studies on H₂O₂¹⁹². On the other hand, a theoretical determination of $\Delta\rho$ for H₂S₂²²⁰ leads to $\Delta\rho > 0$ along the bond axis. Obviously the interpretative value of density difference descriptions is poor in the case of bonds between valence-electron-rich atoms like oxygen.

A more appealing way of analysing ρ has been worked out by Bader and coworkers²²¹⁻²²⁴. It involves the evaluation of the gradient vector field $\nabla\rho(\mathbf{r})$ from *ab initio* (or experimental) electron density functions and the determination of its critical points at which the field vanishes. In Figures 27 and 28 a contour line diagram and the corresponding gradient vector field of **23** are shown²²⁵. All the gradient paths terminating at one of the four nuclei define a subspace of the total molecular space, which can be assigned to the atom in question. There is a saddle point of ρ , at location \mathbf{r}_c between each pair of bonded atoms. This is an O—O or O—H bond critical point of ρ , which serves as the origin for two gradient paths connecting neighbouring nuclei. Together they define the bond path, along which the charge density is a maximum with regard to a lateral displacement. Gradient paths terminating at \mathbf{r}_c form the interatomic surfaces between the O and H atoms²²¹.

In Table 30, $\rho(\mathbf{r}_c)$ and the eigenvalues λ_i ($i = 1, 2, 3$) of the Hessian matrix of ρ at \mathbf{r}_c (O—O) are listed for H₂O₂²²⁵. The negative sign of $\nabla^2\rho(\mathbf{r}_c)$ is indicative of O—O bonding. The curvature of ρ along the internuclear axis is positive ($\lambda_1 > 0$), while it is negative perpendicular to the axis ($\lambda_2, \lambda_3 < 0$). Normally, accumulation of electron density between the nuclei, characteristic of a strengthening of the bond, reduces the

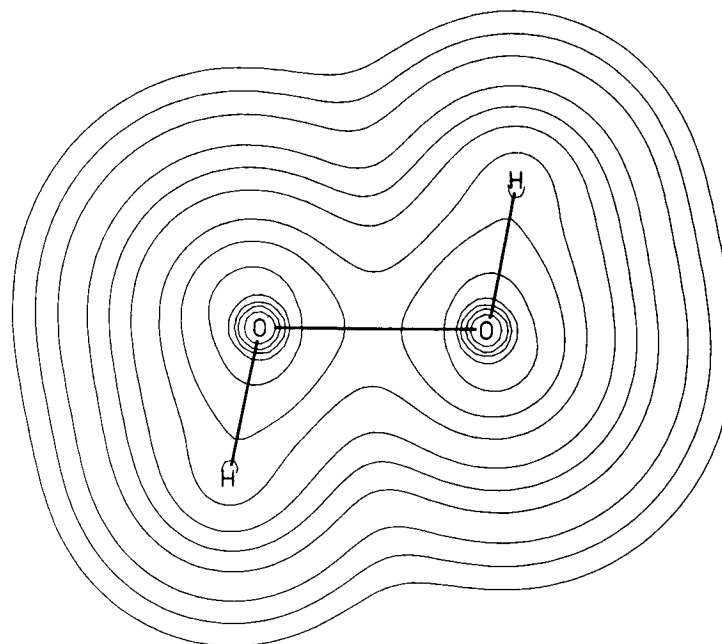


FIGURE 27. Contour plot of $\rho(\mathbf{r})$ for *trans* H₂O₂. (Wave function and geometry from Reference 101.)

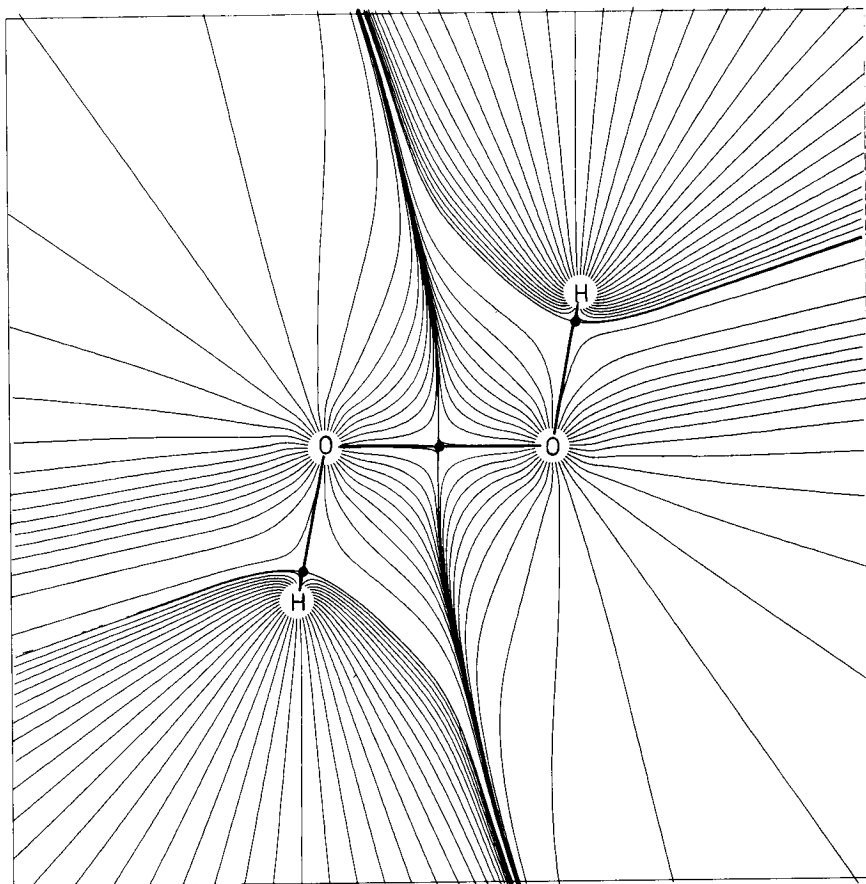


FIGURE 28. Representation of gradient paths of $\rho(\mathbf{r})$ for *trans* H_2O_2 . Bond paths connecting the nuclei are indicated by heavy lines. The bond critical points are marked by dots. (R. F. W. Bader, private communication.)

TABLE 30. Properties of the electron density distribution at the O—O bond critical point of H_2O_2^a

Position $\mathbf{r}_c(\text{OO})$	<i>cis</i> (21)	skew (22)	<i>trans</i> (23)
ρ	0.329	0.352	0.328
$\nabla^2\rho$	-0.225	-0.231	-0.218
λ_1	1.328	1.346	1.323
λ_2	-0.822	-0.807	-0.813
λ_3	-0.730	-0.770	-0.729

^aR. F. W. Bader, unpublished results; geometry and wave function from Ref. 101.

magnitude of λ_1 , thus making $\nabla^2\rho(\mathbf{r}_c)$ more negative. Although both $\rho(\mathbf{r}_c)$ and $\nabla^2\rho(\mathbf{r}_c)$ suggest a maximum of the O—O bond strength for the skewed form, the eigenvalues of the Hessian matrix reveal that the decrease of λ_3 rather than λ_1 influences the value of $\nabla^2\rho(\mathbf{r}_c)$.

In the planar forms $|\lambda_2| > |\lambda_3|$, i.e. a lower curvature perpendicular to the molecular plane signals a 'π-like' nature of the charge distribution in this direction. The fact that at $\tau = 120^\circ$ the value of λ_3 adjusts to that of λ_2 , thus causing the decrease of $\nabla^2\rho(\mathbf{r}_c)$ in skewed H_2O_2 , indicates that 'π-like' charge arranges more uniformly around the O—O bond. This is in line with the MO description of n delocalization discussed in Section IV.B.

Noteworthy is the computed deviation of the O—O bond path from the internuclear axis for $\tau < 180^\circ$. At \mathbf{r}_c a displacement of 0.012 Å for 22 and 0.032 Å for 21 is computed. This is strongly suggestive of the bent-bond picture of strained molecules and, therefore, may be interpreted as increasing strain for τ going to 0° .²²³

RHF calculations close to the HF limit^{107,226} predict a molecular dipole moment μ for skewed H_2O_2 , which is 0.3–0.6 D lower than the experimental value of 2.26 D²²⁷. Although RHF dipole moments cannot directly be compared with vibrationally averaged values, such a large difference is indicative of a sizeable contribution to the theoretical value of μ due to correlation effects. The importance of correlation corrections has been demonstrated in calculations on O_3 ⁴⁹. In this case, RHF theory leads to an overestimation of μ by 0.3 D⁴⁵ while GVB-CI/DZd calculations yield $\mu = -0.54$ D⁴⁹, in line with an experimental value of 0.53 D²²⁸. Recently, a value of 2.0 D has been predicted for HO_2 ⁸⁰.

One-electron properties of H_2O_2 have been determined at various levels of theory^{92,98,106,215}. At present the only quantity which can be compared with an experimental value seems to be the ^{17}O nuclear quadrupole coupling constant K observed in the ^{17}O nuclear quadrupole resonance spectrum of a 90% H_2O_2 solution²²⁹. The calculated K values are 5–15% too large, while the theoretical values of the asymmetry parameter η , which describes how the electric field gradient \mathbf{q} departs from cylindrical symmetry ($0 < \eta < 1$; $\eta = 0$ corresponds to axial symmetry around the principal axis z' , see footnote a of Table 31), exceed the observed value by 20–40% (Table 31).

In Table 32 some selected one-electron properties of skewed H_2O_2 are listed^{98,106}. Although the comparison of values obtained by different methods reveals no dramatic changes, the accuracy of one-electron properties may vary considerably. At least this is suggested by RHF/DZd calculations on O_3 . Rothenberg and Schaefer⁴⁵ have found surprisingly good agreement between experimental and RHF second moments of the electronic charge distribution while, for example, the computed quadrupole moment tensor elements bear little resemblance to experimental values.

TABLE 31. Theoretical and experimental quadrupole coupling constants (MHz) at ^{17}O of H_2O_2

Property ^a	RHF/DZ (Ref. 215)	RHF/MBS ^b (Ref. 98)	RHF/DZdp (Ref. 106)	Exp. (Ref. 229)
$K_{z'z'} = eq_{z'z'}/h$	-17.11	-18.23	-18.70	16.31(7)
η	0.814	0.930	0.953	0.687(11)

^a $Q(^{17}\text{O}) = -0.0256$ barn from H. F. Schaefer, R. A. Klemm and F. E. Harris, *Phys. Rev.*, **176**, 49 (1968). $\eta = (q_{y'y'} - q_{x'x'})/q_{z'z'}$ with $|q_{y'y'}| < |q_{x'x'}| < |q_{z'z'}|$; $q_{x'y'}$, etc. are zero in the principal axes system of H_2O_2 , which is defined in footnote a of Table 32. See T. D. Das and E. L. Hahn, *Nuclear Quadrupole Resonance Spectroscopy*, Academic Press, New York, 1958.

^bMBS calculations with STFs.

TABLE 32. Selected one-electron properties for skewed H₂O₂

Property ^a		RHF/MBS (Ref. 98)	RHF/DZdp (Ref. 106)	APSG ^c (Ref. 106)
Quadrupole moment ^b (10 ⁻²⁶ esu cm ²)	$\theta_{x'x'}$	5.48	5.83	5.64
	$\theta_{y'y'}$	-1.35	-1.34	-1.39
	$\theta_{z'z'}$	-4.12	-4.49	-4.25
	ψ	32.5	36.1	36.7
Electric field gradient at O (10 ⁻¹⁶ esu cm ⁻³) at H	$q_{x'x'}$	0.95	0.98	0.93
	$q_{y'y'}$	0.03	0.02	-0.01
	$q_{z'z'}$	-0.98	-1.01	-0.92
	$q_{x'x'}$	0.10	0.09	0.09
	$q_{y'y'}$	0.07	0.06	0.06
Asymmetry parameter	$q_{z'z'}$	-0.17	-0.15	-0.15
	η^H	0.19	0.20	0.21

^aThe molecular *x* and *z* axes are parallel to the C₂ symmetry axis and the O—O bond, respectively. Primed coordinates denote the principal axes of the tensor. The eulerian angles (ψ , $\varphi = 90^\circ$, $\vartheta = -90^\circ$) relate these axes to the molecular axes.

^bCalculated with the centre of mass as origin.

^cCalculations with the antisymmetrized product of strongly orthogonal geminals (APSG) only consider intrapair electron correlation.

G. Excited States

Because of the importance of O₂ and O₃ in atmospheric chemistry and photochemistry, their excited states have been theoretically studied by various groups^{36,38-40,42,48-50,53,54,230,231}. A detailed discussion of these investigations would go beyond the scope of this chapter. Therefore, just some of the results for ozone are cited here.

Table 33 contains computed vertical transition energies to the excited states shown in Figure 5 (Section III.A.2). MRD-CI results of Thunemann, Peyerimhoff and Buenker⁵³ agree quite well with observed spectral features, while HF calculations lead to a false order of states and an underestimation of excitation energies. Hay, Dunning and Goddard⁴⁸⁻⁵⁰ have reported state diagrams, adiabatic excitation energies, geometries, force constants, frequencies and dipole moments for excited states of bent, cyclic and linear O₃. In a recent MCSCF-CI investigation the potential surface of the ³B₂ state has been explored⁶². This state is found to be bound with an O₂—O binding energy of 0.4 eV.

The importance of the HO₂ radical in atmospheric chemistry has triggered elaborate studies on its excited states only recently. In Table 34, vertical excitation energies and oscillator strengths taken from MRD-CI calculations of Shih, Peyerimhoff and Buenker⁷⁷ and an extensive CI investigation of Langhoff and Jaffe⁷⁹ are compared with the available experimental data²³²⁻²³⁵. Adiabatic potential energy curves for the covalent 1²A', the ionic 2²A" (Figure 4, Section III.A.2) and the ionic 2²A' state, can be found in Reference 79. Covalent or ionic character is reflected by theoretical dipole moments of 4 D (2²A") and 3 D (2²A') as compared with 2.3 D (1²A") and 2 D (1²A')⁷⁹.

In the 1²A' (4π) state the O—O bond is elongated to about 1.41 Å, which causes a decrease of the O—O stretching frequency to 968 cm⁻¹⁷⁹ (exp. 951²³², 881 cm⁻¹²³³). This is indicative of the higher O—O antibonding character of the 2a" MO (Figure 8, Section III.B.2). Shih and coworkers⁷⁷ have calculated a radiation lifetime of the 1²A' state of $\tau_{1/2} = 7.6 \times 10^{-3}$ s as compared with 1.1×10^{-3} s found by Langhoff and Jaffe⁷⁹ and Buenker and Peyerimhoff⁷⁵.

TABLE 33. Calculated vertical transition energies (eV) of ozone^a

No.	State	Excitation	HF	MRD-CI	Exp. ^b
			DZb + diff		
1	1 ¹ A ₁ (4π)	... 1a ₂ ² , 4b ₂ ² , 6a ₁ ²	0	0	0
2	1 ³ B ₂ (4π)	1a ₂ → 2b ₁	-2.27	1.20	Peaks at 1.29, 1.43, 1.55, 1.67, 1.80, 1.92 eV
3	1 ³ A ₂ (5π)	4b ₂ → 2b ₁	0.73	1.44	
4	1 ³ B ₁ (5π)	6a ₁ → 2b ₁	0.69	1.59	
5	1 ¹ A ₂ (5π)	4b ₂ → 2b ₁	1.18	1.72	
6	1 ¹ B ₁ (5π)	6a ₁ → 2b ₁	1.51	1.95	2.1 (Chappuis)
7	2 ³ B ₂ (6π)	4b ₂ , 6a ₁ → 2b ₁ ²	-0.55	3.27	3.5-4.2 (Huggins)
8	2 ¹ A ₁ (6π)	36% 4b ₂ ² → 2b ₁ ² + 45% 6a ₁ ² → 2b ₁ ²		3.60	
9	1 ¹ B ₂ (4π)	1a ₂ → 2b ₁	3.73	4.97	4.86 (Hartley)
10	3 ¹ A ₁ (4π)	50% 1a ₂ ² → 2b ₁ ² + 23% 1b ₁ → 2b ₁		7.60	
11	2 ³ A ₂ (5π)	6a ₁ , 1a ₂ → 2b ₁ ²	4.38	5.58	
12	2 ³ B ₁ (5π)	4b ₂ , 1a ₂ → 2b ₁ ²	4.98	6.50	
13	2 ¹ A ₂ (5π)	6a ₁ , 1a ₂ → 2b ₁ ²	5.10	6.37	
14	2 ¹ B ₁ (5π)	4b ₂ , 1a ₂ → 2b ₁ ²	6.14	7.26	7.18

^aRef. 53. Calculated at $R = 1.277$ Å and $\alpha = 116.8^\circ$ with a DZ basis augmented by bond functions and diffuse Rydberg functions.

^bFor quotations of the experimental work see Ref. 53.

TABLE 34. Vertical excitation energies (eV) and oscillator strengths for HO₂

State	Excitation	Vertical excitation energies			Oscillator strength (Ref. 77)
		Ref. 79	Ref. 77	Exp.	
1 ² A" (3π)	... 7a' 2a" 1	0	0	0	0
1 ² A' (4π)	7a' → 2a"	1.02	0.93	0.88 ^c , 0.87 ^b	3.9 × 10 ⁻⁶
2 ² A" (3π)	1a" → 2a"	6.26	5.90	5.9-6.2 ^c	0.065
2 ² A' (4π)	6a' → 2a"	6.73	6.49		0.0012

^aRef. 232.

^bRef. 233.

^cRefs. 234 and 235.

According to Table 34 the UV spectrum of HO₂ is dominated by a single continuous feature corresponding to the 2²A" ← 1²A" transition with a peak near 2100 Å. The 2²A' ← 1²A" transition is far too weak to be observed. Theory suggests that if the 1²A' state is appreciably populated, it may be possible to observe photoabsorption at about 2500 Å corresponding to the 2²A' ← 1²A' transition.

Some excited states of H₂O₂ have been investigated by Rauk and Barriol²³⁶ with the aid of perturbative CI calculations. Only singly excited configurations were considered and an empirical correction for correlation and orbital relaxation effects applied. This was based on the assumption that computed Rydberg state energies of H₂O₂ may suffer from an error similar in magnitude to that found for the Koopmans' value $-\epsilon_i$ of the occupied MO ϕ_i from which excitation takes place²³⁶ (equation 8), where I^{exp} is the experimentally observed vertical IP.

$$\Delta E_{\text{cor}} = \Delta E_{\text{calc}} + I_i^{\text{exp}} + \epsilon_i \quad (8)$$

In Table 35 results of Rauk and Barriol²³⁶ are summarized. The experimental UV spectrum of H₂O₂ lacks any absorption bands below 6.7 eV (1850 Å)²³⁷. The absorption increases towards 10.3 eV (1200 Å) where the spectrum becomes obscured due to H₂O contamination. There is a single broad maximum at 7.5 eV (1650 Å) and the suggestion of a shoulder at 7 eV (1770 Å). Corrected excitation energies for the third and fourth singlet states, ¹B and ¹A, are of comparable magnitude (Table 35). These states arise from excitation to a bonding (a symmetry) combination of the 3s(O) orbitals and, hence, should be bound states.

Excitation to the corresponding antibonding combination (b symmetry) from the n MOs yields two states in the 4–6 eV region, which are probably dissociative. Rauk and Barriol²³⁶ assume on the basis of the higher oscillator strength of the ¹B state that photolytic decomposition of H₂O₂ occurs via this state. Rupture of the O—O bond of alkyl peroxides has been observed in the first absorption region, 3100–2500 Å, while below 2300 Å C—O rupture appears as a new primary dissociative mode²³⁸.

Rupture of the O—O bond in peroxides has been classified by Dauben, Salem and Turro²³⁹ as being of the tetratopic (σπ)(σπ) type, thus yielding the four pairs of diradical states shown in Figure 29. In the case of H₂O₂, only the GS is bonding while the three excited S states and all the T states are repulsive in nature. These states correlate with the GS of two OH radicals as has been confirmed by Evleth on the basis of CNDO-CI calculations^{240,241}. The key to this correlation lies in the doubly degenerate character of the ²Π ground state of OH, which leads in double combination to four S and four T states. This eightfold energetic degeneracy is an essential feature of O—O bond rupture. It is responsible for an extreme complexity of surfaces in O—O dissociation processes of larger peroxides.

TABLE 35. Vertical excitation energies and oscillator strengths for H₂O₂^a

State	Excitation ^b	Energy (eV)			Oscillator strength
		ΔE _{calc}	ΔE _{cor} ^c	ΔE _{exp}	
¹ A	n(4b) → 3sσ*	6.2	4.0		0.0013
¹ B	81% n(5a) + 14% n(4a) → 3sσ*	7.5	5.6		0.0207
¹ B	n(4b) → 3sσ	9.1	6.9	7.0	0.0054
¹ A	73% n(5a) + 16% n(4b) → 3sσ	9.7	7.8	7.5	0.0078
¹ A	15% n(5a) + 72% n(4b) → 3sσ*	10.5	8.3		0.0131
¹ B	71% n(4b) + 20% n(4a) → 3pπ	11.1	8.9		0.1371
¹ B	n(5a) → 3pπ*	11.2	9.3		0.0388

^aRef. 236. Computed at R = 1.475 Å, R' = 0.95 Å, α = 94.8°, τ = 111.5° with a DZ basis augmented by diffuse Rydberg functions.

^bFractional excitations out of more than one occupied MO are given in percent. Rydberg character of excited states is indicated. Note that valence or Rydberg character of computed states also depends on the inclusion of double excitations. Compare with Ref. 241.

^cCorrection for n(4b) calculated with ε = -13.71, I_{vert} = 11.4 eV and for n(5a) with ε = -14.47 and I_{vert} = 12.56 eV (Ref. 236).

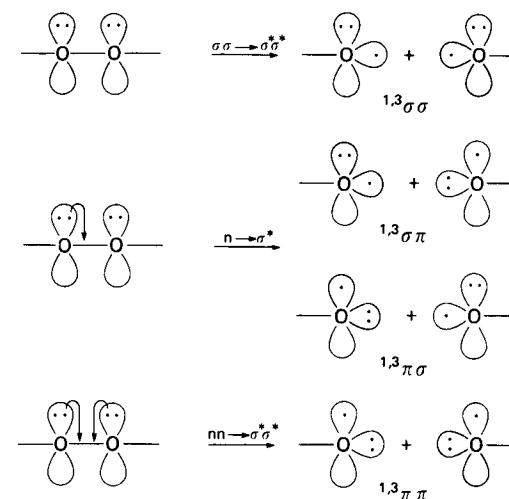


FIGURE 29. Photoexcitation and dissociation of H₂O₂. Mode of excitation and diradical states of OH fragments are given.

V. SUBSTITUENT EFFECTS

A. General Trends

1. Peroxy compounds XO₂

Apart from the parent compounds HO₂ and O₃ only scattered data on XO₂ peroxides are available. Experimental and/or theoretical investigations on structure and bonding in LiO₂^{182,214,242–246}, MeO₂²⁴⁷, NH₂O₂²⁴⁸, HO₃ (X = HO)^{73,249}, FO₂^{189,250–252} and ClO₂²⁵³ with monovalent X have been reported. As for XO₂ systems with divalent X, most attention has been focused on carbonyl oxide and dioxirane^{58,67,69,254–259} because of their important role in the ozonolysis¹² and other oxidation reactions of hydrocarbons¹³. Dioxirane has recently been detected by microwave spectroscopy in the low-temperature reaction of O₃ with ethylene³³. Other theoretical investigations considered the bent or cyclic form of NOO^{260,261}, NOO⁻²⁶² and HNOO^{67,263,264}.

When varying the monovalent substituent X from F to Li, the O—O bond strength decreases. This is reflected by corresponding changes in the bond distance, stretching frequency and force constant (e.g. $f_{RR} = 10.5, 9.7, 5.6 \text{ aJ } \text{Å}^{-2}$ for X = F²⁵⁰, Cl²⁵³ and Li¹⁸²). Spratley and Pimentel²⁶⁵ have suggested that—depending on the electronegativity of X—electron charge is either withdrawn from or donated to the antibonding π_g MO of O₂, thus strengthening or weakening the OO bond. This description has been corroborated by McCain and Palke²⁵², who have investigated trends in electron spin g values for peroxy radicals on the basis of *ab initio* calculations on HO₂ and FO₂. They consider bonding in XO₂ to result from Lewis acid–base reactions between a diamagnetic group X and a O₂⁺ or O₂⁻ radical. The unoccupied π_g MO in O₂⁺ is an electron acceptor which acts as a Lewis σ acid, whereas the filled level of O₂⁻ is an electron donor or Lewis σ

base. In addition, the open shell π_g MO on either O_2^+ or O_2^- can act as a Lewis π acid or base toward a π orbital on X.

Strong acid–base interactions lead to relatively strong XO bonding. Conversely, weak interactions lead to ionic bonding. The latter situation obtains when X is a weak σ/π donor ($X = BF_4^-, AsF_6^-$) or a weak σ/π acceptor ($X = Li^+, Na^+$). Accordingly, ionicity of the XO bond is revealed by OO bond features typical for O_2^+ or O_2^- .

This prediction has been verified in the case of LiO_2 . Bonding between Li and O_2 is essentially ionic with at least 0.77 e transferred from the alkali metal to the O_2 moiety²⁴⁶. In order to maximize Coulomb attraction between a positively charged Li and the negatively charged O atoms, the molecule adopts the C_{2v} , symmetrical cyclic structure **2**. This has been confirmed by matrix IR measurements^{214,242,243} and *ab initio* calculations^{244–246} ($R = 1.30 \text{ \AA}$, $R' = 1.77 \text{ \AA}$, $\alpha = 68.5^\circ$, $\alpha' = 43^\circ$ ²⁴⁶; $\nu_1(O-O \text{ stretch}) = 1097 \text{ cm}^{-1}$ ²¹⁴; compare with Tables 9 and 23 of Section IV). Alkali-metal superoxides all seem to prefer structure **2** since the ionic character varies only slightly for $X = Li, Na$ (maximum), K, Rb, Cs , as is indicated by the corresponding O–O stretching frequencies²⁴³.

For $X = BeH$ or BH_2 the equilibrium geometry should also correspond to an isosceles triangle, yet with less ionic X–O bonding character. This, at least, is suggested by the relative energies of XO_2 peroxides with divalent X (Table 36), which we have calculated in order to compare OO bonding in these compounds at a consistent level of theory²⁶⁶. From Be to F^+ the energy difference ΔE between bent (linear) and cyclic XO_2 increases steadily from -80 to 80 kcal mol^{-1} , i.e. for $X = Be, BH$ and CH_2 structure **2** is more stable than **1**, while for $X = NH, O$ and F^+ the reverse is true (see Table 6, Section III.B.3). Cyclic NO_2^- with $\Delta E = 27 \text{ kcal mol}^{-1}$ ($R = 1.47 \text{ \AA}$, $R' = 1.50 \text{ \AA}$, $\alpha' = 59^\circ$)²⁶² nicely fits into this trend. Parallel to the increase in ΔE , the O–O bond length R and the angle α of structures **1** and **2** decrease. Again, this is indicative of a stepwise depopulation of the π_g MOs of O_2^- and a smooth change from ionic to covalent XO bonding. For example, the charge of the O_2 moiety changes from a surplus of 0.55–0.65 e for Be and BH to a lack of 0.13 e for F^+ .

It is interesting to note that peroxyntrene, HNO_2 , prefers the *syn* form by about 2 kcal mol^{-1} , probably due to Coulomb attraction between H and the terminal oxygen atom²⁶⁶. A similar effect has been found for alkyl-substituted carbonyl oxides^{58,267}.

TABLE 36. Energies and geometries of some XO_2 peroxides calculated at the RSMP/SVd level of theory^{58,266}

No. of valence electrons	No. of π electrons ^a	Molecule	Abs. energy ^b (hartree)	Geometry ^b			ΔE^c (kcal mol ⁻¹)	Geometry ^c		
				R (Å)	R' (Å)	α (deg.)		R (Å)	R' (Å)	α' (deg.)
20	8/4	BeOO	-164.5230	1.34	1.33	180	-82	1.66	1.44	70
22	8/4	HBOO	-175.2611	1.36	1.21	180	-70	1.62	1.37	72
24	4/6	H_2COO^d	-189.0528	1.29	1.30	120	-34	1.53	1.40	66
24	4/6	HNOO	-205.0625	1.27	1.38	119	10	1.49	1.45	62
24	4/6	OOO ^e	-224.8768	1.31	1.31	116	35	1.48	1.48	60
24	4/6	FOO ⁺	-248.9809	1.28	1.33	113	78	1.43	1.59	54

^aNumber of π electrons in the chain/cyclic state.

^bAbsolute energy and geometry (linear or bent) of chain structure **1**.

^cRelative energy and geometry of cyclic structure **2**. The angle OXO is denoted by α' .

^d r_e geometry of dioxirane: $R = 1.516 \text{ \AA}$, $R' = 1.388 \text{ \AA}$, $\alpha' = 66.2^\circ$ ³³.

^e r_e geometry of ozone: $R = 1.2716 \text{ \AA}$, $\alpha = 117.79^\circ$ ⁷⁰.

There, through-space interactions between a pseudo- π orbital of a methylene group and the $2p\pi$ AO of the terminal O atom (homoaromatic 6π system) can lead to additional stabilization of the *syn* forms. In this respect, the configurational and conformational preferences of carbonyl oxides may be considered to represent examples of the *cis* effect²⁶⁷.

Rupture of the XO or OO bond in the acyclic GS of XO_2 leads to $XO(^3P\sigma)$ and $O(^3P)$ or $X(^3\Pi\sigma)$ and $O_2(^3\Sigma_g^-)$ (compare with Figure 5, Section III.A.2). In the case of carbonyl oxide, these processes have been calculated to require about 43 and 56 kcal mol^{-1} , respectively²⁵⁴. Hence, the 4π state of H_2CO_2 is stable with respect to dissociation although it is actually higher in energy than $H_2CO(^1A_1) + O(^3P)$. Because of the high reactivity of carbonyl oxide in the presence of electrophilic, nucleophilic or dipolarophilic agents, there is only indirect evidence for its existence¹².

2. Peroxides $XOOH$ and $XOOX$

A number of theoretical investigations have been carried out in order to establish equilibrium geometry and conformational behaviour of closed-shell peroxides. To be mentioned are *ab initio* studies on the hydroperoxides $LiOOH$ ²⁶⁸, $MeOOH$ ^{100,150,269}, $EtOOH$ ²⁷⁰, $PhOOH$ ²⁷¹, CF_3OOH ¹³⁶, NH_2OOH ¹⁵⁰, $HOOOH$ ^{73,150,272,273}, $FOOH$ ^{100,150} and the peroxides $LiOOLi$ ^{182,246,267,274,275}, $NaOONa$ ²⁷⁵, $KOOK$ ²⁷⁵, BH_2OOBH_2 ²⁷⁶, $MeOOMe$ ²⁷⁷, CF_3OOCF_3 ²⁷⁷, CF_3OOF ¹³⁶, $HOOOOH$ ²⁷² and $FOOF$ ²⁷⁸. We have supplemented these investigations by RHF/SV calculations on $XOOH$ and $XOOX$ varying X systematically from Li to F²⁶⁶. Our results are condensed into Table 37.

Almost all hydroperoxides adopt a bent–bent form. Exceptions are $LiOOH$ and $HBeOOH$ which seem to prefer a linear–bent form with a positively charged X ($\sim +0.7 e$) and a bent OOH moiety with some anionic character. However, the stability of the bridged forms may be underestimated by as much as 20 kcal mol^{-1} (compare with RSMP/SVdp results for H_2O_2 , Table 10, Section IV.A) due to basis set and correlation errors at the RHF/SV level. Accordingly, the bridged form of $LiOOH$ is likely to be the most stable one as has been suggested by Peslak²⁶⁸.

If both hydrogens are replaced by Li or BeH, the stability of the bridged form increases. This is in line with experimental^{180,214} and theoretical results^{182,246,268,274,275} on alkali-metal peroxides. For Li, Na and K, the planar rhombic form is the most stable one since it minimizes Coulomb repulsion between the positively charged metal atoms. Puckering leads to an energy increase^{266,274}. Obviously, the electrostatic factor outweighs stabilizing orbital interactions found for the puckered form of H_2O_2 . As soon as the ionic character of the X–O bond is reduced, puckering will lead to stabilization. This is true for the persulphide analogue of Li_2O_2 ²⁷⁴, namely Li_2S_2 , which is more stable in the puckered geometry (puckering angle $\delta = 53^\circ$ ²⁷⁴; compare with Table 10). According to RHF/SV calculations the planar form is destabilized by $1.7 \text{ kcal mol}^{-1}$ ²⁷⁴.

On the other hand, increased covalent bonding between X and O leads to destabilization of the bridged forms. For $X = NH_2, OH$ and F the bicyclic forms open to monocyclic forms with very weak O–O interactions. Their relative energy is considerably larger than the usual O–O dissociation energies (Table 16, Section IV.C). For example, ΔE of $\overset{\cdot}{O}FO\overset{\cdot}{F}$ is 2.5 times larger than $D_0(FO-OF)$ (ca. 62 kcal mol^{-1} ²⁷⁹). This holds also for the linear geometries, which represent the most unstable peroxide forms of Table 37. Their relative energy increases steadily from $X = Li$ towards $X = F$, probably because of enhanced repulsion between electron lone pairs.

The data of Table 37 suggest that Y forms are stable under certain experimental conditions. The relative energies of the planar geometries represent an upper limit of their

TABLE 37. Absolute and relative energies (in hartree and kcal mol⁻¹) of hydroperoxides XOOH and peroxides XOOX calculated at the RHF/SV level of theory for optimized geometries²⁶⁶

Structure (geometry)	H	Li	BeH	BH ₂	CH ₃	NH ₂	OH	F
XOOH								
Bent-bent (<i>trans</i>)	-157.4631 ^a	-165.2282 ^a	-175.8255	-189.5311	-205.4516	-225.2052	-249.1634	
Bridged (planar)	17	23	59	115	60	81	61	
Linear	59	67	110	143	167	180	210	
XOOX								
Bent-bent (<i>trans</i>)	-150.5599	-164.3484 ^b	-179.9047 ^c	-201.0896	-228.5023	-260.3441	-299.8534	
Y (planar)	26	Nonstable ^d	29	28	49	34	39	
Bridged (planar)	88	-48	-33	36	155	133	155	
Linear	144	0	3	78	143	209	271	

^aEnergy of linear-bent form.

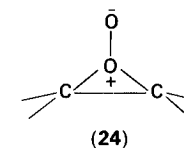
^bEnergy of linear form.

^cEnergy of *cis* form.

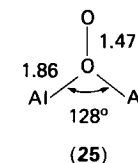
^dGeometry collapses to bridged form.

actual stability since pyramidalization and solvent effects will decrease this energy. The first experimental evidence for the existence of Y forms was found in persulphide chemistry. Kuczowski²⁸⁰ identified by microwave and mass-spectrometric studies two stable F₂S₂ isomers, namely FSSF and F₂SS, the latter with pyramidal geometry. Recent *ab initio* calculations of Hinchliffe²⁸¹ suggest that a H₂SS isomer may also exist.

In connection with the reaction of ¹O₂ with alkenes, the intermediacy of the peroxirane **24** has been discussed^{10,11}. Dewar and Thiel²⁸² have predicted the formation of **24** on the basis of MINDO/3 calculations. However, more recent GVB/CI²⁸³ and HF investigations²⁸⁴⁻²⁸⁶ indicate that **24** is much higher in energy than other possible reaction intermediates.



Unambiguous evidence for the existence of a peroxide with Y structure has recently been given by Atwood and coworkers²⁸⁷. They have synthesized the stable complex [K·dibenzo-18-crown-6] [Al₂Me₆O₂], which according to X-ray measurements contains the Y structure **25** with normal AlO single bonds and a long O—O bond. Since $\nu(\text{O—O})$ of **25** (851 cm⁻¹) is similar to the O—O stretching frequency found for hemerythrins (844 cm⁻¹)²⁸⁸, a group of oxygen-carrying proteins, it is likely that **25** models the bonding situation in these compounds²⁸⁷.



Additional information about the influence of the group X is provided by the RHF/SV bond separation energy (*BSE*) of formal reactions leading to H₂O₂ and XOH (Table 38). Positive *BSEs* are indicative of stabilizing bond interactions, probably via an electron transfer of the type



TABLE 38. RHF/SV bond separation energies (kcal mol⁻¹) of the formal reactions (1), (2) and (3)^a

Bond separation reaction for X =	Li	BeH	BH ₂	CH ₃	NH ₂	OH	F
(1) XOOH + H ₂ O → H ₂ O ₂ + XOH	-3.2	-19.2	-1.6	5.7	5.3	4.7	3.1
(2) XOOX + 2 H ₂ O → H ₂ O ₂ + 2 XOH	30.5	0.5	-4.1	11.3	11.1	4.8	1.0
(3) XOOX + H ₂ O ₂ → 2 XOOH	36.9	38.9	-0.9	-0.1	0.5	-4.6	-5.2

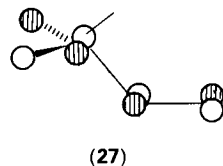
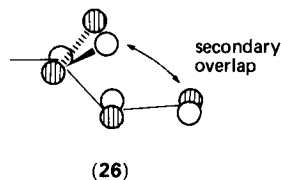
^aGeometries of molecules XOH and XOOX have been completely optimized at the RHF/SV level²⁶⁶. *BSE* values at standard geometries are 6.0, 7.8, 9.3 and 6.3 kcal mol⁻¹ for XOOH with X = CH₃, NH₂, OH and F, respectively¹⁵⁰.

involving π -type donation and σ - or π -type acceptance of electrons as shown in Figure 21 of Section IV.B. These stabilizing interactions are smaller for X^1OX^2 than for $X^1CH_2X^2$ or X^1NHX^2 ¹⁵⁰. An electropositive substituent like Li, BeH or BH₂ leads to destabilization, which, however, is partially offset by attractive Coulomb interactions, especially if a second Li or BeH substituent is attached to the O—O group. Disproportionation of XOOX (reaction 3 of Table 38) becomes more likely with increasing electronegativity of the substituent X. In this case the BSEs decrease rather than double upon going from XOOH to XOOX (reactions 1 and 2 of Table 38).

The σ, π interactions discussed in Section IV.B and illustrated in Figure 21 are primarily responsible for stabilization of skewed forms of peroxides. The equilibrium angle τ is close to 90° if X is both a π donor and a strong σ acceptor like OH or F (dominance of V_2 term in equation 1, Section IV.B). However, if X is a σ electron donor with weak π acceptor property, repulsion between bond dipoles $+X-O^-$ leads to a shift of the conformational minimum towards 180° (dominance of V_1 term). These trends are confirmed by the geometrical data of Table 39 which provides a comparison between peroxide and persulphide geometries determined by gas-phase measurements or *ab initio* calculations.

Noteworthy are the changes in R for increasing electronegativity of the group X. The O—O and S—S bond lengths in the difluoro derivatives are abnormally short, being close to bond lengths in O₂ (1.207 Å, Table 23) and S₂ (1.888 Å, Reference 281). A simple explanation in descriptive VB terms is that structures like $F^-O=O^+F$ and $F^-S=S^+F$ are very important. *Ab initio* theory is presently unable to reproduce the experimental R values of F₂O₂ and F₂S₂ (see Table 39).

If the substituent X possesses a low-lying unoccupied π^* or pseudo- π^* orbital, secondary overlap with the occupied π^* MO of the peroxy group will increase stabilizing two-electron interactions. This explains why conformation **26** rather than **27** is more stable for methyl- or amino-peroxides²⁶⁶.



B. Special Compounds

1. Peroxy acids and acyl peroxides

The structure of organic peroxy acids poses some interesting questions. IR measurements have led to the proposal of a planar conformation of the $-C(O)OOH$ moiety with a *cis-cis* (**28**) rather than a *cis-trans* (**29**) geometry, the former being stabilized by an intramolecular hydrogen bond. Recent RHF/SV calculations of the harmonic and anharmonic force field and the fundamental frequencies of performic acid published by Bock, Trachtman and George²⁹³ add support to this argument as do *ab initio*

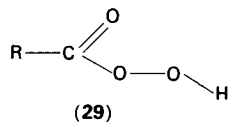
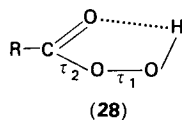


TABLE 39. Comparison between experimental and theoretical geometries (distances in Å, angles in deg.) and barriers for internal rotation (kcal mol⁻¹) obtained for some peroxides and persulphides

Molecule	Geometry			Barriers (<i>trans</i> ; <i>cis</i>)	Method ^d	Ref.
	R	R'	α			
HOOH	1.464	0.965	99.4	120.0	IR, MW	197, 122
CH ₃ OOH	1.46 ^b	1.43 ^b	109.5 ^b	140	RHF/SV	100
CF ₃ OOH	1.447	1.376; 0.974	107.6; 100 ^b	95 ^b	ED	124
HOOOH	1.436	1.404; 0.96 ^b	109.5; 109.5 ^b	90 ^b	RHF/SV	136
FOOH	1.442	0.98	106.1; 100.3	78.5	RSMP/SV ^d	272
CM _{e3} OO _{e3}	1.419	1.441; 0.960	104.5; 104.2	81.8	RHF/SV	266, 100
CF ₃ OO _{e3}	1.480 ^b	1.460	103.9	165.8	ED	123
CF ₃ OO _F	1.419	1.399	107.2	123.3	ED	185
CF ₃ OO _{Cl}	1.366	1.419; 1.449	108.2; 104.5	97.1	ED	124
SiMe ₃ OO _{SiMe₃}	1.417	1.423; 1.440	110.0; 105.0	97	RHF/SV	136
SF ₅ OO _{SF₅}	1.447	1.372; 1.699	108.1; 110.8	93.2	ED	124
FOOF	1.480	1.681	106.6	143.5	ED	123
	1.447	1.667	101.2	136.5	RHF/SV	289
	1.47	1.66	105	107	ED	127
	1.217	1.575	109.5	87.5	MW	126
	1.395	1.432	104.7	83.6	RHF/SV	278
	1.29	1.49	109.5 ^b	87.5 ^b	CI/DZd ^d	278
HSSH	2.055	1.327	91.3	90.6	MMW	128
CH ₃ SSCH ₃	1.922	1.298	95.9	90.7	RHF/FSGO	290
CH ₃ SSC ₂ H ₅	2.022	1.806	104.1	83.9	ED	129
	2.029	1.816	103.2	85.3	ED	130
	2.031	1.817 ^c	103.2 ^c	84.4	ED	130
FSSF	2.030	1.821 ^c	104.0 ^c	83.5	MM	291
CISSCI	1.888 ^e	1.635	71.7	87.9	MW	280
BrSSBr	1.97	2.07	107	82.5	ED	292
	1.98	2.24	105	83.5	ED	292

^aIR = infrared, ED = electron diffraction, MW = microwave, MMW = millimetre-wave, MM = molecular mechanics.

^bAssumed values.

^cAveraged values.

^dOnly O-centred polarization functions used.

^eRHF/DZd: 1.957 Å, Ref. 281.

investigations on peroxyacetic acid^{294,295} and peroxytrifluoroacetic acid²⁹⁵. Another RHF/SV study²⁹⁶ on performic acid, however, has described **29** to be more stable than **28** by about 1 kcal mol⁻¹, the two forms being separated by a rotational barrier of less than 2 kcal mol⁻¹.

Since none of these studies has employed an augmented basis set, care has to be taken when referring to the published *ab initio* results. On the other hand, both theory and experiment clearly establish the *cis* conformation of the O=C—O—O fragment. The *cis* arrangement is stabilized by secondary overlap effects between the π^* orbitals of C=O and O—O, similar to those encountered in methyl- or amino-peroxides (Section V.A). These overlap effects are also responsible for an equilibrium value of τ_1 equal to 0 or 180°.

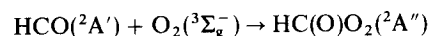
Organic peroxy acids convert alkenes to oxiranes by an electrophilic attack on the double bond. The *cis-cis* form (**28**) plays an important part in the epoxidation reaction. Exploratory RHF/MBS calculations by Plesničar and coworkers^{297,298} on the oxidation of ethylene and methylenimine with performic acid suggest that the reaction is characterized by an asymmetric but highly ordered transition state and an intramolecular transfer of the proton. Since the O atoms of **28** all bear negative charges, it has been argued²⁹⁵ that the electrophilic attack is overlap- rather than charge-controlled. The availability of a low-lying peroxide σ^* MO, especially in compounds like peroxytrifluoroacetic acid, is in line with this reasoning.

A low-lying σ^* MO of the peroxy group seems to play a similar role in the radical-induced decomposition of dibenzoyl peroxide:



Semiempirical MINDO-CI calculations²⁹⁹ on the decomposition of diformyl peroxide (DFP) reveal that a charge transfer from the SOMO of the radical to the LUMO of DFP (σ^*_{OO}) is very important in the TS of the reaction. Therefore, an electron-withdrawing substituent at the acyl group and an electron-donating group at the radical enlarge the charge transfer and, hence, speed up the reaction.

Some of the attention, which acyl peroxides and acylperoxy radicals have received in the past years, has stemmed from their role in the chemistry of polluted atmospheres^{17,18,300}. In photochemical smog, the latter are formed in a rapid reaction between O₂ and an acyl radical. This can lead to the ²A' excited state rather than the ²A" GS of the peroxy radical (Figure 4, Section III.A.2). HF/DZ calculations on the formylperoxy radical (FPR)³⁰¹ show that the reaction



is exothermic by 36 kcal mol⁻¹ whereas the ²A" → ²A' excitation energy is lower than 20 kcal mol⁻¹. In the ²A' state the SOMO is in the right position to facilitate H migration (Figure 4) and, hence, the decomposition to CO₂ and an OH radical. This mechanism is in line with the observed generation of methoxy radicals from acetyl radicals via MeC(O)O₂(²A')³⁰².

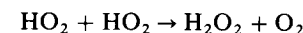
2. Polyoxides

The structural and conformational features of the polyoxides H₂O_n and their F, Me and CF₃ derivatives are affected by *n* electron-pair interactions^{272,273,277,303}. The determining electronic factor is the tendency of a *n* electron pair to delocalize into a coplanar vicinal bond (Section IV.B). This leads to stable *helix* conformations of H₂O_n with dihedral angles of 80–90° (Figure 30), as has been demonstrated by *ab initio* calculations^{272,273,277}.

For H₂O₃ the theoretically determined conformational surface²⁷³, spanned by two rotational angles τ_1 and τ_2 , is shown in Figure 31 in form of a contour-line diagram. Least-

energy paths connecting the potential minima (two global minima, GMIN, at $\tau_1 = \tau_2 = 78^\circ$ and -78° corresponding to helix forms of H₂O₃; two local minima, LMIN, at $\tau_1 = \pm 92^\circ$, $\tau_2 = \mp 92^\circ$ corresponding to forms with both OH bonds either above or below the heavy-atom plane) are shown by dashed lines. There are barriers of 6.5 kcal mol⁻¹ (S points in Figure 31), which have to be surmounted to convert one GMIN form into the other. This interconversion corresponds to successive rotations of the OH bonds through the heavy-atom plane (*flip-flop* rotation, see Figure 32). It needs 16 kcal mol⁻¹ less energy than synchronous rotation of the OH bonds. Flip-flop rotations are the preferred conformational modes of geminal double rotors since they involve only smooth changes of the electronic structure and, hence, the geometry of the rotor molecule as has been demonstrated extensively for H₂O₃ (see Figures 12, 13 and 14 in Reference 273). If flip-flop rotations of adjacent bonds of a cyclic compound are coupled, ring pseudorotation results. Pseudorotation generally requires less energy than ring-inversion³⁰⁴, which can be understood by inspection of Figures 31 and 32²⁷³.

Tetroxides are probably intermediates in the self-reaction of peroxy radicals. Experimental observations suggest that the gas-phase reaction between HO₂ radicals:



proceeds via a H₂O₄ conformer with an intramolecular hydrogen bond³⁰⁵. (Actually, a double hydrogen-bonded association complex could not be excluded by experiment.) Such a conformer is probably 6 kcal mol⁻¹ less stable than the helix conformation of H₂O₄²⁷². Both ¹⁸O labelling experiments³⁰⁵ and semiempirical CI calculations³⁰⁶ exclude a four-centre TS involving a H₂O₄ conformer with strong *n* pair repulsions.

The observation of the isotopic exchange reaction between ¹⁶O₂ and ¹⁸O₂ has led to the proposal of a four-membered oxygen ring^{307,308}. According to *ab initio* calculations⁴⁷ the formation of O₄ is endothermic ($\Delta E > 30$ kcal mol⁻¹). This holds also for the hypothetical O₅ ring formed from O₃ and ¹O₂²⁶⁶. The average O—O bond length in O₅ would be 1.46 Å while the actual bond lengths range from 1.43 to 1.48 Å. The ring is expected to be strongly puckered and, like cyclopentane, a free pseudorotor²⁶⁶.

Knowledge on HO_{*n*} (*n* > 3) molecules is meagre. Recent experiments have revealed the existence of HO_{2*n*}⁺ ions³⁰⁹. UHF/SV calculations³¹⁰ show that these are clusters of O₂ molecules sharing a common proton.

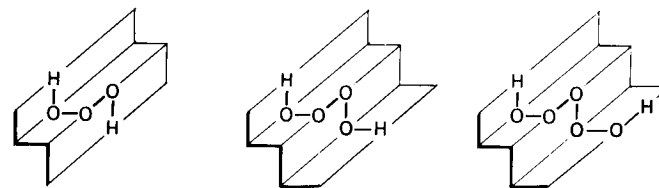


FIGURE 30. Helix conformation of H₂O₃, H₂O₄ and H₂O₅.

3. Ozonides and other cyclic peroxides

Interactions between the *n* electron pairs of oxygen influence the geometry and conformation of cyclic peroxides. If the size of the ring implies a small value of τ , the O—O bond turns out to be rather long. For example, dioxirane contains one of the longest O—O bonds so far observed³³. With increasing ring size, the cyclic peroxide can pucker more strongly. Accordingly *n*-pair delocalization as described for alicyclic peroxides becomes a

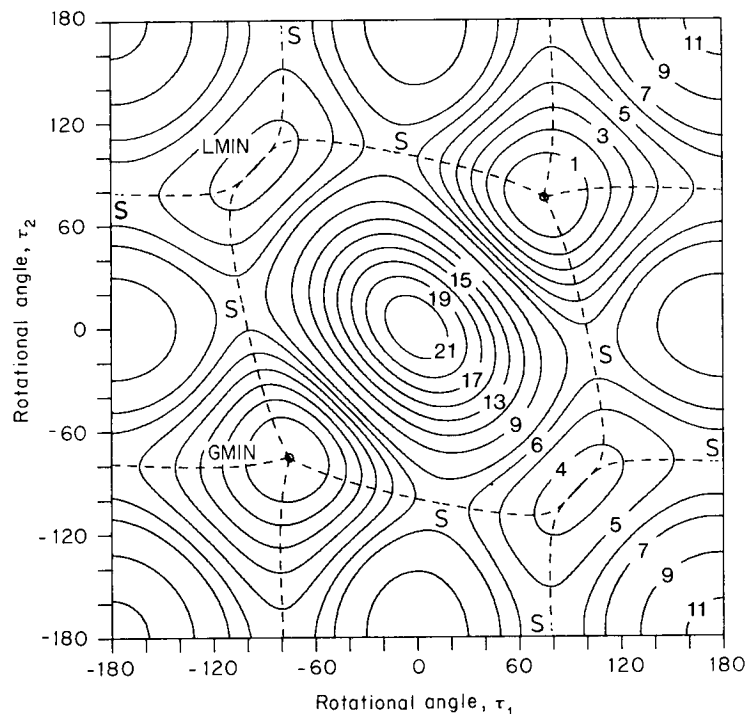


FIGURE 31. Internal rotational potential for H_2O_3 (RSMP/C calculations) as a function of the dihedral angles τ_1 and τ_2 . Contours indicate kcal mol^{-1} above the energy of the global minimum GMIN. The dashed lines represent the steepest descent and ascent paths to and from the saddle-points S. Adapted by permission of the American Institute of Physics from D. Cremer, *J. Chem. Phys.*, **69**, 4456 (1978).

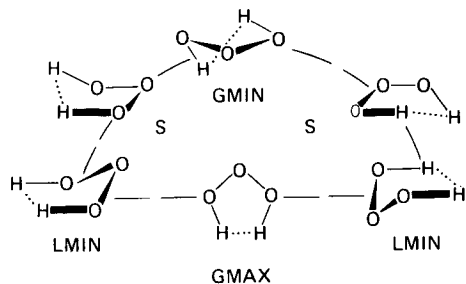


FIGURE 32. Illustration of the relationship between a flip-flop internal rotation of the double rotor H_2O_3 and the pseudorotation of a five-membered ring. GMAX: global maximum; GMIN: global minimum; LMIN: local minimum; S: saddlepoint. Reproduced by permission of the American Institute of Physics from D. Cremer, *J. Chem. Phys.*, **69**, 4456 (1978).

stabilizing factor. This is reflected by the *ab initio* and experimental geometrical data compiled in Table 40.

In a ring of given size, the tendency for puckering is stronger the more O atoms are incorporated into the ring framework. Thus, 1,2,3-trioxolane (primary ozonide) and tetroxolane with 3 and 4 adjacent O atoms are more strongly puckered than 1,2-dioxolane or 1,2,4-trioxolane (final ozonide). Parallel to this trend increases the barrier to inversion (Table 40), which is determined by the energy of the planar ring form.

The mode of puckering is also influenced by n,n interactions. We have shown this by analysing the HOMOs of the trioxolanes, which are primarily out-of-phase combinations of the $2p\pi(\text{O})$ orbitals^{270,316}. Antibonding overlap of the HOMOs is reduced if the rotational angle of the O—O rather than the C—O or C—C bond becomes large. This leads to stable C_2 -symmetrical twist (T) forms for **32**, **33** and **35** but a C_s -symmetrical envelope (E) form for **34** (Table 40). Along the same lines stabilizing or destabilizing substituent effects can be explained^{270,316}.

TABLE 40. Geometries and conformational barriers or cyclic peroxides as determined by experiment or theory

Molecule	R (Å)	R' (Å)	τ (deg.)	q^a (Å)	ϕ^a (deg.)	ΔE_{PR}^b (kcal mol ⁻¹)	ΔE_{IV}^c (kcal mol ⁻¹)	Method	Ref.
(30)	1.516	1.388	0					MW	33
	1.529	1.398	0					RSMP/DZd	58
(31)	1.491	1.475 ^d	22.1	0.28			0	X-ray ^e	311
	1.497	1.473	0	0				RHF/SV	285
(32)	1.483	1.451 ^d	20					X-ray ^f	312
	1.461	1.439	50.2	0.45	90; 270	2.2	5.7	RHF/SVd	313
(33)	1.461	1.415	49.4	0.46	90; 270			MW	314
	1.467	1.433	47.4	0.45	90; 270	3.3	6.3	RHF/SVd	269
(34)	1.454	1.437	48.9	0.47	0; 180	3.0	7.9	RHF/SVd	269
(35)	1.450 ^d	1.441	52.3	0.49	90; 270	2.5	10.9	RHF/SVd	313
(36)	1.45	1.46	60.2					X-ray ^g	315
			68.3					PE ^h	176

^aPuckering amplitude q and pseudorotational phase angle ϕ of most stable conformer; $\phi = 0^\circ$ or 180° corresponds to envelope, $\phi = 90^\circ$ or 270° to twist forms. See Refs. 269 and 317.

^bPseudorotational barrier.

^cInversion barrier of most stable conformer.

^dAveraged value.

^eX-ray analysis of dispiro(adamantane-2,3'-(1,2)dioxetane-4'2''-adamantane) ('adamantylidene-adamantane peroxide').

^fX-ray analysis of 10,10-dimethyl-3,4-dioxatricyclo[5.2.1.0^{1,5}]decane-2-spiro-2'-adamantane. See also Table 22, Section IV.D.

^gX-ray analysis of 3,3,6,6-tetra(bromomethyl)-1,2,4,5-tetroxane. Average value of R' is given. Ideal chair form assumed: the q value corresponds to q_3 , q_2 is zero (see Refs. 317 and 318).

^hPE analysis of 3,3,6,6-tetramethyl-1,2,4,5-tetroxane.

In Figure 33 the theoretically determined conformational surface of the final ozonide (33) is shown in the form of a contour-line diagram²⁶⁹. There the conformational space of the five-membered ring is spanned by the puckering amplitude q and the phase angle ϕ ($0^\circ \leq \phi < 360^\circ$)^{317,318}. The dashed line indicates the energetically most favourable pseudorotation itinerary. The energy difference between E and T forms determines the pseudorotational barriers. For compounds 32–35 these are $\leq 3 \text{ kcal mol}^{-1}$ (Table 40), which means that five-membered ring peroxides and ozonides are rather flexible in spite of relatively large barriers to ring inversion. Again, this is due to relatively small changes of the electronic structure during pseudorotation.

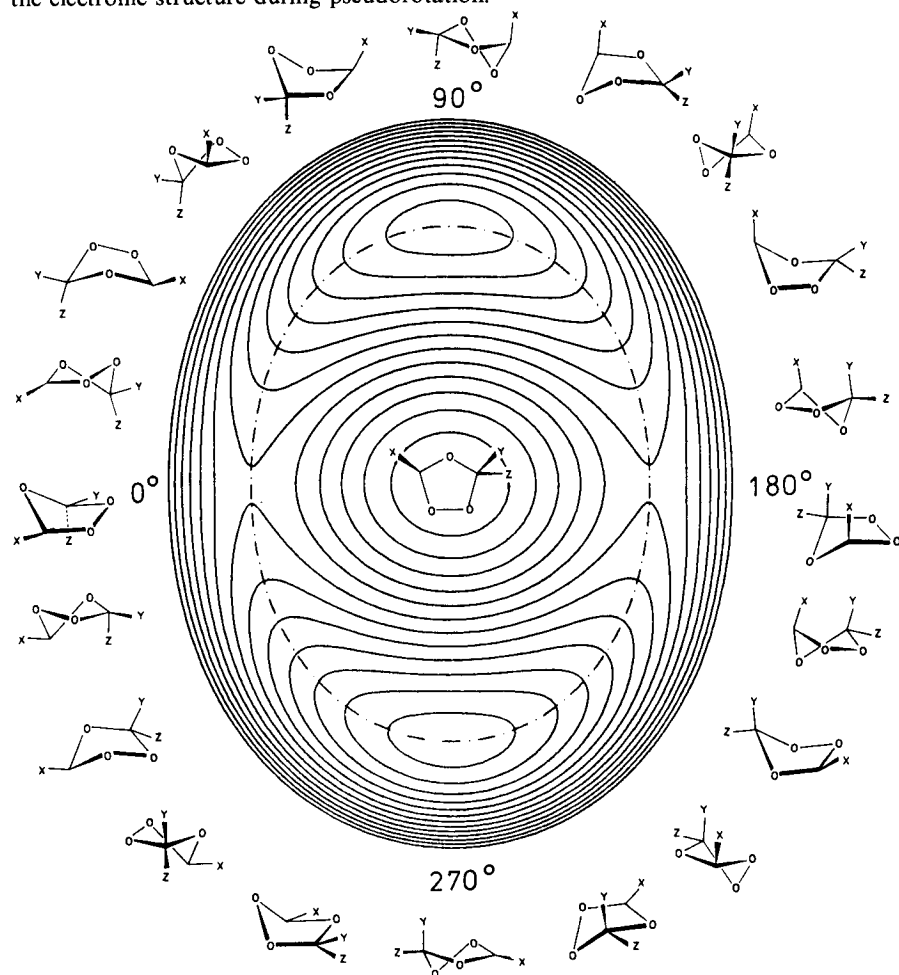


FIGURE 33. Pseudorotational surface of 1,2,3-trioxolane (RHF/C calculations). The potential is zero at the centre of the (q, ϕ) diagram, the innermost contour line corresponds to $-0.5 \text{ kcal mol}^{-1}$. The vertical spacing of two contour lines is $0.5 \text{ kcal mol}^{-1}$. The dashed line indicates the energetically most favourable pseudorotation path. Conformers are shown along this path in intervals of 18° . Substituents X, Y, Z correspond to hydrogen. Reproduced by permission of the American Institute of Physics from D. Cremer, *J. Chem. Phys.*, **70**, 1898 (1979).

Since the ozonides are important intermediates in the ozonolysis reaction, their conformational properties have been extensively discussed on both experimental¹² and theoretical grounds^{319,320}.

VI. ABBREVIATIONS, SYMBOLS, CONSTANTS AND CONVERSION FACTORS

A. List of Abbreviations

AO	Atomic Orbital
APSG	Antisymmetrized Product of Strongly-orthogonal Geminals
BSE	Bond Separation Energy
CEPA	Coupled Electron Pair Approximation
CI	Configuration Interaction
DZ	Double Zeta (Basis with 2 GTFs or STFs per AO)
DZb	Double Zeta basis augmented by bond functions
DZb + diff	Double Zeta basis augmented by bond functions and diffuse Rydberg functions
DZd	Double Zeta basis augmented by 3d functions in the heavy-atom part
DZdp	Double Zeta basis augmented by 3d functions in the heavy-atom part and 2p functions in the H part
ED	Electron Diffraction spectroscopy
ESCA	Electron Spectroscopy for Chemical Analysis
FSGO	Floating Spherical Gaussian Orbital
GS	Ground State
GTF, GTO	Gaussian Type Function, GT Orbital
GVB	Generalized Valence Bond
HF	Hartree-Fock
HOMO	Highest Occupied Molecular Orbital
INDO	Intermediate Neglect of Differential Overlap
IP	Ionization Potential
IR	Infrared spectroscopy
INO	Iterative Natural Orbital
LMO	Localized Molecular Orbital
LUMO	Lowest Unoccupied Molecular Orbital
MB, MBS	Minimal Basis Set (1 GTF or STF per AO; e.g. STO-3G)
MBPT	Many-Body Perturbation Theory
MCSCF	MultiConfiguration Self-Consistent Field
MINDO	Modified Intermediate Neglect of Differential Overlap
MM	Molecular Mechanics
MMW	MilliMetre-Wave spectroscopy
MO	Molecular Orbital
MOL	Molecule
MRD-CI	Multi-Reference Double-excitation Configuration Interaction
MW	Microwave spectroscopy
PE	Photoelectron spectroscopy
REF	Reference State
RHF	Restricted Hartree-Fock
RSMP	Rayleigh-Schrödinger Møller-Plesset perturbation theory
SCF	Self-Consistent Field

SOMO	Singly Occupied Molecular Orbital
STF, STO	Slater Type Function, ST Orbital
SV	Split-Valence basis (basis with two functions per AO of the valence shell; e.g. Pople's 4-31G or 6-31G basis sets)
SVd	Split-valence basis augmented by 3d functions in the heavy-atom part (e.g. Pople's 6-31G* basis)
SVdp	Split-valence basis augmented by 3d functions in the heavy-atom part and 2p functions in the H part (e.g. Pople's 6-31G** basis)
TS	Transition State
UHF	Unrestricted Hartree-Fock
VB	Valence Bond
ZPE	Zero-Point vibrational Energy

B. List of Symbols

A	Arbitrary atom
A,B	Term symbols for nonlinear molecules
Å	Ångstrom; $1 \text{ Å} = 10^{-10} \text{ m}$
<i>a</i>	Radius of spherical cavity (Å) (Section IV.C)
aJ	Atto Joule
a_0	Bohr radius; Atomic unit of length (see conversion factors)
a.u.	Atomic unit
B_0	Rotational constant of lowest vibrational level of ground state
C_i	Coefficient of linear combination
D	Atomic term symbol
D	Debye; unit of dipole moment
D_e	Dissociation energy measured relative to the minimum of the potential energy function ($D_e = D_0 + ZPE$).
D_0	Dissociation energy measured relative to the lowest vibrational level
$DH^0, DH^0(T)$	Dissociation enthalpy measured at temperature <i>T</i>
E	Envelope form of five-membered ring (Section V.B)
<i>E</i>	Energy
$E(\text{EXP})$	Absolute energy (hartree) at lowest vibrational level of molecular ground state
$E(\text{CORR})$	Correlation energy (hartree)
$E(\text{HF})$	Hartree-Fock limit energy (hartree)
$E(\text{HF}/X)$	SCF energy (hartree) obtained with basis set X
$E(\text{REL})$	Relativistic energy (hartree)
$E(\text{S})$	Schrödinger energy (hartree)
$E(\text{THEO})$	Theoretical molecular energy (hartree) for fixed nuclei
$E(\text{VIP})$	Vibrational energy. (hartree)
$E(X)$	SCF energy (hartree) obtained with basis set X
<i>EA</i>	Electron affinity
<i>e</i>	Electron charge (see conversion factors)
<i>f</i>	Force constant (aJ Å^{-n} ; see conversion factors)
f_e	Equilibrium molecular force constant
f_{RR}, f_{rr}	Quadratic OO and HO stretching force constants (aJ Å^{-2})
$f_{\alpha\alpha}$	Quadratic HOO bending force constant (aJ).
$f_{rR}, f_{rr'}$	HO,OO and HO,OH stretch-stretch coupling constants (aJ Å^{-2})

$f_{R\alpha}, f_{r\alpha}, f_{r\alpha'}$	OO,HOO, HO,HOO and HO,OOH stretch-bend coupling constants (aJ Å^{-1})
$f_{\alpha\alpha'}$	HOO,OOH bend-bend coupling constant (aJ)
f_{RRR}, f_{rrr}	Cubic OO and HO stretching constants (aJ Å^{-3})
$f(r, \theta)$	Common radial function of 2p AOs
<i>g</i>	Electron spin <i>g</i> tensor (Section V.A)
<i>g</i>	Subscript used to denote a 'gerade' function
<i>h</i>	Planck's constant (see conversion factors)
<i>I</i>	Ionization potential (eV) (Section IV.D)
I_{vert}	Vertical ionization potential (eV)
I_i^{exp}	Experimentally observed vertical ionization potential (eV)
<i>i</i>	Subscript used to denote molecular orbitals, orbital energies, etc.
<i>i</i>	$\sqrt{-1}$
$K, K_{z'z'}$	Nuclear quadrupole coupling constant (MHz) (Section IV.F)
<i>k</i>	Number of atoms
\hat{L}_z	<i>z</i> component of total orbital angular momentum operator
\hat{l}_z	<i>z</i> component of orbital angular momentum operator for a specific electron
M_L	Eigenvalue of \hat{L}_z operator
M_S	Eigenvalue of \hat{S}_z operator
m_l	Eigenvalue of \hat{l}_z operator
m_s	Eigenvalue of \hat{s}_z operator
N_A	Avogadro number
<i>n</i>	Electron lone pair
occ	Occupied orbitals (summation limit)
P	Atomic term symbol
<i>P, P(AB)</i>	Bond order of bond AB
<i>p, p(AB)</i>	Overlap population between atoms A and B
pm	Picometer; $1 \text{ pm} = 10^{-12} \text{ m}$
$Q, Q(A)$	Electric quadrupole moment of nucleus A (barn, see conversion factors) (Section IV.F)
<i>q</i>	Puckering amplitude (Å) of a nonplanar ring compound; if not otherwise denoted <i>q</i> corresponds to q_2
q_2	Puckering amplitude (Å) of four- and five-membered rings
q_3	Puckering amplitude (Å) of chair form of six-membered ring
<i>q, q(A)</i>	Charge at atom A (e)
$q_{x'x'}$, etc.	Diagonal elements of electric field gradient tensor measured in principal axes system (esu cm^{-3}) (Section IV.F)
$R, R(\text{OO})$	Interatomic OO distance
R_e	Equilibrium distance between O atoms of a peroxide at the minimum of the potential energy function
R_0	Effective OO distance derived directly from ground-state rotational constants
$R', R(\text{OH}), R(\text{OX})$	Interatomic OH or OX distance
R'_e, R'_0	See corresponding definitions of R_e and R_0
r_c	Covalent radius of an atom A
$r_c(\text{AB})$	AB bond critical point of ρ
r_e	Equilibrium geometry determined at the minimum of the potential energy function
r_0	Effective geometry derived directly from ground-state rotational constants

r_s	Effective geometry derived from rotational constants via Kraitchman's equations for a sequence of isotopic substitutions
r_{ip}	Distance between the centres of charge in an ion pair
r, θ, ϕ	Polar coordinates
S	Singlet state
S	Overlap integral
S	Atomic term symbol
\hat{S}_z	z component of total spin angular momentum operator
\hat{s}_z	z component of spin angular momentum operator for a specific electron
T	Triplet state
T	Temperature (Kelvin)
T_e	Energy of excited state relative to the minimum of the ground-state potential energy function
u	Subscript used to denote an 'ungerade' function
V_i^c	Fourier constant
$V_i(\tau)$	Fourier term
X	Arbitrary basis set
x, y, z	Cartesian coordinates (arbitrary axes system)
x', y', z'	Cartesian coordinates (principal axes system)
$\alpha, \alpha(\text{OOH}), \alpha(\text{OOX})$	Bond angle OOH or OOX
α_e	Equilibrium OOH or OOX bond angle at the minimum of the potential energy function
α'	Bond angle OXO
$\alpha, \beta; \alpha(i), \beta(i)$	Spin functions with $m_s = \frac{1}{2}$ and $m_s = -\frac{1}{2}$
Δ	Term symbol for linear molecules
ΔE	Difference between various energy levels
ΔE_{solv}	Solvation energy
ΔH_f^0	Enthalpy (heat) of formation
$\Delta H_f^0(0), \Delta H_f^0(T)$	Enthalpy of formation at 0° and T° Kelvin
ΔI	Difference between succeeding ionization potentials
ΔR_e	Deviation from equilibrium distance R_e
$\Delta \alpha_e$	Deviation from equilibrium bond angle α_e
$\Delta \rho(\mathbf{r})$	Deformation (difference) density function (ea_0^{-3})
$\nabla \rho(\mathbf{r})$	Gradient vector field of electron density distribution
δ	Puckering angle of a four-membered ring
ϵ	Dielectric constant
ϵ_A	Electronegativity of atom A
ϵ_i	Energy of orbital ϕ_i
η, η^A	Asymmetry parameter of atom A (dimensionless) (Section IV.F)
$\theta_{x'x'}, \text{ etc.}$	Diagonal elements of molecular quadrupole moment tensor in principal axes system (esu cm^2) (Section IV.F)
λ_i	Eigenvalue i of Hessian matrix of ρ (matrix of second derivatives) (Section IV.F)
μ	Dipole moment (Debye)
μ_a	Reduced mass (atomic-weight units)
ν_i	Fundamental vibrational frequency i (cm^{-1})
ν_e	Equilibrium vibrational frequency (cm^{-1})
Π	Term symbol for linear molecules
π	Orbitals being antisymmetrical with respect to the molecular plane

π^*	Antibonding π orbitals
ρ, ρ^A	Electron density of atom A (ea_0^{-3})
$\rho(\mathbf{r})$	Electron density distribution at point \mathbf{r} (ea_0^{-3})
Σ	Term symbol for linear molecules
\sum	Summation symbol
σ	Orbital being symmetrical with respect to molecular plane or specified bond axis
σ^*	Antibonding σ orbital
τ	HOOH or XOOX dihedral angle
$\tau_1, \tau_2, \text{ etc.}$	Dihedral angles in a polyoxide
τ'	Angle between HOO plane and plane defined by OO bond and C_2 axis
$\tau_{1/2}$	Radiation lifetime of excited state(s) (Section IV.G)
Φ	Slater determinant
ϕ_i	Molecular orbital i
φ, ϑ, ψ	Eulerian angles (Section IV.F)
χ	Biradical character given in percent (Section IV.A)
Ψ	Molecular wave function

C. Constants and Conversion Factors

$a_0 = 0.52918 \times 10^{-8} \text{ cm}$
$e = 4.803 \times 10^{-10} \text{ esu} = 1.6022 \times 10^{-19} \text{ C}$
$h = 6.6256 \times 10^{-27} \text{ erg s} = 6.6256 \times 10^{-34} \text{ Js}$
$N_A = 6.0225 \times 10^{23} \text{ mol}^{-1}$
$1 \text{ eV} = 23.06 \text{ kcal mol}^{-1}$
$1 \text{ hartree} = 27.211 \text{ eV} = 627.525 \text{ kcal mol}^{-1}$
$1 \text{ kcal mol}^{-1} = 4.184 \text{ kJ mol}^{-1} = 349.74 \text{ cm}^{-1}$
$1 \text{ aJ} = 10^{-18} \text{ J} = 1 \text{ mdyn } \text{\AA}$
$= 0.2294 \text{ hartree} = 6.24 \text{ eV}$
$1 \text{ barn} = 10^{-24} \text{ cm}^2$
$1 \text{ Debye} = 10^{-18} \text{ esu cm}$
$1 \text{ ea}_0 = 2.54158 \text{ Debye}$
$1 \text{ ea}_0^2 = 1.34492 \times 10^{-26} \text{ esu cm}^2 = 1.34492 \text{ Buckingham}$
$1 \text{ ea}_0^{-2} = 17.1524 \times 10^6 \text{ esu cm}^{-2}$
$1 \text{ ea}_0^{-3} = 32.4140 \times 10^{14} \text{ esu cm}^{-3}$

VII. ACKNOWLEDGEMENTS

The author owes a great debt of gratitude to his wife Susi for her continuous help and patience in the preparation of the manuscript. Useful discussions were held with Prof. R. F. W. Bader, Prof. S. W. Benson, Dr. J. Bull, Dr. H. Freund, Dr. S. L. Manatt, Dr. R. Pachter, Prof. P. Rademacher, Dr. S. Razumovskii, Dr. P. v. Royen, Prof. K. Schank, Prof. P. N. Skancke and Prof. U. Wahlgren. Prof. W. Jorgensen kindly provided an early version of his MO plot program. Technical assistance by J. Normann helped to prepare the MO drawings. The manuscript was partially written during a stay at the Council for Scientific and Industrial Research, Pretoria, SAR. The author thanks the members of the NCRL for accommodating him during this time. Support of the Fonds der Chemischen Industrie, the Deutschen Forschungsgemeinschaft and the Rechenzentrum der Universität Köln is gratefully acknowledged.

VIII. REFERENCES

1. W. C. Schumb, C. N. Satterfield and R. L. Wentworth, *Hydrogen Peroxide*, Reinhold, New York, 1955.
2. W. M. Weigert (Ed.), *Wasserstoffperoxid und seine Derivate*, Chemie und Anwendungen, Hüthig Verlag, Heidelberg, 1978.
3. A. V. Tobolsky and R. B. Mesrobian, *Organic Peroxides*, Interscience, New York, 1954.
4. A. G. Davies, *Organic Peroxides*, Butterworths, London, 1961.
5. E. G. E. Hawkins, *Organic Peroxides*, Van Nostrand, Princeton, 1961.
6. O. L. Mageli and C. S. Sheppard in *Encyclopedia of Chemical Technology*, 2nd ed., Vol. 14 (Eds. K. E. Kirk and D. F. Othmer), John Wiley and Sons, New York, 1967, pp. 746–820.
7. D. Swern (Ed.), *Organic Peroxides*, Volumes I, II and III, Wiley-Interscience, New York-London, 1971.
8. W. A. Waters, *Mechanisms of Oxidation of Organic Compounds*, Methuen, London, 1964.
9. K. B. Wiberg (Ed.), *Oxidation in Organic Chemistry*, Part A. Academic Press, New York, 1965.
10. D. R. Kearns, *Chem. Rev.*, **71**, 395 (1971); A. A. Frimer, *Chem. Rev.*, **79**, 359 (1979); M. Balci, *Chem. Rev.*, **81**, 91 (1981).
11. H. H. Wasserman and R. W. Murray (Eds.), *Singlet Oxygen*, Academic Press, New York, 1979.
12. P. S. Bailey, *Ozonation in Organic Chemistry*, Vol. I, *Olefinic Compounds*, Academic Press, New York, 1978.
13. S. W. Benson and P. S. Nangia, *Acc. Chem. Res.*, **12**, 223 (1979).
14. O. E. Edwards and R. Curci in *Encyclopedia of Chemical Technology*, 2nd ed., Vol. 14 (Eds. K. E. Kirk and D. F. Othmer), John Wiley and Sons, New York, 1967, pp. 820–839.
15. N. J. Turro and P. Lechtken, *Pure Appl. Chem.*, **33**, 363 (1973).
16. W. Adam, *Acc. Chem. Res.*, **12**, 390 (1979).
17. K. L. Demerjian, J. A. Kerr and J. G. Calvert, *Advan. Environ. Sci. Technol.*, **4**, 1 (1973).
18. J. H. Seinfeld, *Air Pollution, Physical and Chemical Fundamentals*, McGraw-Hill, New York, 1975, Chap. 4, pp. 142–217.
19. M. L. Kaplan and A. M. Trozzolo in *Singlet Oxygen* (Eds. H. H. Wasserman and R. W. Murray), Academic Press, New York, 1979, pp. 575–595.
20. M. A. J. Rodgers and E. L. Powers (Eds.), *Oxygen and Oxy-Radicals in Chemistry and Biology*, Academic Press, New York, 1981.
21. R. D. Jones, D. D. Summerville and F. Basolo, *Chem. Rev.*, **79**, 139 (1979).
22. L. Vaska, *Acc. Chem. Res.*, **9**, 175 (1976).
23. A. B. P. Lever and H. B. Gray, *Acc. Chem. Res.*, **11**, 348 (1978).
24. R. T. Sanderson, *Chemical Bonds and Bond Energy*, Academic Press, New York, 1971.
25. L. Pauling, *The Nature of the Chemical Bond*, Cornell University Press, Ithaca, 1969.
26. W. A. Goddard, III, T. H. Dunning, Jr., W. J. Hunt and P. J. Hay, *Acc. Chem. Res.*, **6**, 368 (1973).
27. W. L. Jorgensen and L. Salem, *The Organic Chemist's Book of Orbitals*, Academic Press, New York, 1973, p. 88. There three-dimensional MO drawings of O₂ are shown.
28. M. Kasha and D. E. Brabham in *Singlet Oxygen* (Eds. H. H. Wasserman and R. W. Murray), Academic Press, New York, 1979, pp. 1–33.
29. B. M. Gimarc, *J. Amer. Chem. Soc.*, **93**, 815 (1971); *Acc. Chem. Res.*, **7**, 384 (1974).
30. R. J. Buenker and S. D. Peyerimhoff, *Chem. Rev.*, **74**, 127 (1974).
31. B. M. Gimarc, *Molecular Structure and Bonding, The Qualitative Molecular Orbital Approach*, Academic Press, New York, 1979, Chap. 7, pp. 153–169.
32. D. Cremer, unpublished results.
33. F. J. Lovas and R. D. Suenram, *Chem. Phys. Letters*, **51**, 453 (1977); R. D. Suenram and F. J. Lovas, *J. Amer. Chem. Soc.*, **100**, 5117 (1978).
34. B. M. Gimarc, *J. Amer. Chem. Soc.*, **92**, 266 (1970); see also Reference 31, Chap. 6, pp. 127–131.
35. B. M. Gimarc, *J. Amer. Chem. Soc.*, **100**, 1996 (1978); see also Reference 31, Chap. 8, pp. 194–200.
36. P. H. Krupenie, *J. Phys. Chem. Ref. Data*, **1**, 423 (1972).
37. H. F. Schaefer, III, *J. Chem. Phys.*, **54**, 2207 (1971).
38. B. J. Moss and W. A. Goddard, III, *J. Chem. Phys.*, **63**, 3523 (1975).
39. B. J. Moss, F. W. Bobrowicz and W. A. Goddard, III, *J. Chem. Phys.*, **63**, 4632 (1975).
40. N. H. F. Beebe, E. W. Thulstrup and A. Andersen, *J. Chem. Phys.*, **64**, 2080 (1976).
41. S. L. Guberman, *J. Chem. Phys.*, **67**, 1125 (1977).
42. R. P. Saxton and B. Liu, *J. Chem. Phys.*, **67**, 5432 (1977).

43. W. T. Zemke, G. Das and A. C. Wahl, *Chem. Phys. Letters*, **14**, 310 (1972).
44. G. Das, W. T. Zemke and W. C. Stwalley, *J. Chem. Phys.*, **72**, 2327 (1980).
45. S. Rothenberg and H. F. Schaefer, III, *Mol. Phys.*, **21**, 317 (1971).
46. J. S. Wright, *Can. J. Chem.*, **51**, 139 (1973).
47. J. S. Wright, *Theoret. Chim. Acta*, **36**, 37 (1974).
48. P. J. Hay, T. H. Dunning, Jr. and W. A. Goddard, III, *Chem. Phys. Letters*, **23**, 457 (1973).
49. P. J. Hay, T. H. Dunning, Jr. and W. A. Goddard, III, *J. Chem. Phys.*, **62**, 3912 (1975).
50. P. J. Hay and T. H. Dunning, Jr., *J. Chem. Phys.*, **67**, 2290 (1977).
51. L. B. Harding and W. A. Goddard, III, *J. Chem. Phys.*, **67**, 2377 (1977).
52. S. Shih, R. J. Buenker and S. D. Peyerimhoff, *Chem. Phys. Letters*, **28**, 463 (1974).
53. K. H. Thunemann, S. D. Peyerimhoff and R. J. Buenker, *J. Mol. Spectro.*, **70**, 432 (1978).
54. D. Grimbert and A. Devaquet, *Mol. Phys.*, **27**, 831 (1974).
55. R. R. Lucchese and H. F. Schaefer, III, *J. Chem. Phys.*, **67**, 848 (1977).
56. P. G. Burton, *Intern. J. Quant. Chem., Symp.*, **11**, 207 (1977); *J. Chem. Phys.*, **77**, 961 (1979).
57. G. Karlström, S. Engström and B. Jönsson, *Chem. Phys. Letters*, **57**, 390 (1978).
58. D. Cremer, *J. Amer. Chem. Soc.*, **101**, 7199 (1979).
59. D. Cremer, to be published.
60. J. S. Wright, S. Shih and R. J. Buenker, *Chem. Phys. Letters*, **75**, 513 (1980).
61. C. W. Wilson, Jr. and D. G. Hopper, *J. Chem. Phys.*, **74**, 595 (1981).
62. M. J. S. Dewar, S. Olivella and H. S. Rzepa, *Chem. Phys. Letters*, **47**, 80 (1977).
63. S. W. Benson and A. E. Axworthy Jr., *J. Chem. Phys.*, **26**, 1718 (1957).
64. E. F. Hayes and A. K. Q. Siu, *J. Amer. Chem. Soc.*, **93**, 2090 (1971).
65. K. Yamaguchi, K. Ohta and T. Fueno, *Chem. Phys. Letters*, **50**, 266 (1977).
66. K. Yamaguchi, *Intern. J. Quant. Chem.*, **28**, 101 (1980).
67. P. C. Hiberty and C. Leforestier, *J. Amer. Chem. Soc.*, **100**, 2012 (1978).
68. W. D. Laidig and J. F. Schaefer, III, *J. Chem. Phys.*, **74**, 3411 (1981).
69. L. B. Harding and W. A. Goddard, III, *J. Amer. Chem. Soc.*, **100**, 7180 (1978).
70. J. C. Depannemaecker and J. Bellet, *J. Mol. Spectro.*, **66**, 106 (1977).
71. D. H. Liskow, H. F. Schaefer, III and C. F. Bender, *J. Amer. Chem. Soc.*, **93**, 6734 (1971).
72. J. L. Gole and E. F. Hayes, *J. Chem. Phys.*, **57**, 360 (1972).
73. R. J. Blint and M. D. Newton, *J. Chem. Phys.*, **59**, 6220 (1973).
74. W. A. Lathan, L. A. Curtiss, W. J. Hehre, J. B. Lisle and J. A. Pople, *Progr. Phys. Org. Chem.*, **2**, 175 (1974).
75. R. J. Buenker and S. D. Peyerimhoff, *Chem. Phys. Letters*, **37**, 208 (1976).
76. S. K. Shih and S. D. Peyerimhoff, *Chem. Phys. Letters*, **28**, 299 (1978).
77. S. K. Shih, S. D. Peyerimhoff and R. J. Buenker, *Chem. Phys.*, **28**, 299 (1978).
78. C. F. Melius and R. J. Blint, *Chem. Phys. Letters*, **64**, 183 (1979).
79. S. R. Langhoff and R. L. Jaffe, *J. Chem. Phys.*, **71**, 1475 (1979).
80. A. Komornicki and R. L. Jaffe, *J. Chem. Phys.*, **71**, 2150 (1979).
81. T. H. Dunning, Jr., S. P. Walch and M. M. Goodgame, *J. Chem. Phys.*, **74**, 3482 (1981).
82. Y. Beers and C. J. Howard, *J. Chem. Phys.*, **64**, 1541 (1976).
83. B. R. De and A. B. Sannigrahi, *J. Comp. Chem.*, **1**, 334 (1980).
84. M. E. Boyd, *J. Chem. Phys.*, **37**, 1317 (1962).
85. S. N. Foner and R. L. Hudson, *J. Chem. Phys.*, **36**, 2681 (1962).
86. P. Gray, *Trans. Faraday Soc.*, **55**, 408 (1959).
87. D. Cremer, to be published.
88. U. Kaldor and I. Shavitt, *J. Chem. Phys.*, **44**, 1823 (1966).
89. W. H. Fink and L. C. Allen, *J. Chem. Phys.*, **46**, 2261 (1967); **46**, 2276 (1967).
90. L. Pedersen and K. Morukuma, *J. Chem. Phys.*, **46**, 3941 (1967).
91. W. E. Palke and R. M. Pitzer, *J. Chem. Phys.*, **46**, 3948 (1967).
92. P. F. Franchini and C. Vergani, *Theoret. Chim. Acta*, **13**, 46 (1969).
93. A. Veillard, *Chem. Phys. Letters*, **4**, 51 (1969); *Theoret. Chim. Acta*, **18**, 21 (1970).
94. R. M. Stevens, *J. Chem. Phys.*, **52**, 1397 (1970).
95. I. H. Hillier, V. R. Saunders and J. F. Wyatt, *Trans. Faraday Soc.*, **66**, 2665 (1970).
96. R. B. Davidson and L. C. Allen, *J. Chem. Phys.*, **55**, 519 (1971).
97. J. P. Ranck and J. Johansen, *Theoret. Chim. Acta*, **24**, 334 (1972).
98. C. Guidotti, U. Lamanna, M. Maestro and R. Moccia, *Theoret. Chim. Acta*, **27**, 55 (1972).

99. T. H. Dunning, Jr. and N. W. Winter, *Chem. Phys. Letters*, **11**, 194 (1971).
100. L. Radom, W. J. Hehre and J. A. Pople, *J. Amer. Chem. Soc.*, **94**, 2371 (1972).
101. T. H. Dunning, Jr. and N. W. Winter, *J. Chem. Phys.*, **63**, 1847 (1975).
102. P. Botschwina, W. Meyer and A. M. Semkow, *Chem. Phys.*, **15**, 25 (1976).
103. R. E. Howard, M. Levy, H. Shull and S. Hagstrom, *J. Chem. Phys.*, **66**, 5181 (1977); **66**, 5189 (1977).
104. P. B. Ryan and J. D. Todd, *J. Chem. Phys.*, **67**, 4787 (1977).
105. P. G. Burton and B. R. Markey, *Australian J. Chem.*, **30**, 231 (1977).
106. W. R. Rodwell, N. R. Carlsen and L. Radom, *Chem. Phys.*, **31**, 177 (1978).
107. D. Cremer, *J. Chem. Phys.*, **69**, 4440 (1978).
108. M. P. Melrose and R. G. Parr, *Theoret. Chim. Acta*, **8**, 150 (1967).
109. W. H. Fink and L. C. Allen, *J. Chem. Phys.*, **46**, 3270 (1967).
110. G. F. Musso and V. Magnasco, *J. Chem. Phys.*, **60**, 3754 (1974).
111. W. England and M. S. Gordon, *J. Amer. Chem. Soc.*, **94**, 4818 (1972).
112. P. A. Christiansen and W. E. Palke, *J. Chem. Phys.*, **67**, 57 (1977).
113. E. Lombardi, G. Tarantini, L. Pirola and P. Torsellini, *J. Chem. Phys.*, **64**, 5229 (1976).
114. J. A. Pople in *The World of Quantum Chemistry* (Ed. R. Daudel and B. Pullman), Reidel Publishing Co., Dordrecht, Holland, 1974, p. 49.
115. A. Golebiewski and A. Parczewski, *Chem. Rev.*, **74**, 519 (1974).
116. A. Veillard in *Internal Rotation in Molecules* (Ed. W. J. Orville-Thomas), John Wiley and Sons, London, 1974, p. 385.
117. P. W. Payne and L. C. Allen in *Modern Theoretical Chemistry*, Vol. 4, *Applications of Electronic Structure Theory* (Ed. H. F. Schaefer, III), Plenum Press, New York, 1977, p. 29.
118. K. F. Freed, *Chem. Phys. Letters*, **2**, 255 (1968).
119. R. L. Redington, W. B. Olson and P. C. Cross, *J. Chem. Phys.*, **36**, 1311 (1962).
120. R. H. Hunt, R. A. Leacock, C. W. Peters and K. T. Hecht, *J. Chem. Phys.*, **42**, 1931 (1965).
121. W. C. Oelfke and W. Gordy, *J. Chem. Phys.*, **51**, 5336 (1969).
122. C. S. Ewig and D. O. Harris, *J. Chem. Phys.*, **52**, 6268 (1970).
123. D. Käss, H. Oberhammer, B. Brandes and A. Blaschette, *J. Mol. Struct.*, **40**, 65 (1977).
124. C. J. Marsden, D. D. DesMarteau and L. S. Bartell, *Inorg. Chem.*, **16**, 2359 (1977).
125. C. J. Marsden, L. S. Bartell and F. P. Diodati, *J. Mol. Struct.*, **39**, 253 (1977).
126. R. H. Jackson, *J. Chem. Soc.*, 4585 (1962).
127. R. B. Harvey and S. H. Bauer, *J. Amer. Chem. Soc.*, **76**, 859 (1954).
128. G. Winnewisser, M. Winnewisser and W. Gordy, *J. Chem. Phys.*, **49**, 3465 (1968).
129. B. Beagley and K. T. McAlloon, *Trans. Faraday Soc.*, **67**, 3216 (1972).
130. A. Yokozeki and S. H. Bauer, *J. Phys. Chem.*, **80**, 618 (1976).
131. O. J. Sovers, C. W. Kern, R. M. Pitzer and M. Karplus, *J. Chem. Phys.*, **49**, 2592 (1968).
132. K. Ruedenberg, *Rev. Mod. Phys.*, **34**, 326 (1962).
133. T. K. Brunck and F. Weinhold, *J. Amer. Chem. Soc.*, **101**, 1700 (1979).
134. L. C. Allen, *Chem. Phys. Letters*, **2**, 597 (1968).
135. A. Liberles, B. O'Leary, J. E. Eilers and D. R. Whitman, *J. Amer. Chem. Soc.*, **94**, 6894 (1972).
136. J. F. Olsen, *J. Mol. Struct.*, **49**, 361 (1978).
137. C. Romers, C. Altona, H. R. Buys and E. Havinga in *Topics in Stereochemistry*, Vol. 4 (Ed. E. L. Eliel and N. L. Allinger), Wiley-Interscience, New York-London, 1969, p. 39.
138. J. D. Cox and G. Pilcher, *Thermochemistry of Organic and Organometallic Compounds*, Academic Press, London, 1970.
139. D. D. Wagman, W. H. Evans, V. B. Parker, I. Halow, S. M. Bailey and R. H. Schumm, 'Selected values of chemical thermodynamic properties', *National Bureau of Standards Technical Note*, No. 270-3, Washington D.C., 1968; D. R. Stull and H. Prophet, *Natl. Stand. Ref. Data Ser., Natl. Bur. Stand.*, No. 37 (1971).
140. S. W. Benson, F. R. Cruickshank, D. M. Golden, G. R. Hangen, H. E. O'Neal, A. S. Rodgers, R. Shaw and R. Walsh, *Chem. Rev.*, **69**, 279 (1969).
141. S. W. Benson, *Thermochemical Kinetics*, 2nd ed., John Wiley and Sons, New York, 1976.
142. S. W. Benson and R. Shaw in *Organic Peroxides*, Vol. 1 (Ed. D. Swern), Wiley-Interscience, New York-London, 1971, p. 105.
143. P. S. Nangia and S. W. Benson, *J. Phys. Chem.*, **83**, 1138 (1979).
144. S. W. Benson and P. S. Nangia, *Acc. Chem. Res.*, **12**, 223 (1979).

145. P. S. Nangia and S. W. Benson, *Intern. J. Chem. Kinet.*, **12**, 29, 43, 169 (1980).
146. S. W. Benson and P. S. Nangia, *J. Amer. Chem. Soc.*, **102**, 2843 (1980).
147. P. S. Nangia and S. W. Benson, *J. Amer. Chem. Soc.*, **102**, 3105 (1980).
148. S. W. Benson, private communication.
149. D. Cremer, *J. Comp. Chem.*, in press.
150. L. Radom, W. J. Hehre and J. A. Pople, *J. Amer. Chem. Soc.*, **93**, 289 (1971).
151. A. C. Hopkinson, K. Yates and I. G. Csizmadia, *Theoret. Chim. Acta*, **23**, 369 (1972).
152. A. C. Hurley, *Advan. Quant. Chem.*, **7**, 315 (1973).
153. H. v. Hirschhausen and K. Wenzel, *Theoret. Chim. Acta*, **25**, 293 (1974).
154. J. G. Calvert and J. N. Pitts, Jr., *Photochemistry*, John Wiley and Sons, New York, 1967, pp. 824-826.
155. J. G. Kirkwood, *J. Chem. Phys.*, **2**, 351 (1934).
156. T. Koopmans, *Physica*, **1**, 104 (1934).
157. G. D. Purvis and Y. Öhrn, *J. Chem. Phys.*, **62**, 2045 (1975).
158. K. Siegbahn, C. Nordling, G. Johansson, J. Hedman, P. F. Heden, K. Hamrin, U. Gelius, T. Bergmark, L. O. Werme, R. Manne and Y. Baer, *ESCA Applied to Free Molecules*, North-Holland, Amsterdam, 1969.
159. O. Edqvist, E. Lindholm, L. E. Selin and L. Åsbrink, *Phys. Scripta*, **1**, 25 (1970).
160. J. L. Gardner and J. A. R. Samson, *J. Chem. Phys.*, **62**, 4460 (1975).
161. P. S. Bagus and H. F. Schaefer, III, *J. Chem. Phys.*, **56**, 224 (1972); P. S. Bagus, M. Schrenck, D. W. Davis and D. A. Shirley, *Phys. Rev.*, **9A**, 1090 (1974).
162. D. C. Frost, S. T. Lee and C. A. McDowell, *Chem. Phys. Letters*, **24**, 149 (1974).
163. C. R. Brundle, *Chem. Phys. Letters*, **26**, 25 (1974).
164. J. M. Dyke, L. Golob, N. Jonathan, A. Morris and M. Okuda, *J. Chem. Soc. Faraday Trans. 2*, 1828 (1974).
165. H. Basch, *J. Amer. Chem. Soc.*, **97**, 6047 (1975).
166. L. S. Cederbaum, W. Domcke, W. v. Niessen and W. P. Kramer, *Mol. Phys.*, **34**, 381 (1977).
167. H. Sambe and R. H. Felton, *J. Chem. Phys.*, **61**, 3862 (1974); but see also R. P. Messmer and D. R. Salahub, *J. Chem. Phys.*, **65**, 779 (1976).
168. A. J. B. Robertson, *Trans. Faraday Soc.*, **48**, 228 (1952).
169. K. Osafune and K. Kimura, *Chem. Phys. Letters*, **25**, 47 (1974).
170. R. S. Brown, *Can. J. Chem.*, **53**, 3439 (1975).
171. F. S. Ashmore and A. R. Burgess, *J. Chem. Soc., Faraday Trans. 2*, **73**, 1247 (1977).
172. C. R. Brundle, M. B. Robin and H. Basch, *J. Chem. Phys.*, **53**, 2196 (1970).
173. D. W. Davies, *Chem. Phys. Letters*, **28**, 520 (1974).
174. C. Batich and W. Adam, *Tetrahedron Letters* 1467 (1974).
175. R. S. Brown and R. W. Marcinko, *J. Amer. Chem. Soc.*, **100**, 5584 (1978).
176. P. Rademacher and W. Elling, *Liebigs Ann. Chem.*, 1473 (1979).
177. K. Kimura and K. Osafune, *Bull. Chem. Soc. Japan*, **48**, 2421 (1975).
178. M. J. W. Boness and G. J. Schulz, *Phys. Rev.*, **A2**, 2182 (1970).
179. R. J. Celotta, R. A. Bennett, J. L. Hell, M. W. Siegel and J. Levine, *Phys. Rev.*, **A6**, 631 (1972).
180. H. Föppl, *Z. Anorg. Allgem. Chem.*, **291**, 12 (1957).
181. N. L. Summers and J. Tyrrell, *J. Amer. Chem. Soc.*, **99**, 3960 (1977).
182. J. H. Yates and R. M. Pitzer, *J. Chem. Phys.*, **66**, 3592 (1977).
183. T. Tanaka and Y. Morino, *J. Mol. Spectry*, **33**, 552 (1970).
184. A. Barbe, C. Secroun and P. Jouve, *J. Mol. Spectry*, **49**, 171 (1974).
185. M. L. Vestal and G. H. Mauclair, *J. Chem. Phys.*, **67**, 3767 (1977).
186. S. E. Novick, P. C. Engelking, P. L. Jones, J. H. Futrell and W. C. Lineberger, *J. Chem. Phys.*, **70**, 2652 (1979).
187. G. P. Smith and L. C. Lee, *J. Chem. Phys.*, **71**, 2323 (1979).
188. J. F. Hiller and M. L. Vestal, *J. Chem. Phys.*, **74**, 6096 (1981).
189. D. C. McCain and W. E. Palke, *J. Chem. Phys.*, **56**, 4957 (1972).
190. P. A. Giguère and V. Schomaker, *J. Amer. Chem. Soc.*, **65**, 2025 (1943).
191. W. R. Busing and H. A. Levy, *J. Chem. Phys.*, **42**, 3054 (1965).
192. J. M. Savariault and M. S. Lehmann, *J. Amer. Chem. Soc.*, **102**, 1298 (1980).
193. S. F. Trevino, C. S. Choi and M. K. Farr, *J. Chem. Phys.*, **63**, 2620 (1975).
194. S. W. Peterson and H. A. Levy, *Acta Cryst.*, **10**, 70 (1957).

195. H. Kim, E. F. Pearson and E. H. Appelman, *J. Chem. Phys.*, **56**, 1 (1972).
 196. I. N. Przhivalskii and G. A. Khachkuruzov, *Opt. Spectry*, **36**, 172 (1974).
 197. D. Cremer and D. Christen, *J. Mol. Spectry*, **74**, 480 (1979).
 198. P. A. Giguère and T. K. K. Srinivasan, *J. Mol. Spectry*, **66**, 168 (1977).
 199. D. Cremer, *Fresenius Z. Anal. Chem.*, **304**, 261 (1980).
 200. B. F. Pedersen, *Acta Cryst.*, **B28**, 1014 (1972).
 201. B. F. Pedersen, *Acta Chem. Scand.*, **23**, 1871 (1969).
 202. B. F. Pedersen and B. Pedersen, *Acta Chem. Scand.*, **18**, 1454 (1964).
 203. B. F. Pedersen, *Acta Chem. Scand.*, **21**, 779 (1967).
 204. J. M. Adams, V. Ramdas and A. W. Hewat, *Acta Cryst.*, **B36**, 570 (1980).
 205. J. M. Adams and R. G. Pritchard, *Acta Cryst.*, **B32**, 2438 (1976).
 206. J. M. Adams and V. Ramdas, *Acta Cryst.*, **B34**, 2150 (1978).
 207. G. A. Khachkuruzov and I. N. Przhivalskii, *Opt. Spectry*, **33**, 127, 434 (1972).
 208. P. A. Giguère and T. K. K. Srinivasan, *J. Raman Spectry*, **2**, 125 (1974).
 209. D. W. Smith and L. Andrews, *J. Chem. Phys.*, **60**, 81 (1974).
 210. J. W. Johns, A. R. W. McKellar and M. Riggan, *J. Chem. Phys.*, **68**, 3957 (1978).
 211. J. D. Rogers and J. J. Hillman, *J. Chem. Phys.*, **75**, 1085 (1981).
 212. G. A. Khachkuruzov and I. N. Przhivalskii, *Opt. Spectry*, **36**, 175 (1974).
 213. G. Herzberg, *Molecular Spectra and Molecular Structure: I. Spectra of Diatomic Molecules*, Van Nostrand, New York, 1950.
 214. L. Andrews, *J. Chem. Phys.*, **50**, 4288 (1969).
 215. L. C. Snyder and H. Basch, *Molecular Wave Functions and Properties*, Wiley-Interscience, New York-London, 1972, p. T-88.
 216. R. Janoschek, *Z. Naturforsch.*, **25a**, 311 (1970).
 217. R. E. Christoffersen and K. A. Baker, *Chem. Phys. Letters*, **8**, 4 (1971).
 218. S. Bratož, R. Daudel, M. Roux and M. Allavena, *Rev. Mod. Phys.*, **32**, 412 (1960).
 219. P. Coppens and E. D. Stevens, *Advan. Quantum Chem.*, **10**, 1 (1977).
 220. J. Rys and M. Dupuis, results cited in P. Coppens, Y. W. Yang, R. H. Blessing, W. F. Cooper and F. K. Larsen, *J. Amer. Chem. Soc.*, **99**, 760 (1977).
 221. R. F. W. Bader, S. G. Anderson and A. J. Duke, *J. Amer. Chem. Soc.*, **101**, 1389 (1979).
 222. R. F. W. Bader, T. T. Nguyen-Dang and Y. Tal, *J. Chem. Phys.*, **70**, 4316 (1979).
 223. R. F. W. Bader, *J. Chem. Phys.*, **73**, 2871 (1980).
 224. R. F. W. Bader, T. H. Tang, Y. Tal and F. W. Biegler-König, *J. Amer. Chem. Soc.*, to be published.
 225. R. F. W. Bader, private communication.
 226. L. C. Snyder, *J. Chem. Phys.*, **61**, 747 (1974).
 227. J. T. Massey and D. R. Bianco, *J. Chem. Phys.*, **22**, 442 (1954).
 228. M. Lichtenstein, J. J. Gallagher and S. A. Clough, *J. Mol. Spectry*, **40**, 10 (1971).
 229. O. Lumpkin and W. T. Dixon, *J. Chem. Phys.*, **71**, 3550 (1979).
 230. R. J. Buenker and S. D. Peyerimhoff, *Chem. Phys. Letters*, **34**, 225 (1975).
 231. R. P. Messmer and D. R. Salahub, *J. Chem. Phys.*, **65**, 779 (1976).
 232. H. E. Hunziker and H. R. Wendt, *J. Chem. Phys.*, **60**, 4622 (1974).
 233. K. H. Becker, E. H. Fink, P. Langen and U. Schurath, *J. Chem. Phys.*, **60**, 4623 (1974).
 234. T. T. Paukert and H. S. Johnston, *J. Chem. Phys.*, **56**, 2824 (1972).
 235. C. J. Hochenadel, J. A. Ghormley and P. J. Ogram, *J. Chem. Phys.*, **56**, 4426 (1972).
 236. A. Rauk and J. M. Barriol, *Chem. Phys.*, **25**, 409 (1977).
 237. M. Schürgers and K. H. Welge, *Z. Naturforsch.*, **23a**, 1508 (1968).
 238. J. G. Calvert and J. N. Pitts Jr., *Photochemistry*, Wiley-Interscience, London-New York, 1967, pp. 443, 447-450.
 239. W. G. Dauben, L. Salem and N. J. Turro, *Acc. Chem. Res.*, **8**, 41 (1975).
 240. E. M. Evleth, *J. Amer. Chem. Soc.*, **98**, 1637 (1976).
 241. E. M. Evleth and E. Kassab, *J. Amer. Chem. Soc.*, **100**, 7859 (1978).
 242. D. A. Hatzenbuehler and L. Andrews, *J. Chem. Phys.*, **56**, 3398 (1972).
 243. L. Andrews and R. R. Smardzewski, *J. Chem. Phys.*, **58**, 2258 (1973).
 244. F. B. Billingsley and C. Trindle, *J. Phys. Chem.*, **76**, 2295 (1972).
 245. S. V. O'Neill, H. F. Schaefer, III and C. F. Bender, *J. Chem. Phys.*, **59**, 3608 (1973).
 246. D. T. Grow and R. M. Pitzer, *J. Chem. Phys.*, **67**, 4019 (1977).
 247. K. Ohkubo, T. Fujita and H. Sato, *J. Mol. Struct.*, **36**, 101 (1977).

248. K. Yamaguchi and S. Iwata, *Chem. Phys. Letters*, **76**, 375 (1980).
 249. M. M. L. Chen, R. W. Wetmore and H. F. Schaefer, III, *J. Chem. Phys.*, **74**, 2938 (1981).
 250. P. N. Noble and G. C. Pimentel, *J. Chem. Phys.*, **44**, 3641 (1966).
 251. J. L. Gole and E. F. Hayes, *Intern. J. Quantum Chem.*, **3S**, 519 (1970).
 252. D. C. McCain and W. E. Palke, *J. Magn. Res.*, **20**, 52 (1975).
 253. A. Arkell and I. Schwager, *J. Amer. Chem. Soc.*, **89**, 5999 (1967).
 254. W. R. Wadt and W. A. Goddard, III, *J. Amer. Chem. Soc.*, **97**, 3004 (1975).
 255. P. C. Hiberty, *J. Amer. Chem. Soc.*, **98**, 6088 (1976).
 256. C. A. Hull, *J. Org. Chem.*, **43**, 2780 (1978).
 257. K. Yamaguchi, K. Ohta, S. Yabushita and T. Fueno, *J. Chem. Phys.*, **68**, 4323 (1978).
 258. G. Karlström, S. Engström and B. Jönsson, *Chem. Phys. Letters*, **67**, 343 (1979).
 259. K. Yamaguchi, S. Yabushita, T. Fueno, S. Kato and K. Morokuma, *Chem. Phys. Letters*, **71**, 563 (1980).
 260. H. F. Schaefer, III, C. F. Bender and J. H. Richardson, *J. Phys. Chem.*, **80**, 2035 (1976).
 261. P. A. Benioff, G. Das and A. C. Wahl, *J. Chem. Phys.*, **67**, 2449 (1977); G. Das and P. A. Benioff, *Chem. Phys. Letters*, **75**, 519 (1980).
 262. P. K. Pearson, H. F. Schaefer, III, J. H. Richardson, L. M. Stephenson and J. I. Brauman, *J. Amer. Chem. Soc.*, **96**, 6778 (1974).
 263. K. Yamaguchi, S. Yabushita and T. Fueno, *J. Chem. Phys.*, **71**, 2321 (1979).
 264. W. A. Lathan, L. Radom, P. C. Hariharan, W. J. Hehre and J. A. Pople, *Topics Curr. Chem.*, **40**, 1 (1973).
 265. R. D. Spratley and G. C. Pimentel, *J. Amer. Chem. Soc.*, **88**, 2394 (1966).
 266. D. Cremer, to be published.
 267. E. Block, R. E. Penn, A. A. Bazzi and D. Cremer, *Tetrahedron Letters*, **22**, 29 (1981).
 268. J. Peslak, Jr., *J. Mol. Struct.*, **12**, 235 (1972).
 269. D. Cremer, *J. Chem. Phys.*, **70**, 1898 (1979).
 270. D. Cremer, *J. Chem. Phys.*, **70**, 1911 (1979).
 271. W. J. Hehre, L. Radom and J. A. Pople, *J. Amer. Chem. Soc.*, **94**, 1486 (1972).
 272. B. Plesničar, S. Kaiser and A. Ažman, *J. Amer. Chem. Soc.*, **95**, 5476 (1973).
 273. D. Cremer, *J. Chem. Phys.*, **69**, 4456 (1978).
 274. J. Kao, *J. Mol. Struct.*, **56**, 147 (1979).
 275. M. Allavena, E. Blaisten-Barojas and B. Silvi, *J. Chem. Phys.*, **75**, 787 (1981).
 276. O. Gropen, *J. Mol. Struct.*, **32**, 85 (1976).
 277. B. Plesničar, D. Kocjan, S. Murovec and A. Ažman, *J. Amer. Chem. Soc.*, **98**, 3143 (1976).
 278. R. R. Luchese, J. F. Schaefer, III, W. R. Rodwell and L. Radom, *J. Chem. Phys.*, **68**, 2507 (1978).
 279. A. D. Kirshenbaum, A. V. Grosse and J. G. Aston, *J. Amer. Chem. Soc.*, **81**, 6398 (1959).
 280. R. L. Kuczowski, *J. Amer. Chem. Soc.*, **85**, 3047 (1963); **86**, 3617 (1964).
 281. A. Hinchliffe, *J. Mol. Struct.*, **55**, 127 (1979).
 282. M. J. S. Dewar and W. Thiel, *J. Amer. Chem. Soc.*, **97**, 3978 (1975); **99**, 2338 (1977).
 283. L. B. Harding and W. A. Goddard, III, *J. Amer. Chem. Soc.*, **99**, 4520 (1977); **102**, 439 (1980).
 284. K. Yamaguchi, T. Fueno, I. Saito and T. Matsuura, *Tetrahedron Letters*, **21**, 4087 (1980).
 285. K. Yamaguchi, S. Yabushita and T. Fueno, *Chem. Phys. Letters*, **78**, 572 (1981).
 286. K. Yamaguchi, S. Yabushita, T. Fueno and K. N. Houk, *J. Amer. Chem. Soc.*, **103**, 5043 (1981).
 287. D. C. Hrnčir, R. D. Rogers and J. L. Atwood, *J. Amer. Chem. Soc.*, **103**, 4277 (1981).
 288. D. M. Kurtz, Jr., D. F. Shriver and I. M. Klotz, *J. Amer. Chem. Soc.*, **98**, 5033 (1976).
 289. H. Oberhammer and J. E. Boggs, *J. Amer. Chem. Soc.*, **102**, 7241 (1980).
 290. P. H. Blustin, *Theoret. Chim. Acta*, **48**, 1 (1978).
 291. N. L. Allinger, J. Kao, H.-M. Chang and D. B. Boyd, *Tetrahedron*, **32**, 2867 (1976).
 292. E. Hirota, *Bull. Chem. Soc. Japan*, **31**, 130 (1958).
 293. C. W. Bock, M. Trachtman and P. George, *J. Mol. Spectry*, **84**, 256 (1980); *J. Mol. Struct.*, **71**, 327 (1981).
 294. L. M. Hjelmeland and G. H. Loew, *Chem. Phys. Letters*, **32**, 309 (1975).
 295. L. M. Hjelmeland and G. Loew, *Tetrahedron*, **33**, 1029 (1977).
 296. C. Petrongolo, *Chem. Phys.*, **26**, 243 (1977).
 297. B. Plesničar, M. Tasevski and A. Ažman, *J. Amer. Chem. Soc.*, **100**, 743 (1978).
 298. A. Ažman, J. Koller and B. Plesničar, *J. Amer. Chem. Soc.*, **101**, 1107 (1979).
 299. O. Kikuchi, K. Suzuki and K. Tokumaru, *Bull. Chem. Soc. Japan*, **52**, 1086 (1979).

300. K. Ohkubo and J. Sato, *Bull. Chem. Soc. Japan*, **52**, 1525 (1979).
301. N. W. Winter, W. A. Goddard, III and C. F. Bender, *Chem. Phys. Letters*, **33**, 25 (1975).
302. G. R. McMillan and J. G. Calvert, *Oxidation Combustion Rev.*, **1**, 83 (1965).
303. P. Brant, J. A. Hashmall, F. L. Carter, R. DeMarco and W. B. Fox, *J. Amer. Chem. Soc.*, **103**, 329 (1981).
304. D. Cremer and J. A. Pople, *J. Amer. Chem. Soc.*, **97**, 1358 (1975).
305. H. Niki, P. D. Maker, C. M. Savage and L. P. Breitenbach, *Chem. Phys. Letters*, **73**, 43 (1980).
306. T. Minato, S. Yamabe, H. Fujimoto and K. Fukui, *Bull. Chem. Soc. Japan*, **51**, 682 (1978).
307. H. F. Carroll and S. H. Bauer, *J. Amer. Chem. Soc.*, **91**, 7727 (1969).
308. A. Bar-nun and A. Lifshitz, *J. Chem. Phys.*, **47**, 2878 (1967).
309. K. Hiraoka, P. P. S. Saluja and P. Kebarle, *Can. J. Chem.*, **57**, 2159 (1979).
310. S. Yamabe and K. Hirao, *J. Amer. Chem. Soc.*, **103**, 2176 (1981).
311. J. Hess and A. Voss, *Acta Cryst.*, **B33**, 3527 (1977).
312. P. B. Hitchcock and I. Beheshti, *J. Chem. Soc., Perkin 2*, 126 (1979).
313. D. Cremer, *J. Amer. Chem. Soc.*, to be published.
314. C. W. Gillies and R. L. Kuczkowski, *J. Amer. Chem. Soc.*, **94**, 6337 (1972); R. L. Kuczkowski, C. W. Gillies and K. L. Gallaher, *J. Mol. Spectry*, **60**, 361 (1976); U. Mazur and R. L. Kuczkowski, *J. Mol. Spectry*, **65**, 84 (1977).
315. M. Schulz, K. Kirschke and E. Hohne, *Chem. Ber.*, **100**, 2242 (1967).
316. D. Cremer, *J. Chem. Phys.*, **70**, 1928 (1979).
317. D. Cremer and J. A. Pople, *J. Amer. Chem. Soc.*, **97**, 1354 (1975).
318. D. Cremer, *Israel J. Chem.*, **20**, 12 (1980).
319. D. Cremer, *J. Amer. Chem. Soc.*, **103**, 3619, 3627, 3633 (1981).
320. D. Cremer, *Angew. Chem.*, **93**, 934 (1981).